AD NUMBER

AD853475

LIMITATION CHANGES

TO:

Approved for public release; distribution is unlimited.

FROM:

**Distribution authorized to U.S. Gov't. agencies and their contractors;
Administrative/Operational Use; MAR 1969. Other requests shall be referred to Naval Weapons Center, China Lake, CA.**

AUTHORITY

NWC ltr 24 Oct 1973

NWC TP 4393

EXPERIMENTAL STUDIES ON THE OSCILLATORY COMBUSTION OF SOLID PROPELLANTS

by

Aerothermochemistry Division

Research Department

ABSTRACT. This report describes the results of testing a series of composite and double-base propellants in a T-burner facility. The investigation reveals the unstable combustion behavior that is susceptible of excitation under acoustic pressure-coupled conditions. The degree of instability is quantitatively described in terms of the response function, which is a well-defined characteristic of the propellant. The effect of pressure and frequency has been systematically investigated for the frequency range of 500-10,000 cps and for pressures up to nearly 3,000 psia. Such an extended coverage has permitted the determination of a very general pattern of behavior, including the maximum instability conditions, the isoresponse function contours, and the neutral boundary separating the unstable and stable combustion regimes in the 1.5-inch T-burner.

NAVAL WEAPONS CENTER
CHINA LAKE, CALIFORNIA * MARCH 1969

BLANK PAGE

NAVAL WEAPONS CENTER
AN ACTIVITY OF THE NAVAL MATERIAL COMMAND

M. R. Etheridge, Capt., USN ..... Commander
Thomas S. Amlie, Ph.D. ..... Technical Director

FOREWORD

This report summarizes results of an extensive study of the effect of formulation variables on the combustion stability of solid propellants. The test results and discussion provide a useful guide to stability trends, and pose some basis for evaluation of existing theories of combustion perturbation behavior.

This study was supported under Navy Bureau of Weapons Task Assignment RMMP-22 095/216 1/F009-06-04, and was carried out between 1964 and 1967.

This report is released at the working level for information purposes and does not represent the final judgment of the Center.

Released by
E. W. PRICE, Head
Aerothermochemistry Division
25 March 1969

Under authority of
HUGH W. HUNTER, Head
Research Department

NWC Technical Publication 4393

Published by.....Research Department
Collation.....Cover, 56 leaves, DD Form 1473, abstract cards
First printing.....225 unnumbered copies
Security classification.....UNCLASSIFIED

CONTENTS

NOMENCLATURE

c	Velocity of sound
E	Acoustic energy in a column of unit cross-sectional area and length L
$\dot{E}$	Rate of change of E with respect to time
E_1	E during growing oscillations with attenuation
e	Acoustic energy per unit volume
e''	e during decaying oscillations
f	Frequency
L	Length of T-burner
m	Mass flow rate per unit area
p	Amplitude of pressure oscillations at time t = 0
p'	Amplitude at time t = 0 for case of oscillations growing in presence of attenuation
r	Linear regression rate of the burning surface
t	Time
U	Mean flow velocity just outside the combustion zone
Y	Real part of the acoustic admittance (Eq. 16)
Y'	Effective admittance (real part) including contribution due to convection through the burning surface
y	Y/(U/P)
y'	Y'/(U/P)
α	Exponential growth rate of oscillations in absence of attenuation

γ	Ratio of specific heats of product gas
ΔP	Amplitude of pressure oscillations
ΔP_1	Amplitude of pressure oscillations during period of growth
$\Delta P'$	Amplitude at specific time
$\Delta P''$	Amplitude at one cycle after time for which $\Delta P = \Delta P'$
ΔU	$(\Delta U)_m \cos \theta$
$(\Delta U)_m$	Amplitude of velocity oscillations just outside the combustion zone (velocity perpendicular to the burning surface).
ϵ	Amplitude of pressure oscillation divided by mean pressure
θ	Phase of the velocity oscillation relative to the pressure oscillation
μ	Amplitude of in phase component of mass rate oscillation divided by mean mass rate
ρ	Density of combustion product gas
ρ_s	Density of the solid propellant
σ	Amplitude of in phase component of density oscillation divided by mean density

SUBSCRIPTS

1	Pertaining to period of growing oscillations
2	Pertaining to period of decaying oscillations
m	Pertaining to period of constant oscillations

INTRODUCTION

The Problem

The combustion of solid propellants in rocket motors is often accompanied by a phenomenon known as unstable burning, or combustion instability. This phenomenon can manifest itself in several different ways, depending upon the type of propellant, the configuration of the motor, and the operational pressure (Ref. 1). Most cases of combustion instability result in motor-pressure fluctuations which have a detrimental effect on motor performance. The advent of very large motors, together with the development of very-fast-burning propellants, made combustion instability an even more critical problem. Some reliable criteria for rating combustion instability are therefore needed.

Among the types of combustion instability most frequently impairing motor performance, that defined as "acoustic instability" is, as a rule, the hardest to eradicate. It is encountered when the motor pressure oscillates at a frequency equal to or near that of any of the acoustic standing waves of the motor cavity, either in longitudinal or transverse modes. The peak-to-peak amplitude of the acoustic pressure oscillations that develop in very severe cases of instability can reach levels comparable to the mean motor pressure. The engineering approach to control of such behavior has mainly consisted of the application of mechanical methods to reduce the amplitude of the acoustic pressure oscillations to tolerable limits, disregarding the basic causative principles of the problem.

The dynamic interaction of the acoustic field with the propellant combustion is twofold, due to the pressure and velocity components associated with the sound field. The nature of this mutual interaction is highly involved because of the peculiarities of the acoustic field prevailing in the cavity and because of the complexity of the physical and chemical processes occurring during the combustion of the propellant. In order to make the problem tractable, the nature of the combustion and sound-field interaction had to be resolved into its basic elements, and thus the approach was taken of studying the "pressure-coupled" and "velocity-coupled" contributions separately. Practical experience, however, has suggested that the contribution through pressure coupling is by far the stronger of the two in the frequency range above 500 cps (Ref. 1).

Much effort has been devoted to the development of burner systems in which either attribute of acoustic combustion instability could be studied independently of the other. Considerable success has been achieved in developing a burner system that exhibits pressure-coupled instability spontaneously, uncomplicated by the presence of velocity coupling. The resulting laboratory design is known as the T-burner, and the technique of testing has received extensive study (Ref. 2).

The Investigation

The main objective of the investigation was to experimentally determine the acoustic pressure-coupled unstable combustion behavior of a selected group of composite and double-base propellants, using the existing T-burner facility at the Naval Weapons Center (NWC). Emphasis was placed on the effect of pressure and frequency to try to detect as much of an overall mode of behavior as possible. Experimentation at increasingly higher pressures (up to 2,400 psia) over the available frequency range (500 to 10,000 cps) has led to the establishment of a very general pattern of behavior which had so far remained unknown. Propellants that exhibit instability in rocket motors can generally be characterized in the 1.5 inch diameter T-burner over the ranges of frequency and pressure of importance. An exception is the class of aluminized propellants, which propellants are less suited for study because they usually become stable at frequencies in the effective test range of this burner (above 500 cps) due to the stabilizing effect of Al_2O_3 smoke.

The principal information obtained from the T-burner tests is

1. The susceptibility of the propellant to pressure coupled instability, as a function of frequency and mean pressure

2. The stability limits of the T-burner

Various propellant compositions have been studied in order to compare their behavior. Only a few typical double-base propellants were tested (N-4, N-5, JPN, and X-14). The main objective has been to determine the effect of burning rate through the linear, mesa, and plateau modalities and to establish the major differences of behavior between double-base and composite propellants. The objective with the composite propellants has been primarily to determine the effect of (1) ammonium perchlorate particle size and (2) combustion catalysts. A secondary objective has been to determine the effect of (1) type of binder, (2) type of oxidizer, and (3) amount of aluminum. Some of the compositional influences appear to be strong and individualistic, and although certain trends are clearly discernible, a formulistic categorization is not possible at present. This report does not contain theoretical work or a review of theories; the brief notes in "Fundamentals of the T-Burner Method" are for conceptual definition only.

Applicability of Results

The merit of the T-burner method rests on its ability to produce results that can be defined as being a fundamental property of propellant combustion. The combustion amplification constant α, or the response function μ/ε, are true representations of that property, and in this respect the importance of the T-burner method is unquestionable. The significance of the results, however, has often been doubted or even ignored (Ref. 3) on the grounds of irrelevance to actual rocket-motor situations. Nevertheless, a balanced judgment on the matter would prove the inconsistency of that premise as a basis to reckon the validity of T-burner results, since the argument does not rest so much on the results as on how to apply them to the fullest advantage.

Rocket-motor instability, in a broad sense, is the combined outcome of two contributing behaviors, that of the propellant and that of the combustion chamber. Therefore, in any scheme intended to predict rocket-motor instability, T-burner data is a necessary element of information among the several needed. The T-burner method does provide a representation of propellant combustion instability that is adequate at high frequencies when pressure-coupled conditions are predominant; however, as lower frequencies are approached, the results do not completely fill the need because of the appearance of velocity-coupled contributions. As no technique has yet been successfully devised to study the effect of velocity-coupled contributions, their relative importance at low frequencies remains a matter of conjecture.

The present T-burner system is operated under a standardized procedure, and measurements can be obtained cheaply and routinely down to 500 cps. Some operational improvements might afford a lower-frequency coverage or greater accuracy at marginal, unstable conditions. The effect of scaled-up parameters, such as burner diameter, remains uncertain, but there is no reason to assume that such an effect would change the validity of the results presented herein, at least insofar as differences in behavior of different propellants are concerned.

FUNDAMENTALS OF THE T-BURNER METHOD

Character of the Experiment

The unstable combustion behavior of solid propellants under acoustic pressure-coupled conditions was investigated in a T-burner. The standard design of this laboratory burner has a double-end-burning configuration and is vented at the center to a surge tank to afford constant-pressure control during the test (Ref. 4). The location of the propellant specimens and the axial mode of oscillation of the burner ensure that the coupling between the combustion zone and the acoustic field is pressure-coupled only. In the standard design, the propellant specimens have the same cross-sectional area as the burner. Thus, the burner exhibits one-dimensional, self-excited pressure oscillations which are interpreted in terms of linear acoustics and treated under the stipulation that all the interaction between the combustion zone and the acoustic field occurs via the first longitudinal acoustic standing-wave mode of the burner cavity. A collective review on the theory and use of the T-burner technique can be found in Ref. 5.

In general, the intensity of acoustic pressure-coupled instability will depend upon the combined effect of several variables:

1. The amount of energy released at sites in the motor cavity that could become antinodes for acoustic pressure oscillations

2. The modes of energy released at the combustion zone through kinetic and diffusion processes and the corresponding reaction times associated with these processes

3. The acoustic damping or attenuation properties of the propellant and combustion products

4. The acoustic damping or attenuation properties of the motor cavity.

The type of propellant and the pressure, frequency, and motor geometry will determine in each case the magnitude of the above variables and the degree of their interaction. T-burner experiments cannot resolve the individual contribution of each variable, since they essentially show the "global" amplification and attenuation as a function of pressure and frequency. To properly elucidate the amplification mechanism, which is mainly dependent upon amount and mode of energy release, and the attenuation mechanism, which is mainly dependent upon particulate

damping by the combustion products and cavity damping, techniques of greater versatility than the present one will have to be applied.

Propellant Combustion Amplification

The purpose of this experiment was to determine (1) the propellant combustion amplification constant α and (2) the limiting conditions at which attenuation cancels amplification. Both were determined as functions of combustion pressure and oscillation frequency. In unstable tests, the acoustic pressure oscillations appear spontaneously and grow exponentially from a small pressure disturbance. If a system with no attenuation is assumed (an ideal case), the exponential growth of the pressure oscillations would continue indefinitely until burnout and would remain constant thereafter, as indicated in Fig. 1(a). In such a case, the amplitude of the pressure oscillations ΔP, as a function of time, would be given during the period of growing oscillations by

$$\Delta P = pe^{\alpha t} \tag{1}$$

In a system with attenuation, the growth rate of oscillations is less, and is designated by

$$\Delta P_1 = p_1 e^{\alpha_1 t_1}$$

In practice, the amplitude of oscillations is limited by nonlinearities, which leads to constant-amplitude oscillations after the initial growth period (Fig. 1b). Upon burnout of the propellant, the oscillations decay in an approximately exponential manner

$$\Delta P_2 = p_2 e^{\alpha_2 t_2}$$

In interpreting the test results, it is assumed that the attenuation effects responsible for α_2 are the same as the attenuation present during the growth of oscillations,[1] in which case the combustion amplification of oscillations is

$$\alpha = \alpha_1 + \alpha_2 \tag{2}$$

[1] This assumption has not been systematically evaluated, and is known to be a source of appreciable error, particularly under test conditions where α_2 is comparable to α (i.e., near the combustor stability limits). In particular, the timewise variation during the flushing time of the combustor is large when condensed phase products are involved and the combustor is long (low frequency).

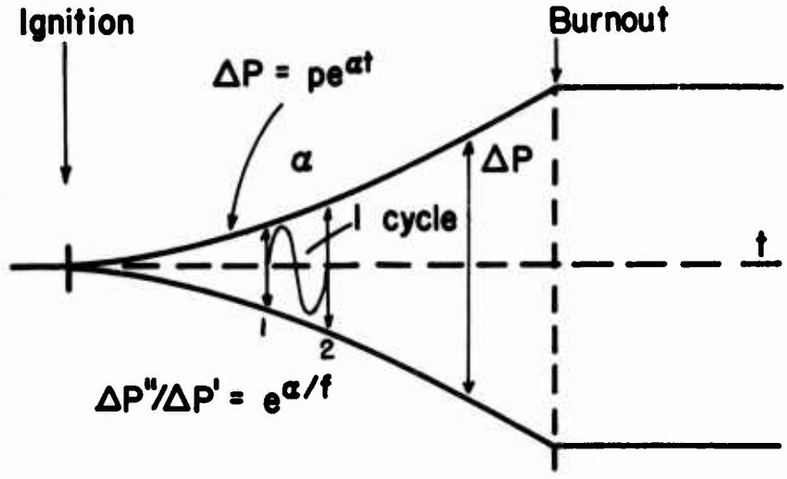

(a) System with no acoustic losses ($\alpha_2 = 0$)

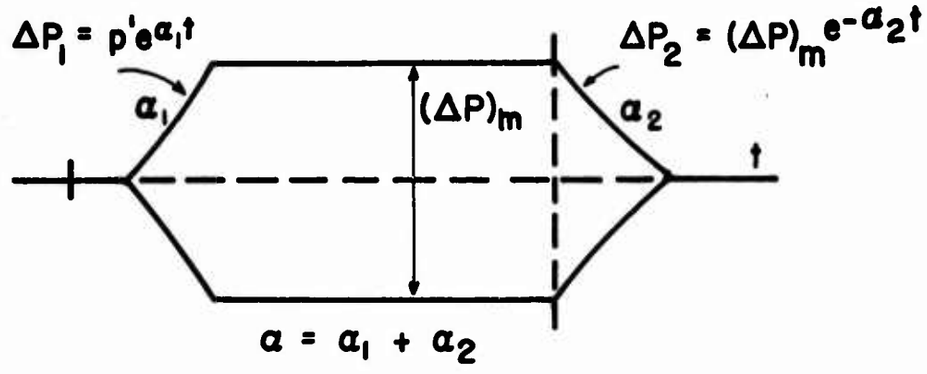

(b) System with acoustic losses ($\alpha > \alpha_2$)

(c) System with acoustic losses ($\alpha \leq \alpha_2$)

$\alpha_1 = 0$

FIG. 1. Schematic Representation of Oscillatory Behavior in T-Burner.

Figure 1(c) shows the situation when attenuation overrides amplification; the outcome is stable burning. The pressure and frequency conditions, for a given T-burner, at which α exactly matches α_2 (i.e., α_1 becomes zero) define the neutral boundary separating the stable and unstable regimes; this boundary is a property of the system and not of the propellant alone. Conversely, it should be emphasized that α is an inherent property of the propellant. It follows from Eq. 1, as illustrated in Fig. 1(a), that α can also be expressed in terms of the pressure amplitudes over 1 cycle of oscillation:

$$\alpha = f\,[\ln\,(\Delta P''/\Delta P')] \tag{3}$$

where f is the frequency of the pressure oscillations. The word "constant" used in connection with α, α_1, and α_2 is somewhat misleading and should be taken with reservation. For a given burner and propellant, these quantities are assumed to be constant only at a fixed pressure and frequency and when considered in the context of the defining relationships; it will be later seen that they have a strong and definite parametric relationship to the related variables.

Acoustic Energy Levels

Unstable burning conditions imply the appearance of certain acoustic energy levels and a direct relationship exists between these levels and α. Referring to the T-burner experiment, as illustrated in Fig. 1(b), the growth of the amplitude of the pressure oscillations ΔP_1, as a function of time, is given by

$$\Delta P_1 = p' e^{\alpha_1 t} \tag{4}$$

where p' is the initial pressure disturbance in the burner cavity, from which the spontaneous development of the full-scale pressure oscillations is accounted to originate (with $t = 0$ at the time of the disturbance p'). The nature of this pressure disturbance is left unidentified, although the level of turbulence in the burner cavity, once propellant burning is under way, might adequately justify the disturbance. In any case, the presence of this pressure disturbance does not necessarily have prior connection with the oscillatory behavior that it helps to trigger.

ΔP_1 attains a maximum value $(\Delta P)_m$ when nonlinearities develop and a balance is reached with no net change in acoustic energy after time $t > t_m$, or roughly

$$(\Delta P)_m = p' e^{\alpha_1 t_m} \tag{5}$$

After burnout, the decay of the amplitude of the pressure oscillations ΔP_2, as a function of time, follows the relation

$$\Delta P_2 = (\Delta P)_m e^{-\alpha_2 t} \tag{6}$$

For a standing sound wave in a closed cavity, the acoustic energy e per unit volume, at isentropic conditions, is given by

$$e = \frac{\rho(\Delta U)_s^2}{4} = \frac{(\Delta P)_s^2}{4\rho c^2} \tag{7}$$

where ρ is the gas density, $(\Delta U)_s$ is the antinodal amplitude of the gas velocity oscillations, $(\Delta P)_s$ is the antinodal amplitude of the gas pressure oscillations, and c is the speed of sound. Considering a T-burner of length L, the acoustic energy per unit cross section area during the growth of the pressure oscillations will be denoted by

$$e_1 L = E_1 = \frac{(\Delta P_1)^2 L}{4\rho c^2} \tag{8}$$

If α_1 in Eq. 4 is assumed to remain invariant during the growth of the pressure oscillations, Eq. 4 may be used with Eq. 8 to write the specific input rate of acoustic energy in the system as

$$\frac{1}{E_1}\frac{\Delta E}{\Delta t} = \frac{\dot{E}_1}{E_1} = 2\alpha_1 \tag{9}$$

Under similar assumptions, the corresponding specific output rate of acoustic energy in the system during the decay of the pressure oscillations will be

$$e_2 L = E_2 = \frac{(\Delta P_2)^2 L}{4\rho c^2} \tag{10}$$

and

$$\frac{1}{E_2}\frac{\Delta E_2}{\Delta t} = \frac{\dot{E}_2}{E_2} = -2\alpha_2 \tag{11}$$

therefore, the specific input rate of acoustic energy in the system due to combustion will become

$$\frac{\dot{E}_1}{E_1} - \frac{\dot{E}_2}{E_2} = \frac{\dot{E}}{E} = 2\,(\alpha_1 + \alpha_2) = 2\alpha \qquad (12)$$

or twice the value of α, i.e., α can be used as a measure of the amplification of pressure waves by the combustion. Experimentally, α would be obtained from observed values of α_1 and α_2, in combination with Eq. 12.

Acoustic Admittance

In most rocket motor situations, the combustion processes are localized near the propellant surface. Under this condition, the combustion layer can be viewed for the purposes of stability analyses as an acoustically active surface, whose acoustic properties can be characterized by an acoustic admittance. The value of the admittance depends on the combustion dynamics, which in principle can be determined either from analytical models of the combustion dynamics or from experiments. If the admittance were known as a function of pressure, frequency and propellant composition, the prediction of combustor stability would be greatly simplified. There is no sound basis for such predictions from existing models. The purpose of the present work is to determine the admittance or related functions from experimentally observed combustor behavior, using the T-burner. In the following, the relation between the admittance and the burner behavior is presented as a basis for explaining the data reduction procedure.

Referring to a plane just outside the (thin) combustion zone in the T-burner, the amplitudes of velocity and pressure oscillations are denoted by $(\Delta U)_m$ and ΔP, and the phase between velocity and pressure is denoted by θ. The component of $(\Delta U)_m$ in phase with pressure is

$$\Delta U = (\Delta U)_m \cos\theta \qquad (13)$$

The acoustic energy that results per unit time and unit area of combustion zone is calculated to be

$$\dot{E} = \tfrac{1}{2}\,(\Delta P)\,(\Delta U) \qquad (14)$$

with $\dot{E}$ representing the same quantity as in Eq. 12. This term can also be interpreted as the work done by a pressure ΔP acting on a unit of surface which moves a distance ΔU each unit time as a consequence of the pressure action. From Eq. 14 it follows that

$$\dot{E} = \tfrac{1}{2} (\Delta P)^2 \left(\frac{\Delta U}{\Delta P}\right) = - \tfrac{1}{2} (\Delta P)^2 Y \tag{15}$$

where Y, the acoustic admittance, takes the form[2]

$$Y = - \left(\frac{\Delta U}{\Delta P}\right) \tag{16}$$

In terms of the combustion-sound field interaction, the requirement for amplification is that $\dot{E}$ has to be positive or Y negative. For practical purposes, however, the minus sign in Eq. 16 can be ignored.

Propellant Response Function

Equation 16 can be transformed into a more workable expression by applying the steady state conservation equation

$$U\rho = r\rho_s = m \tag{17}$$

where U is the mean velocity of the combustion gases, r is the propellant steady state burning rate at mean pressure, ρ_s is the propellant density, and m is the propellant mass burning rate per unit area. Assuming that Eq. 17 remains valid when a variation in U equal to ΔU is imposed, it follows that

$$\Delta U = \Delta\left(\frac{m}{\rho}\right) = \left(\frac{\Delta m}{\rho} - m \frac{\Delta \rho}{\rho^2}\right) \tag{18}$$

where Δm and $\Delta \rho$ are the corresponding variations in mass burning rate and gas density.[3] By rearranging and using Eq. 17, Eq. 18 becomes

$$\Delta U = U \left(\frac{\Delta m}{m} - \frac{\Delta \rho}{\rho}\right) \tag{19}$$

Defining the fractional variations in mass burning rate, pressure, and density as

$$\frac{\Delta m}{m} = \frac{\Delta r}{r} = \mu \tag{20}$$

---

[2] This is the real part of the complex acoustic admittance used in many references.

[3] Incremental quantities refer to component in phase with pressure.

$$\frac{\Delta P}{P} = \varepsilon \tag{21}$$

$$\frac{\Delta \rho}{\rho} = \sigma \tag{22}$$

the admittance function in Eq. 17 can then be written as

$$Y = -\frac{U}{P}\left(\frac{\mu}{\varepsilon} - \frac{\sigma}{\varepsilon}\right) \tag{23}$$

where the ratio μ/ε has become known as the "pressure-coupled propellant response function", and represents the ratio of the fractional variation in burning rate to the fractional variation in pressure. Essentially, this is described by

$$\frac{\mu}{\varepsilon} = \frac{P}{r}\frac{\Delta r}{\Delta P} \tag{24}$$

where P/r is the steady state and $\Delta r/\Delta P$ the oscillatory term of the response function.

Acoustic studies of T-burner cavities (Ref. 6) have shown that the admittance function given by Eq. 23 requires an additional term in order to account for the effect of mean flow in the burner, which is caused by the combustion gases as they proceed downstream in both directions from the burner ends. The effect of the mean flow is a convective transport of acoustic energy, and the value of the correcting term is given by $-(U/P)(1/\gamma)$; therefore, a new expression for an equivalent "no-mean-flow admittance" is

$$Y' = -\frac{U}{P}\left(\frac{\mu}{\varepsilon} - \frac{\sigma}{\varepsilon} + \frac{1}{\gamma}\right) \tag{25}$$

It is apparent that the mean flow has a destabilizing effect (same sign as μ/ε). It should be noted, however, that Eq. 25 is no longer the admittance function of a surface, as is the case with Eq. 23, the relation between the admittance and Y' being

$$Y' = Y - \frac{U}{P}\frac{1}{\gamma} \tag{26}$$

Sometimes a reduced specific admittance function is defined by removing the U/P term, i.e.,

$$y' \equiv Y'/(U/P) = y - \frac{1}{\gamma} \tag{27}$$

At high frequencies, when isentropic or adiabatic conditions should prevail in the burner cavity, the ratio σ/ε exactly matches $1/\gamma$, and the admittance function takes the form

$$Y'_{HF} = -\frac{U}{P}\frac{\mu}{\varepsilon} \tag{28}$$

Conversely, when conditions become isothermal at low frequencies, the ratio σ/ε acquires value unity, and

$$Y'_{LF} = -\frac{U}{P}\left(\frac{\mu}{\varepsilon} - \frac{\gamma-1}{\gamma}\right) \tag{29}$$

The next step is to determine the relationship between α and Y and, through it, the relationship between α and μ/ε. On one hand, the acoustic energy rate in terms of the standing wave equation is given by

$$\dot{E} = 2\alpha E = 2\alpha \frac{(\Delta P)_s^2 L}{4\rho c^2} \tag{30}$$

On the other hand, considering a double-ended T-burner of length L, where there are two unit areas of combustion zone per unit cross section area of cavity, the acoustic energy rate, according to Eq. 15, will be[4]

$$\dot{E} = -2\left[\tfrac{1}{2}(\Delta P)^2 Y\right] \tag{31}$$

thus, from the combination of Eq. 30 and 31, it follows that

$$Y = -\frac{\alpha L}{2\rho c^2} \tag{32}$$

Introducing the relation for the oscillation frequency of the first acoustic longitudinal mode of the cavity

$$f = \frac{c}{2L} \tag{33}$$

[4] $(\Delta P)_s$ in Eq. 30 is the same as ΔP in Eq. 31 because the propellant is located at the pressure antinode.

Eq. 32 may be written

$$Y = -\frac{\alpha}{4c\rho f} \tag{34}$$

this being the same result obtained by a different method in Ref. 7. Alternatively, if the isentropic acoustic relationship is used, namely,

$$c^2 = \frac{\gamma P}{\rho} \tag{35}$$

Eq. 34 becomes

$$Y = -\frac{c\alpha}{4\gamma P f} \tag{36}$$

which clearly shows the dependence of Y upon α and the operating variables of pressure and frequency. Using for the admittance function the corrected expression to account for the effect of mean flow in the T-burner, Eq. 25, it follows, together with Eq. 17 and 34, that

$$\alpha = 4c\rho_s \frac{r}{P} f \left(\frac{\mu}{\epsilon} - \frac{\sigma}{\epsilon} + \frac{1}{\gamma}\right) \tag{37}$$

As the value of α and that of $4c\rho_s$, r/P, and f are known or determined independently, it has become customary to express the results in terms of μ/ϵ. When rearranged, the equation for μ/ϵ at high frequencies takes the form

$$\frac{\mu}{\epsilon} = \left(\frac{P}{4c_s r}\right)\left(\frac{\alpha}{f}\right) \tag{38}$$

It is seen from Eq. 38 that the response function equation involves one factor (α/f), which is descriptive of the oscillatory behavior, and a second factor $(P/c\rho_s r)$, which is descriptive of the steady state combustion of the propellant. T-burner records provide the values of α (as $\alpha_1 + \alpha_2$) and other necessary data (except, of course, ρ_s) from which the value of μ/ϵ is readily calculated. The conditions for α_1 equal to zero that define the neutral boundary are determined by interpolation between the last unstable and first stable tests in a series.

At low frequencies, Eq. 38 would give erroneously high values of μ/ϵ, partly because the average speed of sound in the burner cavity, through thermal losses, becomes smaller than the speed of sound at the

combustion zone and partly because of the assumption that

$$\frac{\sigma}{\varepsilon} - \frac{1}{\gamma} = 0$$

The correction for velocity of sound amounts to $(c/c')^2$, where c represents the average speed of sound in the cavity and c' the speed of sound at the combustion zone. Correction for the heat loss effect is discussed in Ref. 8, but was not used in the present work. At high frequency, when the thermal losses are generally small, both speeds of sound can be assumed to be the same in good approximation.

From Eq. 37 it can be seen that low values of c, r, and μ/ε and high values of P are conducive to stability (making due allowance for interdependence among these variables).

T-BURNER APPARATUS

Burner Assembly

The combustion chamber consists of two equal lengths of steel pipe having an inside diameter of 1 1/2 inches and an outside diameter of 2 1/2 inches, attached to a central nozzle block. The 1/4-inch-thick propellant specimens are mounted flush at both section ends and are bonded to the metal wall with epoxy resin; steel caps close the section ends. The combustion chamber is rigidly connected to a surge tank by a straight, 5-inch-long nozzle neck having an inside diameter of 5/8 inch and an outside diameter of 1 1/2 inches. The two surge tank containers have a total volume of about 6.5 ft^3 or 11,200 in^3. Figure 2 shows a schematic layout of the burner unit and instrumentation. In the present work, propellants were tested over a frequency range from 500 to 10,000 cps and at pressures to 2,400 psig in convenient pressure and frequency steps. The frequency of the pressure oscillations at the first longitudinal mode of the cavity was changed by changing the length of the burner; the mean pressure was varied through initial pressurization of the burner and surge tank assembly.

To help in the selection of frequencies, 15 burner settings were standardized as shown in Table 1. The burner gas column lengths L are given for halfway through burning and include the central nozzle block (3/4 inch), the pipe sections, and the connectors between sections (1/4 inch), when required. The nominal frequencies f_N were calculated on the basis of an average speed of sound decreasing with frequency. The burner volume, excluding the neck, is denoted by V_B. In each test about 1/20 pound of machined propellant was used (two disks 1 1/2 inches in diameter and 1/4 inch thick); the approximate gas evolution from this amount of propellant at 2,000°K is about $V = (130{,}000/P)$ in^3, where P is in psig.

In the extended coverage series, each propellant was tested at three reference pressure levels: (1) 200, 400, and 800 psig, or (2) 200, 800, and 1,600 psig, depending upon the unstable pressure range exhibited by the propellant in the present T-burner. Eleven of the 15 standardized frequencies were chosen as reference frequencies for each pressure level. In addition, selected tests were conducted to delimit the upper reaches of the neutral boundary, including the upper pressure and frequency conditions.

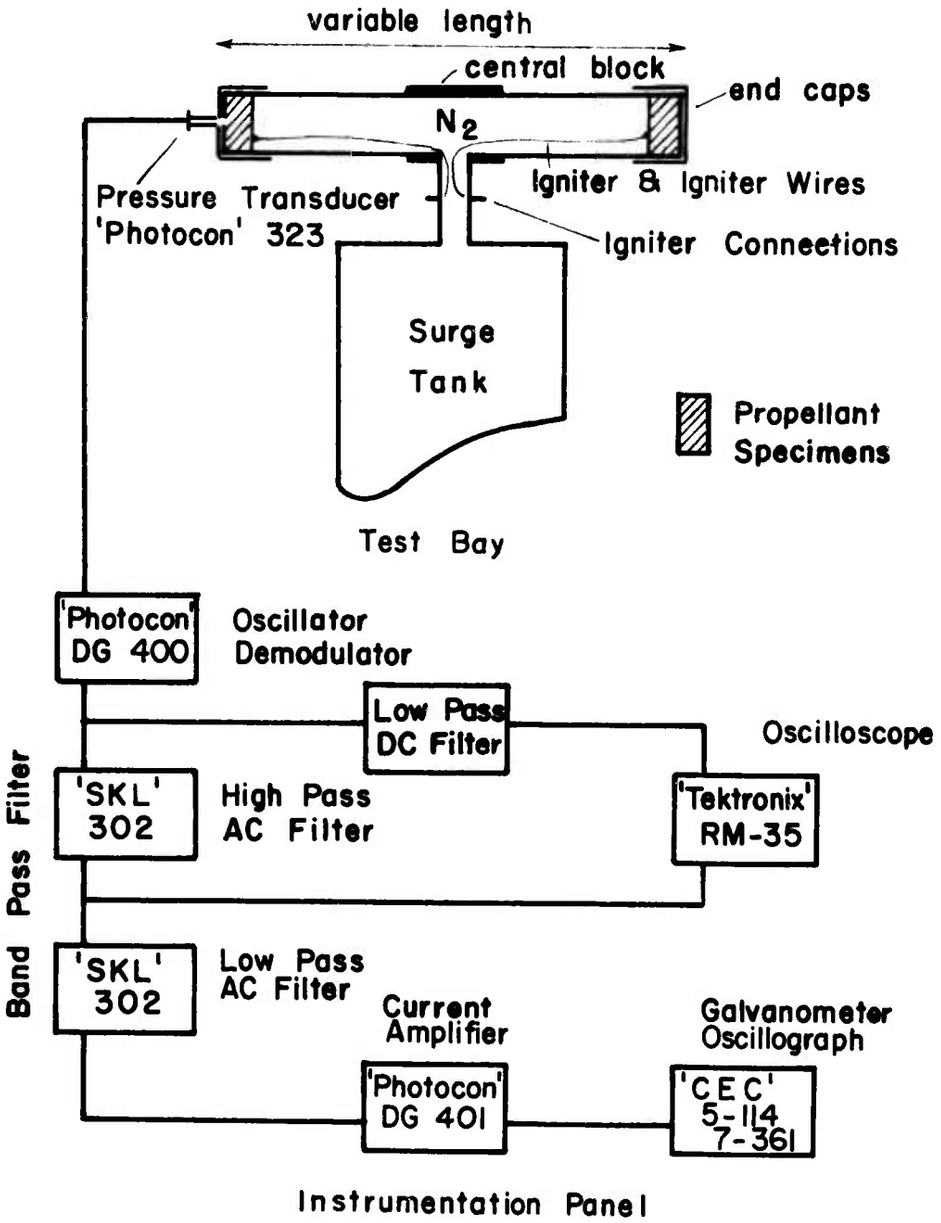

FIG. 2. T-Burner Apparatus Layout.

TABLE 1. Burner Settings and Nominal Frequencies

Setting No.	Section Lengths in.				L in.	1/2 L $in.^{-1}$	f_n cps	c in/sec	V_B in^3
1		3/4	3/4		2.0	0.250	10,000	40,000	3.5
2		1.0	1.0		2.5	0.200	7,900	39,500	4.4
3		1.5	1.5		3.5	0.143	5,590	39,000	6.2
4		2.0	2.0		4.5	0.111	4,280	38,500	7.9
5		2.5	2.5		5.5	0.0909	3,450	38,000	9.7
6		3.0	3.0		6.5	0.0769	2,880	37,500	11.5
7		3.5	3.5		7.5	0.0667	2,460	37,000	13.2
8		4.0	4.0		8.5	0.0588	2,150	36,500	15.0
9		4.5	4.5		9.5	0.0526	1,890	36,000	16.8
10		6.0	6.0		12.5	0.0400	1,400	35,000	22.0
11	2.5			2.5	16.0	0.0312	1,080	34,500	28.2
12	3.5	6.0	6.0	3.5	20.0	0.0250	840	33,500	35.3
13	2.5	10	9.0	3.5	26.0	0.0192	620	32,500	45.9
14	3.0	14	11	6.0	35.0	0.0143	450	31,500	62.0
15	3.0	20	17	6.0	47.0	0.0106	320	30,000	83.0

Instrumentation

The pressure oscillations in the burner cavity are sensed by a water-cooled pressure transducer in contact with the back face of one of the propellant specimens. The transducer is located 1/6 diameter off center, and, provided that the thickness of the propellant disk is kept to about 1/4 inch, there is no apparent reduction in signal strength or quality. The signal is received by an oscillator-demodulator and split into two channels. One channel passes through a low-pass DC filter and is displayed on an oscilloscope, and the other channel is taken by a high-pass AC filter and again split into two channels. One channel is then displayed as an AC trace on the same oscilloscope and the other is directed to a low-pass AC filter. The resulting signal is finally amplified and recorded on photographic chart paper by means of a galvanometer oscillograph. The oscilloscope displays are then recorded on Polaroid film. The high- and low-pass AC filters ensure that the signal registered by the galvanometer oscillograph contains only the first longitudinal mode of the acoustic pressure oscillations in the burner cavity.

The oscilloscope record provides an immediate visualization of the test and simultaneously presents the mean burner pressure and the oscillation pressure. Since the higher frequencies, if present, are unfiltered at this point, the record also indicates the content of higher oscillation

modes. The mean burner pressure trace is used to calculate the burning rate of the propellant at that pressure. The oscillograph record is the main source of data acquisition and measures the actual frequency, α_1 and α_2, and the maximum peak-to-peak value of the acoustic pressure amplitude, $(\Delta P)_m$. The record provides an indication of the quality of the test, showing the effect of the igniter pulse, burning symmetry, and distortions at burnout, from which it can be decided whether or not to repeat the test.

At least three calibrations are needed to ascertain instrumentation performance: (1) static pressure calibration of the pressure transducer by means of a deadweight testing machine at various attenuations in the oscillator-demodulator unit, (2) calibration of the frequency response of the pressure transducer and AC filter units at constant voltage, and (3) calibration of the amplitude response of the pressure transducer and AC filter units at constant frequency. Calibration (1) is carried out periodically to check deterioration or malfunction of the transducer probe, and calibration (2) is made whenever the AC filter units are suspected to be faulty. The pressure transducer response is almost independent of frequency up to about 8,000 cps, but falls sharply at increasingly higher frequencies.

Test Procedure

The test procedure comprises the following steps:

1. Machining the propellant specimens to disk shape with a nominal thickness of 1/4 inch and a diameter of 1 1/2 inches
2. Fitting and bonding the disks to the terminal burner sections with epoxy resin
3. Curing the epoxy bond
4. Fixing the igniter (spreading pyrotechnic material over the surface of the propellant disk and teardrop primer of the same substance, which supports the ignition wires
5. Assembling the burner sections and end caps
6. Soldering the ignition wires inside the burner cavity to the terminal posts at the nozzle neck
7. Mounting the burner unit to the surge tank and connecting the transducer probe
8. Pressurizing the burner atmosphere with nitrogen to the desired pressure level
9. Checking on instrumentation settings and circuit continuity

10. Activating the sequencer, igniting, and recording the test data.

Data Acquisition

The data acquisition procedure is aimed at determining all the necessary terms involved in Eq. 38. The steady state terms are readily known or calculated. P is the initial pressurization level imposed on the burner, r is calculated from the oscilloscope DC pressure trace or from strand burning rate measurements, and the value of ρ_s is easily obtained.

The oscillatory terms are derived from the oscillograph record. The actual frequency of the pressure oscillations is read after it has attained a constant value during the growth of the oscillations, and c is determined as the average slope in the plot of f versus 1/2 L, L being the length of the burner gas column halfway through burning (see Table 1). Most of the data-reduction work goes into determining the growth and decay constants of the pressure oscillations. A standard numerical procedure renders the average value of α_1; the value of f corresponds to this stage in the test, and in most cases it remains substantially the same until the moment of burnout. The calculation of α_2 is not so straightforward and implies a certain degree of arbitrariness. The conditions at burnout are such, mainly through thermal losses, that the decay constant of the pressure oscillations usually undergoes a noticeable change from beginning to end of the decay period; the tendency is toward smaller values (although sometimes the opposite is true at high frequencies) and toward lower corresponding frequencies as the decay proceeds in time. Consequently, each decay event is represented by two constant and frequency combinations, one denoted by (α_2', f_2'), reflecting the beginning, and the other by (α_2'', f_2''), reflecting the end of the decay period. The maximum peak-to-peak value of the amplitude of the acoustic pressure oscillations $(\Delta P)_m$, is calculated from the records with the help of the calibrations mentioned above.

The determination of the final value of α comprises a sequence of plotting steps intended to smooth the raw test data. The following steps have been adopted: (1) plots of α_1 versus f and α_2 versus f_2, whereby each test is represented by a line extending from (α_2', f_2') to (α_2'', f_2'') in the latter plot, (2) graphical averaging of the data by a best fit curve, (3) tabulation of the α_1 and α_2 values for the reference frequencies 500, 1,000, 2,000 cps, etc., (4) replots of these data as α_1/f versus f and α_2/f versus f and further graphical averaging if necessary. The values of α are given by the final α_1 and α_2 values, and the processed data are collected in tabular form as presented under "Experimental Results." The value of the limiting frequencies for $\alpha_1 = 0$ (neutral boundary frequencies) are also determined graphically from the α_1 versus f plots for each pressure.

Attempts were made to obtain directly the logarithmic recordings of the growth and decay of the pressure oscillations by incorporating a Tektronix (Type 0) logarithmic converter amplifier into the instrumentation. Had this approach been successful, the very time-consuming numerical procedure for determining α_1 and α_2 would have been greatly reduced.

Accuracy of Results

There is a multitude of possible sources of error that can adversely affect the quality of the results. They fall into three major categories: (1) the nature of the technique under which the T-burner system operates, (2) the measuring equipment which senses and records the primary data, and (3) the method of data acquisition.

The error contributions by the technique concern

1. Propellant manufacture, whereby batch-to-batch variations in composition or quality tend to impair test repeatability, especially as marginally unstable conditions are approached near the neutral boundary

2. Burner atmosphere, initially composed of almost pure nitrogen, but becoming richer in combustion products as the propellant burns, with the result that the growth and decay of the pressure oscillations must occur in an environment of changing temperature and composition, which weakens the hypothesis of constance of attenuation, especially for propellants that give off a considerable amount of particulate matter

3. Igniter pulse, produced by the rapid burning of the pyrotechnic material, which can distort the growth profile of the pressure oscillations, and also the presence of the ignition wires and their combustion products inside the burner cavity, since their effect as acoustic attenuators cannot be ruled out

4. Nonsimultaneous or nonuniform burning of the propellant specimens caused by different ignition delays or failure of the propellant-to-metal-wall bonding

5. Variations in operating conditions, such as initial propellant temperature or mean burner pressure, when the initial level of pressurization cannot be maintained in the surge tank.

In general, these sources of error become more critical as low frequencies are approached. This is particularly true of (1) the burner atmosphere (because of the increasing larger burner volume as the frequency is reduced, which gives rise to attempts to arrest the growth of the pressure oscillations (hold-off grains, movable acoustic attenuators) until sometime later during burning) and (2) the igniter pulse (because

it tends to persist longer at low frequencies because of small cavity attenuation and because of the long length of ignition wire present in the cavity at low frequencies, much of which remains unconsumed). These combined effects have limited extention of routine testing below about 500 cps, which is considered to be the lowest practical limit of the present T-burner. Uncertainties caused by propellant composition or quality are usually small; as for the unsymmetry in the burning of the propellant specimens, which can happen at any frequency, record distortion is normally great enough for it to pass undetected.

Instrumentation malfunctions can cause errors in oscilloscope and galvanometer oscillograph records. The three components most liable to malfunction are the pressure transducer probe, the oscillator-demodulator, and the AC filters. The pressure transducer can be recalibrated periodically or whenever visual inspection shows a sudden deterioration of the sensing head. Marginal malfunctions of the demodulator-oscillator and AC filters can go undetected for several tests until the warning symptoms become severe. The appearance of minor spurious features in the records is not uncommon and usually can be disregarded unless they become repetitive.

The data reduction procedure, though simple in itself, depends on the operator's judgment, particularly for poorly defined records. In general, the array of uncertainties is such that no estimation of absolute errors is possible; the only way to assure accurate results is by checking repeatability and by adopting a fixed procedure for testing, data acquisition, and data reduction. Scattering of test data points indicates that the final and response function values have an uncertainty no better than $\pm 10\%$ when α_1 and α_2 are both above 10 sec^{-1} and provided α_1 is not much smaller than α_2. This is generally the case for conditions of medium to severe instability in the high-frequency region. At low frequencies, when α_1 and α_2 might fall well below 10 sec^{-1}, or near the high-frequency side of the neutral boundary, when α approaches α_2, the uncertainty increases to $\pm 15\%$ or higher.

PROPELLANTS

Selection of Propellants

Most of the propellants tested belong to an "A" series of research composite propellants formulated to encompass a wide number of compositional variations; others are commercial propellants, including four typical double-base propellants developed years ago. Among the 38 propellants studied, extended testing was confined to nine composite formulations (A-13, A-14, A-15, A-16, A-17, A-18, A-19, A-81, and T-35) and four double-base formulations (N-4, N-5, JPN, and X-14). This selection was made in order to characterize some of the major compositional and burning rate effects on instability, such as (1) differences of behavior between composite and double-base propellants, (2) influence of the linear, mesa, and plateau burning rate modalities for the double-base propellants, (3) effect of ammonium perchlorate particle size and combustion catalysts, and (4) effect of binder, oxidizer types, and aluminum for the composite propellants. Of the remaining propellants, only partial evaluation is available for 16 (A-1, A-2, A-5, A-7, A-10, A-11, A-12, A-20, A-22, A-23, A-24, A-25, A-26, A-27, A-28, and A-44), and five propellants (A-52, A-83, A-91, A-138, and A-139) did not exhibit instability within the frequency covered by the present T-burner.

Propellant Procurement

The A-series propellants are manufactured by the Development Engineering Branch, Propulsion Development Department, at NWC, using routine mixing and curing procedures. Of the three binders used, PBAN, PU, and PS, good quality is observed for the propellants containing PBAN, only marginal quality for those containing PU, and attempts to produce PS formulations resulted in propellants of unacceptable quality. Some quality alteration has been noticed for the PU binder propellants in that aging at room temperature seems to bring about a tendency toward stability.

Each batch yielded approximately 7 pounds of propellant or about 4 pounds of machined propellant specimens, providing material for 80 tests, a number ample enough to evaluate some of the less unstable propellants.

Propellant Composition and Burning Rate

Composite compositions are shown in Table 2, and double-base compositions are shown in Table 3. The burning rates are shown graphically in Fig. 3 and 4 for the composite and in Fig. 5 for the double-base propellants. The composite propellants and the N-4 and JPN double-base propellants exhibited essentially linear burning rates in the usual logarithmic plot of r versus P; the N-5 propellant exhibited mesa, and the X-14 plateau burning characteristics. It should be noted that the PBAN binder ingredient in the A propellants has been mistakenly reported in the past as being PBAA. The A-28 propellant was not formed by casting but through pressing the mixture at 40,000 lb/in^2.

The 85μ AP was a commercial grade designated Lot 90-3 and 90-4 by the American Potash and Chemical Corporation, and the 15μ AP was standard American Potash and Chemical Corporation 15μ grade. Ammonium perchlorate designated by BM in the tables and figures was a 50-50 mixture of micropulverized (approximately 9μ) and as-received (approximately 150μ) material.

TABLE 2. COMPOSITE PROPELLANTS

Ser. No.	Binder		Aluminum		Oxidizer			Catalyst		Ps	r, in/sec at P, psia				Burn Rate Eq.
	Type	%wt.	Size, μ	%wt.	Type	Size, μ	%wt.	Type	%wt.	lb/in^3	215	415	815	1615	r=CP^{n}in/secs,
A-12	PBAN	20	...	...	AP	BM	80	...	...	.063	.21	...	...	...	...
A-1	PBAN	18	...	...	AP	BM	80	cc	2	.063	.34	.47	...	...	...
A-24	PBAN	19.5	...	...	AP	BM	80	cc	.5	.059	.28	...	...	...	$32.6 \times 10^{-3}\ P^{.40}$
A-22	PS	20	...	...	AP	BM	80	...	...	.063	.29	...	...	...	...
A-25	PU	20	...	...	AP	BM	80	...	...	.060	.19	...	...	...	...
A-28	PBAN	10	...	...	AP	80	90	...	...	.061	.24	...	...	...	...
A-27	PBAN	15	...	...	AP	80	85	...	...	.060	.28	...	...	...	...
A-26	PBAN	23.5	...	...	AP	80	76	CB	.5	.057	.16	...	...	...	...
A-44	PS	25	...	...	AP	80	75	...	...	.062	.32	...	...	...	...
A-23	PBAN	23.7	...	...	AP	15	76	cc	.3	.057	.44	...	...	...	...
A-10	PBAN	17.6	.02	.4	AP	BM	80	cc	2	.063	.34	...	...	...	...
A-5	PBAN	17.5	5	.5	AP	BM	80	cc	2	.063	.34	...	...	...	...
A-2	PBAN	17	5	1	AP	BM	80	cc	2	.063	.34	.45	...	...	...
A-7	PBAN	17	20	1	AP	BM	80	cc	2	.063	.34	...	...	...	...
A-11	PBAN	17	2	I(Al_2O_3)	AP	BM	80	cc	2	.063	.34	...	...	...	...
A-20	PBAN	23	20	1	AP	15	76	...	...	.057	.33	...	...	...	...
A-13	PBAN	24	...	...	AP	80	76	...	...	.057	.16	.21	.28	...	$16.8 \times 10^{-3}\ P^{.42}$
A-15	PBAN	23	...	...	AP	80	76	cc	1	.057	.26	.35	.47	...	$24.6 \times 10^{-3}\ P^{.44}$
A-17	PBAN	23	...	...	AP	80	76	LF	1	.057	.12	.16	.22	...	$10.7 \times 10^{-3}\ P^{.45}$
A-81	PBAN	23	...	...	AP	80	75	cc LF	1 1	.057	.25	.34	.45	...	$23.7 \times 10^{-3}\ P^{.44}$
A-14	PBAN	24	...	...	AP	15	76	...	...	.057	.26	...	.42	.53	$37.5 \times 10^{-3}\ P^{.36}$
A-16	PBAN	23	...	...	AP	15	76	cc	1	.057	.51	.64	.82	...	$73.2 \times 10^{-3}\ P^{.36}$
A-18	PBAN	23	...	...	AP	15	76	LF	1	.057	.22	...	.35	.45	$29.8 \times 10^{-3}\ P^{.37}$
A-19	PBAN	24	...	...	AP	80 15	38 38	...	...	.057	.21	...	.34	.44	$27.0 \times 10^{-3}\ P^{.38}$
T-35	PS	26	...	...	AP	15	71	MgO FeO	1 2	.062	.44	.56	.72	...	$60.0 \times 10^{-3}\ P^{.37}$
A-35	PU	25	...	...	AP	80	75	...	...	.060	.17	.23	.31	...	$15.3 \times 10^{-3}\ P^{.45}$
A-83	PU	25	5	4	AP	80	71	...	...	...	...	...	...	...	...
A-91	PU	25	5	8	AP	80	67	...	...	...	...	...	...	...	...
A-52	PU	25	5	16	AP	80	59	...	...	...	...	...	...	...	...
A-139	PU	25	5	8	AP	15	67	...	...	.058	.18	...	...	...	...
A-138	PBAN	24	...	...	KP	46	76	...	...	.068	.25	...	...	...	$3.42 \times 10^{-3}\ P^{.80}$

Binder: % wt. includes curing agents; PBAN = polybutylacrylonitrile acrylic acid, PS = polysulphide, PU = polyurethane. Oxidizer: AP = ammonium perchlorate, KP = potassium perchlorate, BM = bimodal distribution containing micropulverized and "as received" material in equal parts. Catalysts: cc = copper chromite, LF = lithium fluoride, CB = carbon black.

TABLE 3(a). Double-Base Propellants

	JPN	N-4	N-5	X-14
Nitrocellulose	51.40	51.0	50.0	
Nitroglycerin	42.90	34.3	34.9	
Diethl phthalate	3.23	10.6	10.5	
Ethyl centralite	1.00	--	--	
Carbon black	0.20	0.1	--	
Potassium sulfate	1.25	1.5	--	
Candelilla wax	0.02	--	0.2	
2-Nitrodiphenylanime	--	2.0	2.0	
Lead stearate	--	0.5	--	
Lead salicylate	--	--	1.2	
Lead 2-ethylhexoate	--	--	1.2	
	100.0%	100.0%	100.0%	

TABLE 3(b). Burning Characteristics

	JPN	N-4	N-5	X-14
ρ_s, lb/in^3	.059	.056	.056	.058
r, in/sec at P, psia				
215	.22	.17	.16	.51
415	--	--	--	--
815	.55	.34	.44	.93
1615	.89	.48	.41	1.08
Burn rate equation $r = CP^n$, in/sec	$5.4X10^{-3}P^{.69}$	$11.0X10^{-3}P^{.51}$	Mesa	Plateau

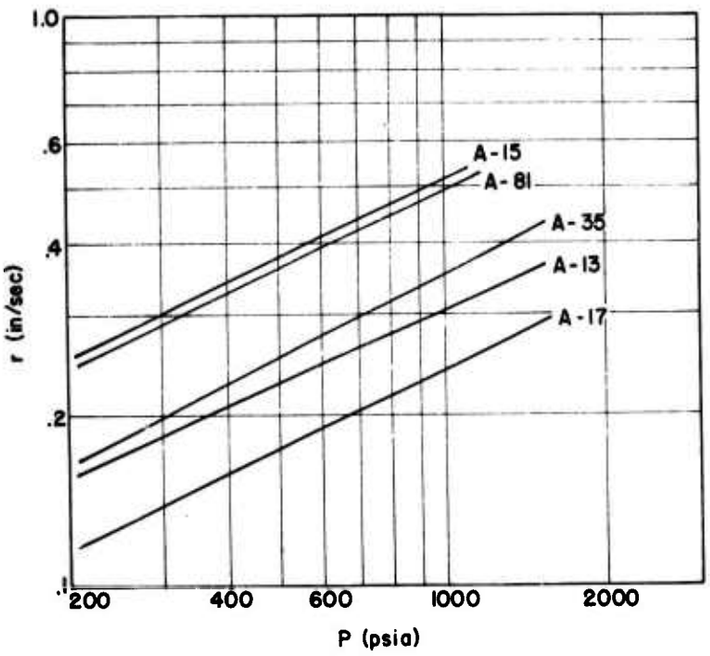

FIG. 3. Burning Rate of Composite Propellants (80°F).

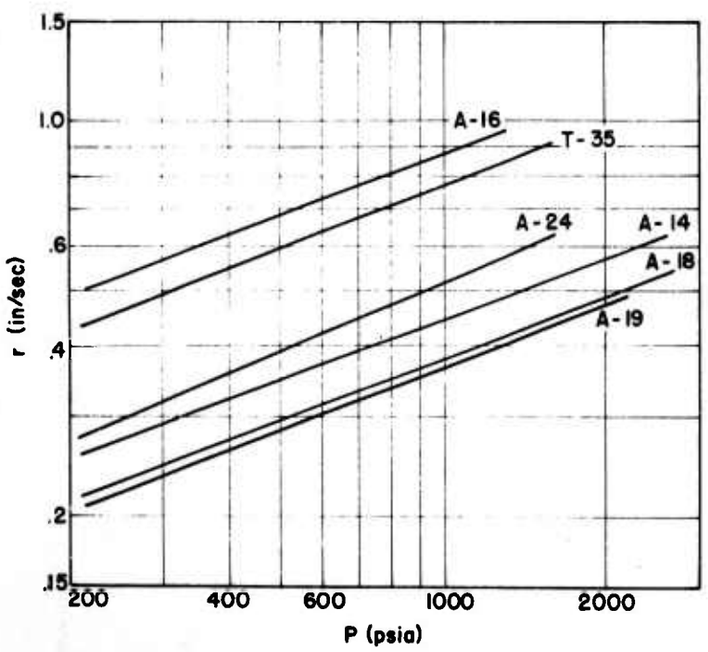

FIG. 4. Burning Rate of Composite Propellants (80°F).

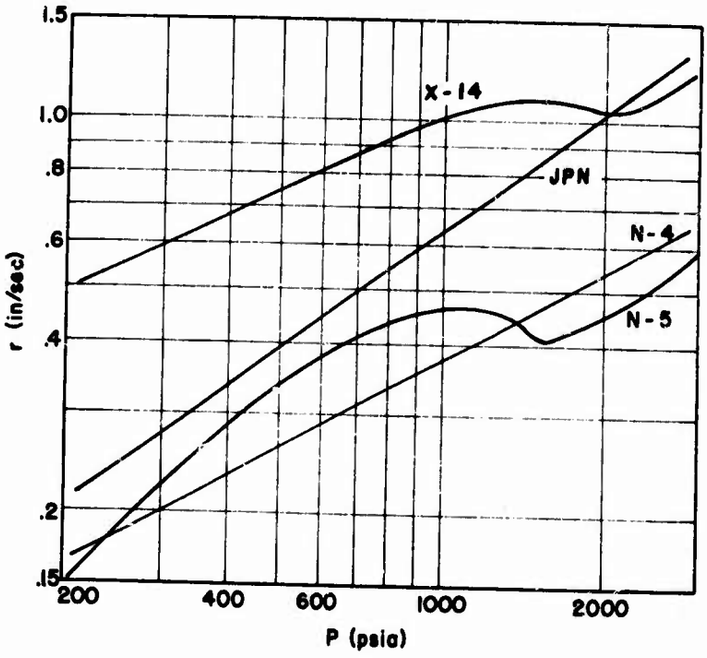

FIG. 5. Burning Rate of Double-Base Propellants ($80^{\circ}F$).

EXPERIMENTAL RESULTS

General Form of Behavior

When a T-burner is fired under unstable conditions, oscillations develop shortly after ignition, grow exponentially, level off at some steady amplitude, and decay more or less exponentially after burnout. Most unmetallized propellants produce unstable behavior under some conditions of pressure and frequency, and determinations can thus be made of the combustion α or response function (real part) μ/ε. Tests are fired at a specific mean pressure with burners of several lengths, and the series is repeated for other mean pressures as needed. From such tests, a graph of response function versus frequency is developed, with curves for various mean pressures (Fig. 6). In an extensive series of tests, the range of burner lengths (frequencies) tested will usually include length extremes for which the burner is stable. These sets of tests delineate not only the response characteristics of the propellant, but also the stability limits of the propellant-combustor combination. These combined properties may be summarized in a diagram such as Fig. 7, which is a contour map of the response function in the pressure-frequency plane. The outer boundaries are the stability limit for the type of burner used, and iso-response contours obtained by cross plotting in the μ/t versus f diagram represent the perturbation combustion characteristics of the propellant. The contour map shows in this case a maximum response function at point P*f*. The two curves through that point are the locus of frequencies for maximum μ/ε as a function of mean pressure, and locus of pressures for maximum μ/ε as a function of frequency (e.g., the f_f curve in Fig. 7 is a plot of the maximum μ/ε points of the curves in Fig. 6). Ideally, one would like to have a three-dimensional plot of these functions for each propellant of interest, but cost considerations will usually limit propellant characterization to determination of the high μ/ε portions of curves like those in Fig. 6

Response Function

The response function values have been calculated from Eq. 39, i.e.,

$$\mu/\varepsilon = \left(\frac{p}{4c\rho_s r}\right)\left(\frac{\alpha_1 + \alpha_2}{f}\right) \tag{39}$$

and α being equal to $\alpha_1 + \alpha_2$, an abbreviation for each pressure level can be written as

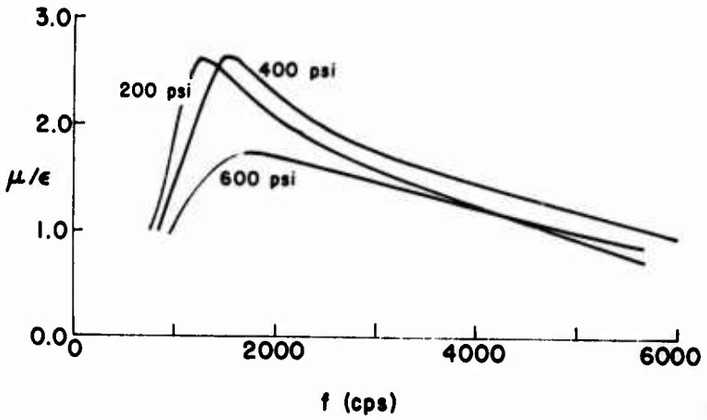

FIG. 6. Variation of Response Function With Frequency for Several Pressures--Typical Trends.

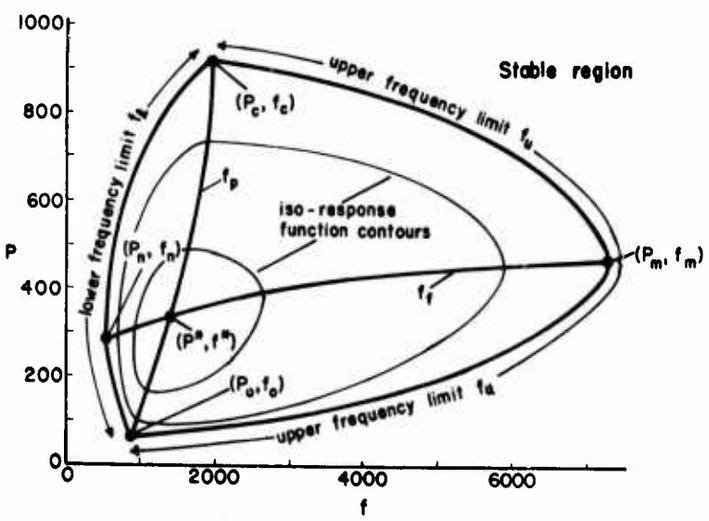

FIG. 7. Instability Behavior Characterized by μ/ε Contour Map and Stability Limit in the P-f Plane.

$$\mu/\varepsilon = Kr\ \left(\frac{\alpha}{f}\right) \tag{40}$$

where Kr is the shortened form of $P/4c\rho_s r$ and is dimensionless.

The response function results are separated into two groups according to the pressure coverage.

Group I comprises the results obtained testing propellants under limited pressure coverage, mainly at 200 psig only; these results are to a great extent recalculations from data already published in Ref. 9 and 10, together with additional data obtained to check previous results or to complete missing information. These results, which contain only response function determinations (since no other information can be reliably derived from scant pressure coverages) are presented collectively in Appendix A along with response function diagrams. The results for the A-44 propellant are suspect because of the poor quality of this propellant.

Group II includes the results obtained testing propellants under extensive pressure coverage; previous data on some of these propellants, Ref. 9 and 11, were entirely retested. These results include determination of combustor stability limits as well as response function. The neutral boundary limits, the pressure and frequency peak lines, and the vertex point are illustrated in the P-f diagrams, also in Appendix B, along with response function diagrams for the three corresponding reference pressures. The conditions yielding maximum response function were calculated by a method described in Appendix C, and are shown in Table 4 for those propellants that were tested extensively.

TABLE 4. Vertex Points (Maximum Response Function)

Propellant Serial No.	f* cps	P* psia	r* in/sec	Propellant Serial No.	f* cps	P* psia	r* in/sec
A-13	1200	320	.19	A-19	1700	500	.28
A-14	2900	640	.39	T-35	1600	370	.54
A-15	1900	250	.28	N-4	1400	500	.25
A-16	4200	300	.58	N-5	1200	460	.32
A-17	820	310	.14	JPN	800	300	.28
A-18	2500	700	.33	X-14	1700	400	.67

Stability Limits

For those propellants that were most extensively tested, a rough estimate of the stability limit of the combustor can be determined. This is illustrated in Fig. 8 for a hypothetical example, where the value of α_1 is plotted as a function of frequency for a particular mean pressure. When the curve is extrapolated to $\alpha_1 = 0$, the stability limit is given by the corresponding values of pressure and frequency.

In principle, a sufficient number of $\alpha_1 = 0$ points $(p, f)_{\alpha=0}$ can be obtained in this way to plot a stability limit profile like that in Fig. 7. Unfortunately, the scatter of measurements becomes very bad as the stability limits are approached, so that determination of the limits is accomplished with only marginal accuracy.

In order to achieve a more systematic correlation of the rather limited data on stability limits, a computational scheme was developed for constructing stability boundaries from the limit points. This scheme, discussed in Appendix C, fits the limit points with segments of two curves, one bounding the high frequency side of the unstable region, the other bounding the low frequency side. These segments can each be fitted when three limit points are available, and can then be described in terms of limiting high and low values of pressure and frequency for the unstable region. Table 5 lists these values, estimated for those propellants having sufficient data for computations. The meaning of the notation is clarified in Fig. 7. Table 4 listed the vertex points (P*,f*) for those propellants with extensive test data.

Acoustic Pressure Results

The maximum acoustic pressure levels, $(\Delta P)_m$, have been calculated for most of the propellants of the extended pressure series. These values are easily derived from the test records and corresponding calibrations. No assessment can be made of their accuracy, which, on the average, should not be regarded as very high. It has sometimes been the practice, mainly from an engineering viewpoint, to describe the degree of combustion instability in terms of the pressure ratio $(\Delta P)_m/P$, although this representation has not yet been theoretically substantiated. The $(\Delta P)_m$ pressure levels and $(\Delta P)_m/P$ pressure ratios for the propellants are listed in Appendix D. Comparison with other instability data seems to suggest a certain resemblance of trends between the α_1/f and $(\Delta P)_m/P$ ratios. Also relevant to this large amplitude aspect of combustion instability (but not explored here) is the change on propellant burning rate effected by the amplitude and frequency of the acoustic pressure oscillations sustained in the burner cavity, as the experimental observations in Ref. 12 and 13 have clearly shown.

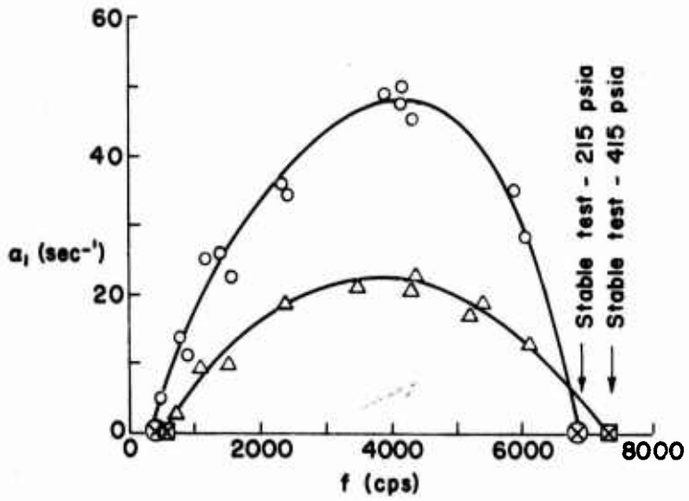

FIG. 8. Plot of α_1 Versus f and Extrapolation to Determine Stability Limits.

Effect of Additives on Attenuation

The presence of particulate material in the reaction products is known to produce a major effect on attenuation of oscillations. Figure 9 shows the trends of α_2 for several of the propellants tested on this program. A comparison of the results for a propellant with "clean" reaction products such as A-14 with the other propellants shows a conspicuous effect even for the low concentrations of condensed products resulting from 2% copper chromite or 1% aluminum.

Detailed Study of A-13 Propellant

Considering that the most adequate description of behavior is given by the P-f diagrams, showing not only the structural lines but also the isoresponse function contours at discrete intervals, further testing with the A-13 propellant was undertaken to determine some of these contours. The A-13 propellant was selected because (1) it has a simple formulation and is easy to manufacture, giving batches of consistent quality, and it does not appreciably deteriorate with time; and (2) its unstable behavior is confined to a pressure and frequency range that is attainable in the present T-burner apparatus.

The testing was extended in two directions: (1) toward low pressures to resolve the steep gradient of the isoresponse function contours

TABLE 5. Terminal Points of Neutral Boundary

Propellant serial no.	fo[b] cps	Po[a] psia	ro[b] in/sec	fr[c] cps	Pr[c] psia	rn in/sec	fm[c] cps	Pm[c] psia	rm in/sec	fc[d] cps	Pc[d] psia	rc in/sec
A-13	170	5	.025	95	270	.18	7,900	530	.23	1,600	1,100	.32
A-14	430	5	.045	245	570	.37	25,300	970	.45	3,900	2,300	.60
A-15	260	5	.035	145	210	.26	14,500	410	.35	2,400	850	.48
A-16	560	5	.075	315	260	.56	26,100	430	.66	5,000	1,000	.88
A-17	90	5	.015	53	270	.13	7,600	600	.19	1,100	1,200	.26
A-18	300	5	.035	192	620	.32	22,400	1,160	.40	3,300	2,600	.54
A-19	270	5	.035	155	420	.26	14,200	750	.33	2,500	1,700	.45
T-35	180	5	.060	105	310	.50	11,700	580	.63	1,900	1,300	.85
A-35	40	5	.020	22	240	.18	3,800	570	.27	600	1,200	.38
N-4	70	5	.012	50	420	.24	49,200	1,400	.45	2,300	2,800	.64
N-5	50	5	.010	36	430	.30	80,000	1,000	.47	1,700	2,900	.59
JPN	32	5	.010	24	250	.25	86,500	1,360	.80	2,200	2,300	1.15
X-14	70	5	.030	48	310	.60	47,500	1,200	1.07	3,400	2,500	1.12

[a] Po has been given an arbitrary value of 5 psia, as the actual pressure will be subatmospheric in most cases.

[b] fo, ro are values derived by curve fitting.

[c] fr, Pr and fm, Pm are calculated values.

[d] fc, Pc are experimentally observed values.

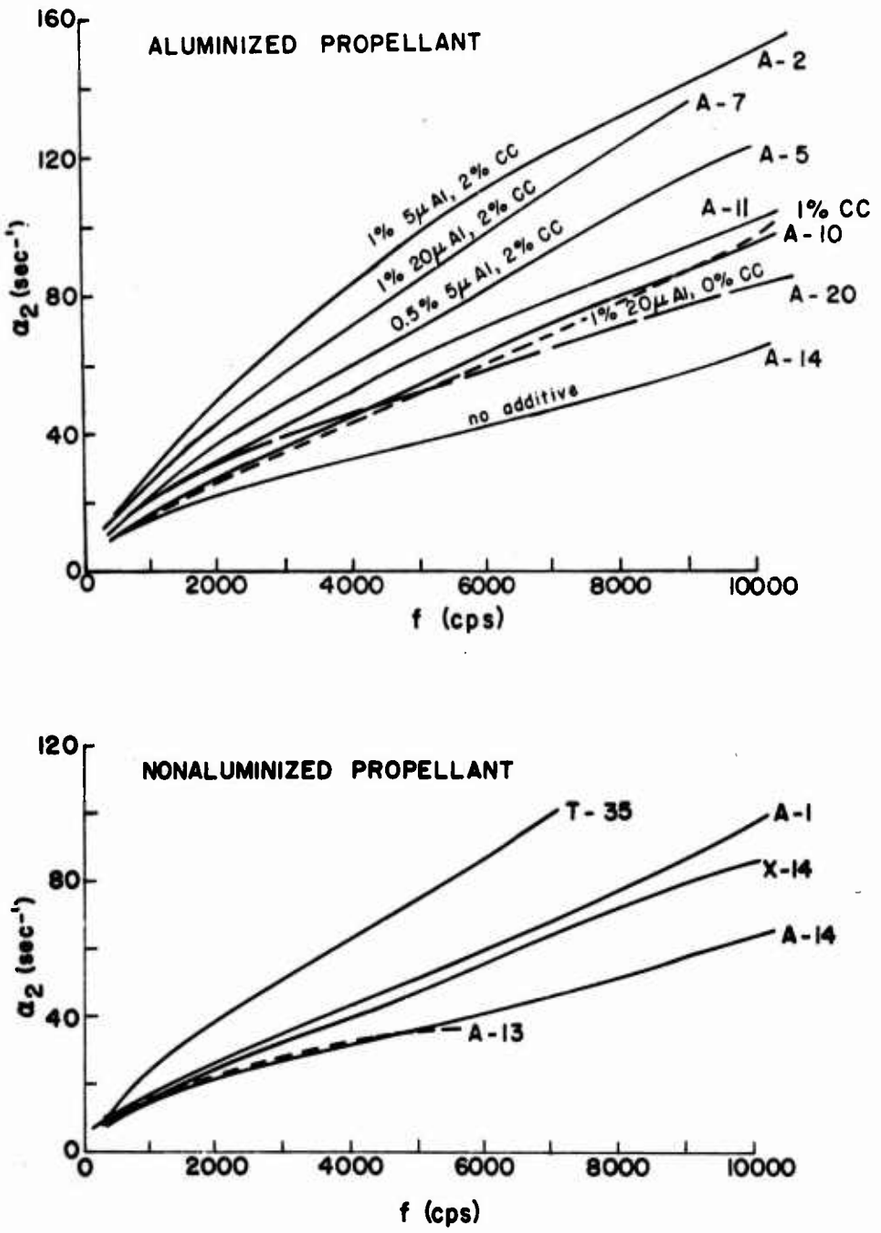

FIG. 9. Decay Constants at 215 psia for Aluminized and Nonaluminized Propellants.

as low pressure and frequencies are approached, and (2) at constant-frequency conditions to further ascertain contour location. A-13 growth and decay constants are shown as functions of frequency in Appendix E. The figures contain individual test data points, showing the scatter that is encountered. In cases where the decay assumes two values, the two points are connected with a thin straight line. The assumed variations of growth and decay constants are shown as heavier curved lines. The cross-plotting of data into p-f diagrams has produced some of the isoresponse function contours as well as the graphical representation of other parameters of interest, including α, α_1, and α_2 and their corresponding frequency ratios. The isoresponse function contours and the remaining diagrams are given in Appendix E. The specimen results gathered from the A-13 propellant illustrate additional trends that should be incorporated into the general form of behavior.

High-Speed Photography of Burning Surfaces

High-speed cinematography of propellant samples burning under steady state conditions has afforded observation of surface and gas phase events that have some qualitative relevance on instability behavior. The observations are summarized for the following propellants.

1. N-4. At 200 psig, black melt and moving dark particles (spherical, 100 to 200 microns) on surface, no flame visible; at 400 psig, larger number of dark particles smaller in size, no flame visible; at 800 psig, same trend for particles, appearance of flame about 1,000 microns from surface, well defined dark zone.

2. N-5. At 200 psig, irregular particles somewhat spectacular (about 200 microns) accumulate on surface prior to shedding, no flame visible; at 400 psig, almost same appearance as before; at 800 psig, larger number of dark, shiny particles, spherical in shape as they move through the flame, which appear about 1,500 microns above surface.

3. X-14. At 400 psig, multitude of small shiny blobs on surface, no flame visible; at 800 psig, visible flame, the particles appear spherical and incandescent as they move through the flame.

Information on composite propellants is summarized below:

1. A-13. At 200 psig, dark blobs of molten binder (150 microns) on surface, orange flame about 1,800 microns high; at 400 psig, blobs of molten binder tend to coalesce, more intense and uniform flame about 1,500 microns high; at 800 psig, blobs of molten binder increase in number and size, more vigorous and higher flame than before.

2. A-14. At 200 psig, no binder melting, weak flame; at 400 psig, no melting, stronger flame; at 800 psig, no melting, stronger flame, particles eject from surface, some ammonium perchlorate crystals appear to protrude as surface regresses.

3. A-15. Same behavior as with A-13, but more intense melting of binder, occasional green flares appear to originate from the burning binder blobs.

4. A-16. Same behavior as with A-14 but more vigorous flame and absence of ammonium perchlorate protrusion.

5. A-17. At 200 psig, less melting of binder and in smaller blobs than with A-13, deposition of soot on surface, weak flame; at 400 psig, considerable increase of molten binder in blobs of larger size, some in filament form, stronger flame; at 800 psig, same trend as before, but distinct flares appear to originate from burning binder blobs.

6. A-18. At 200 psig, similar to A-14; did not sustain burning at higher pressures.

7. A-19. At 200 psig, no binder melting; at 400 psig, incipient binder melt; at 800 psig, enhanced melting of binder and intense flame.

8. T-35. At 200 psig, slight binder melt, burning metallic particles collect on surface and later move through flame (resemblance to aluminum combustion); at 400 and 800 psig, same behavior but with fewer metal particles and increasingly stronger flame.

9. A-52, A-83, A-91, A-139. Since these are aluminized propellants, the most prominently observed feature is the combustion of the metal ingredient; aluminum combustion appears to enhance melting of the binder.

10. A-138. Surface almost covered by a bubbling mass of molten potassium perchlorate and very strong flame.

DISCUSSION

The purpose of the present investigation was to determine the effect of propellant and environmental variables on the oscillatory combustion of propellants, particularly, composite ammonium perchlorate (AP) propellants and homogeneous double-base propellants. The T-burner technique used determines the pressure-coupled response of the combustion (i.e., response to perpendicularly incident pressure waves). The response can be characterized by the normalized acoustic energy flux, $\dot{E}/E$, which is determined in the experiment from the value of α (Eq. 12). For convenience in interpretation of results, the value of $\dot{E}/E$ is represented in terms of several contributing factors by the relation (Eq. 12, 37 and 35)

$$2\alpha = \dot{E}/E = 4c^2 \frac{\rho_s}{L} \frac{r}{P} \frac{\mu}{\epsilon} = \frac{4}{\gamma} \frac{\rho_s r c^2}{\rho L c^2} \frac{\mu}{\epsilon} = \frac{4}{\gamma} \frac{\rho_s r}{\rho L} \frac{\mu}{\epsilon}$$

which pertains for the T-burner in the frequency range used here where $\sigma/\epsilon - 1/\gamma = 0$ in Eq. 37. In the above, the expression

$$\left(\frac{\rho_s c^2 r}{\rho L c^2}\right)$$

is indicative of the energy flux from the combustion zone (per unit area) available for perturbation (normalized by the energy per unit cross section in the cavity), and μ/ϵ is a measure of the susceptibility of that flow to perturbation. A propellant with high values of both $(\rho_s r/\rho)$ and μ/ϵ is very unstable. In the following, attention is directed primarily to the value of μ/ϵ, because it is the quantity most difficult to establish--but the reader should be reminded that the value of $(\rho_s r/\rho)$ is equally important.

In discussion of the response function curves, it may be assumed from current one-dimensional perturbation theories for solid propellant combustion that effects on μ/ϵ due to burning rate or related pressure effects will be minimized by normalization of the frequency scale to a form f/r^2. Such a normalization is used in the following whenever it seems to produce similarity in the frequency dependence of μ/ϵ for different propellants or pressures. In no case where data was available did this correlation eliminate the pressure dependence of μ/ϵ as predicted by theory (Ref. 14), but similarity of frequency dependence was sometimes produced (i.e., μ/ϵ curves assumed similar shapes with maxima at the same frequencies).

In addition to the stability characteristics of the propellants, there is reason for interest in the stability limits of the T-burner. In the present work, considerable emphasis was given to testing near the stability limits, and on correlation of results by analysis. Results of these studies should be of value in future development of T-burner testing and theory, but are not discussed extensively here.

Effect of Binder on Response Function

The test series included a comparison of three propellants that differed only in the type of binder. The response functions for these propellants (A12, A22, and A25) are collected in Fig. 10. The response function was roughly the same for all three binders at the low end of the frequency range tested, but differed significantly at high frequency, with polyurethane being most unstable and PBAN being most stable. Making allowances for the different values of r for these propellants (PBAN, r = 0.21 in/sec; PS, r = 0.29 in/sec; PU, r = 0.19 in/sec), stabilities are roughly equal in the high frequency range, with PS propellant being the most unstable at "low" frequency. This generalization should not, of course, be extended to all pressures or other propellant formulations without considering trends such as those discussed below.

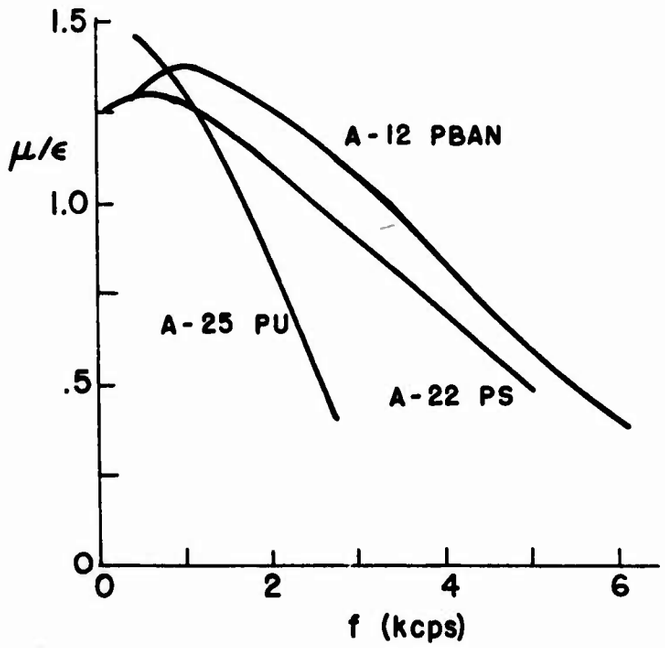

FIG. 10. Effect of Binder on Response Function (80% AP, 50-50 Mix of Micropulverized and As-Received; No Ballistic Modifier).

Effect of Equivalence Ratio

Tests were made on a family of propellants with PBAN binder and 80μ AP, with oxidizer contents of 76, 85 and 90% AP (A13, A27, A28). The response functions are shown in Fig. 11 for tests at 215 psia, along with values of burning rate. From the figure it is evident that the values of the response functions differ conspicuously, although they usually have a maximum at around 1100 cps. Under most conditions, the response function was higher for the formulations with low oxidizer content, a result possibly due to the relatively great importance of the (presumably pressure-sensitive) diffusion flame in fuel-rich formulations.

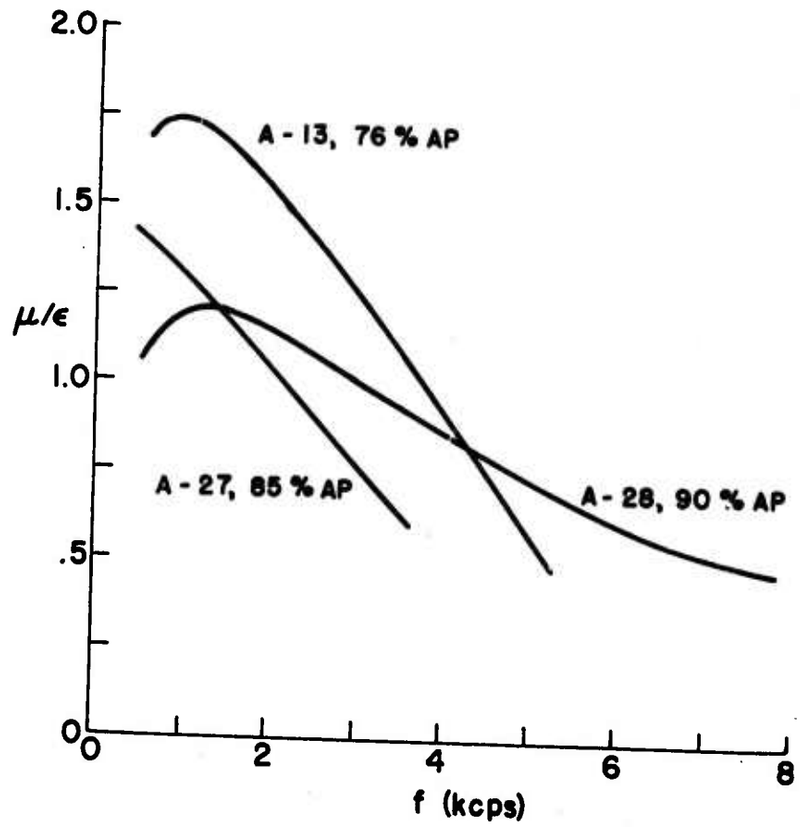

FIG. 11. Effect of Equivalence Ratio on Response Function (PBAN Binder, No Ballistic Modifier, 80μ AP).

Effect of Oxidizer Particle Size

This variable was examined using a PBAN binder, an oxidizer content of 76%, and using either lithium fluoride (LiF), copper chromite (cc), or no ballistic modifier. Results are summarized in Fig. 12(a)-(d), which differ primarily according to ballistic modifier. The formulations with no modifier (Fig. 12(a) and (b)) were tested at 215 psia and 815 psia, with 15μ, bimodal (50-50 mix of 15μ and 80μ), and 80μ particle sizes. The formulations with ballistic modifiers were tested with only 15μ and 80μ unimodal oxidizer (Fig. 12(c) and (d)). The values of μ/ε were better correlated by f/r^2 than by f, and were thus plotted in these figures as μ/ε versus f/r^2.

In all cases where the oxidizer particle size was varied, the response function and burning rate were both increased by going to finer particle size. Bimodal material behaved as though it were of particle size intermediate to its ingredient sizes (with possible exception at low pressure and high frequency (Fig. 12(a)). The pressure dependence of μ/ε was greater with coarse AP than fine AP, except for the copper chromite catalyzed formulation (Fig. 12(d)).

The enhanced response function obtained with fine oxidizer is probably due to an increase in the role of heat release steps at or near the burning surface due to high interfacial area in the propellant (Ref. 14). The higher pressure sensitivity with coarse oxidizer is probably related to the pressure dependence of the AP deflagration in the 200-800 psi range (Ref. 15), and the correspondingly important role of the diffusion flame. The absence of this particle size effect with the formulation containing copper chromite is presumably related to the as-yet-undetermined mode of catalysis by copper chromite, which not only reduces the pressure dependence of μ/ε, but also has a major depressing effect on μ/ε at all pressures. This could be through a decoupling of the gas phase reactions and the surface reactions, but the mechanism remains to be found.

Effect of Ballistic Modifiers

Tests were run on three different families of propellants involving ballistic modifiers. All used PBAN binder. One family contained 76% of 80μ AP and provides a comparison of behavior with 1% LiF, 1% copper chromite, and no modifier. A second family contained 76% of 15μ AP and again provides a comparison of behavior with 1% LiF, 1% copper chromite, and no modifier. The third family contained 80% bimodal AP (50-50 ratio of micropulverized and as-received), and compared behavior with 0, 0.5, and 2.0% copper chromite.

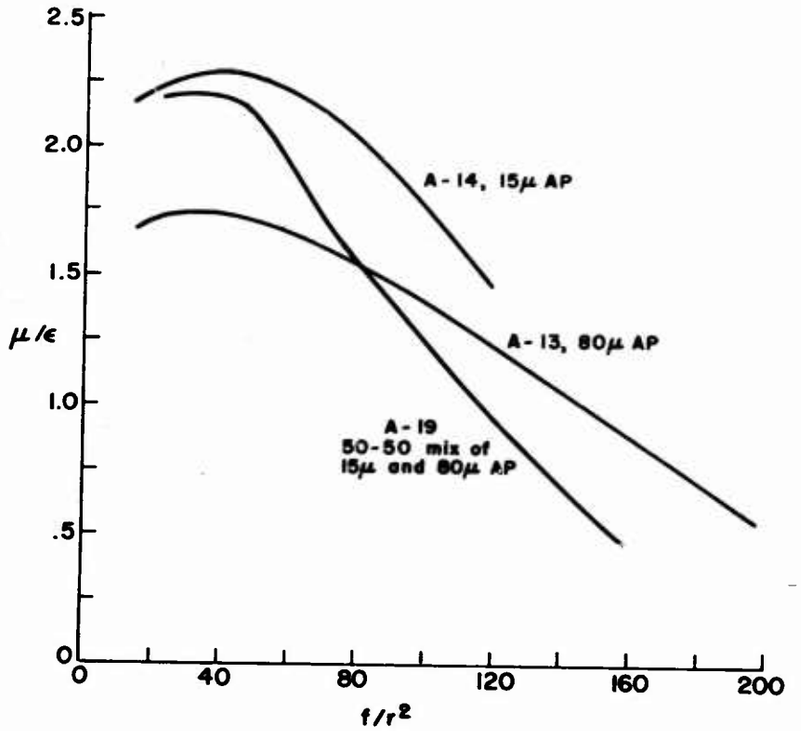

(a) No Ballistic Modifier, 215 psia.

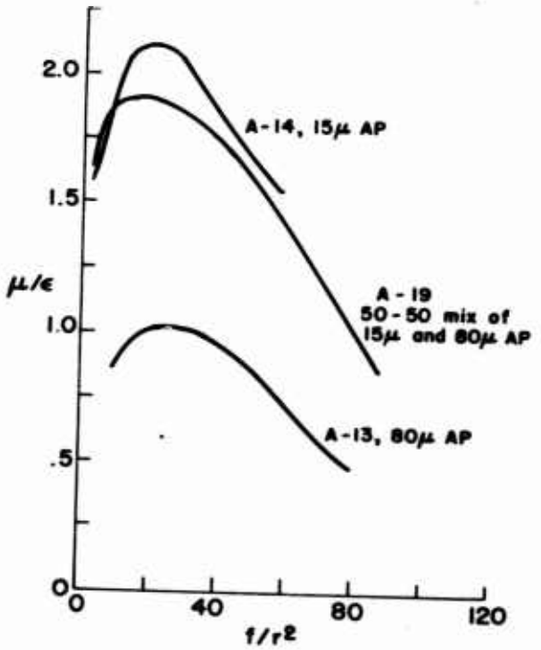

(b) No Ballistic Modifier, 815 psia.

FIG. 12. Effect of Oxidizer Particle Size on Response Function (PBAN Binder, 76% AP).

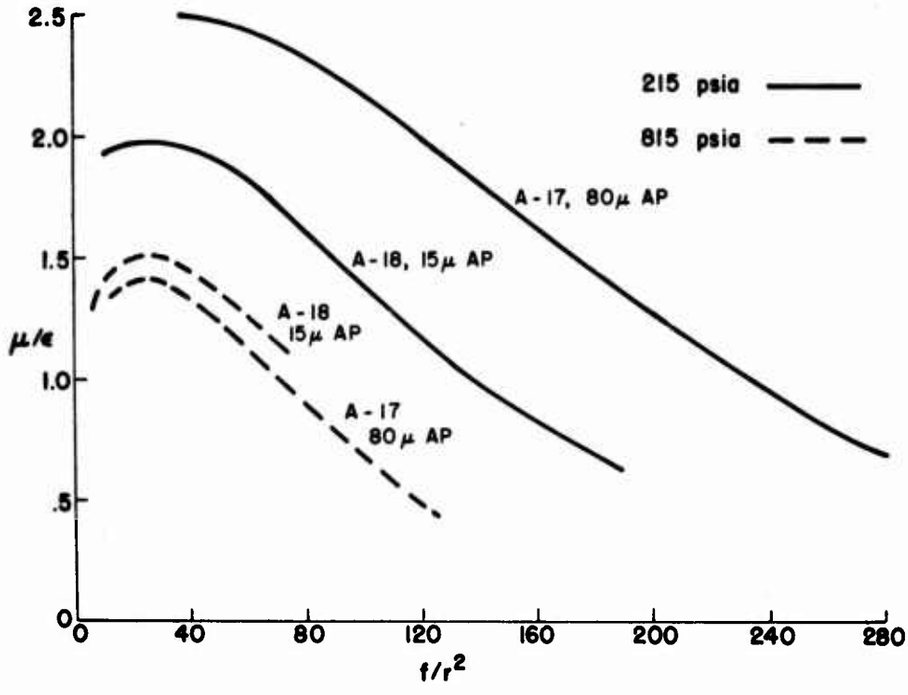

(c) 1% Lithium Fluoride.

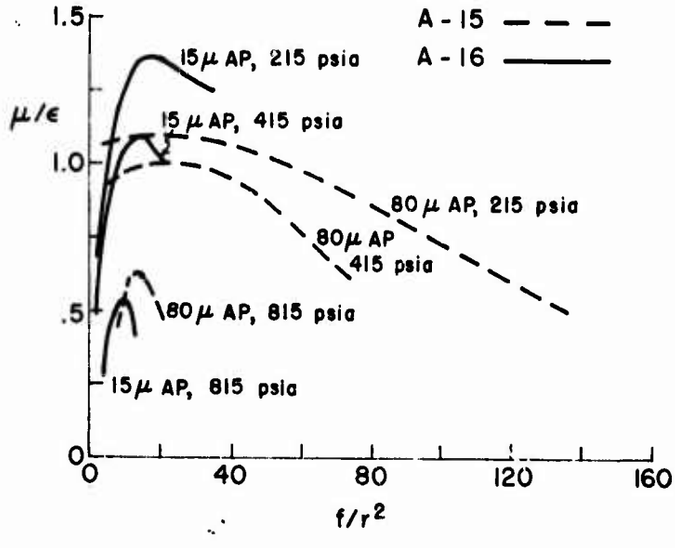

(d) 1% Copper Chromite.

FIG. 12. Effect of Oxidizer Particle Size on Response Function (PBAN Binder, 76% AP).

In the case of 80μ AP, the μ/ε values were fairly well correlated by the f/r^2 abscissa (Fig. 13(a)-(c)) and the value of μ/ε was high for low burning rate formulations (containing LiF) and low pressure, and low for high burning rate formulations (containing copper chromite) and high pressures. Since the susceptibility to unstable combustion is proportional to both burning rate and μ/ε, the net effect of the ballistic modifiers (and pressure)was generally small when compared on a "per unit area of burning surface" basis. The pressure sensitivity of μ/ε was about the same for each formulation.

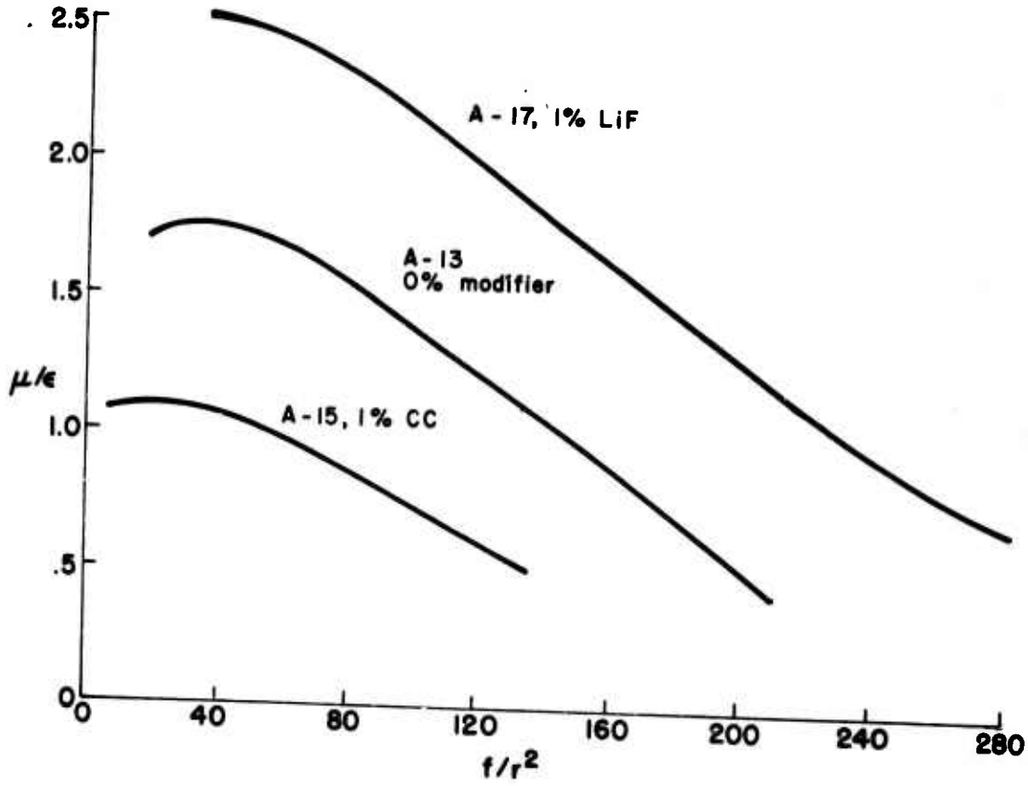

FIG. 13(a). Effect of Ballistic Modifiers on Response Function (PBAN Binder), 76% 80μ AP, 215 psia.

In the case of 15μ AP, the values of μ/ε were again well correlated on a f/r^2 scale insofar as similarity of curves is concerned (Fig. (d) and (e)). The pressure dependence was roughly proportional to the magnitude of μ/ε for the different formulations, and similar to that of the propellants with 80μ AP. As noted in an earlier section, the values of μ/ε were much higher for this family of propellants than for the corresponding family with 80μ AP. Another difference is the depressing effect of LiF on the response function (as contrasted with an enhancing effect with 80μ AP).

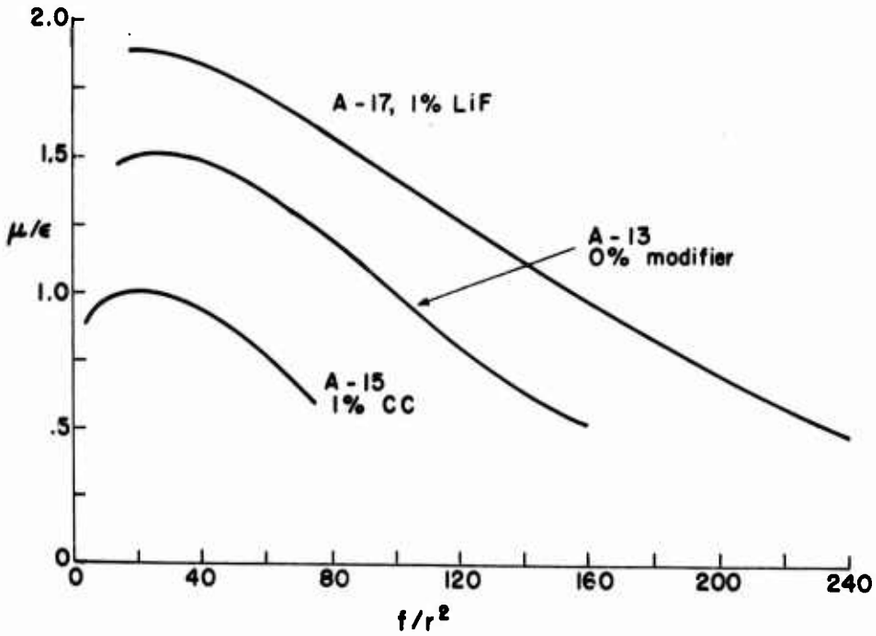

(b) 76% 80μ AP, 415 psia.

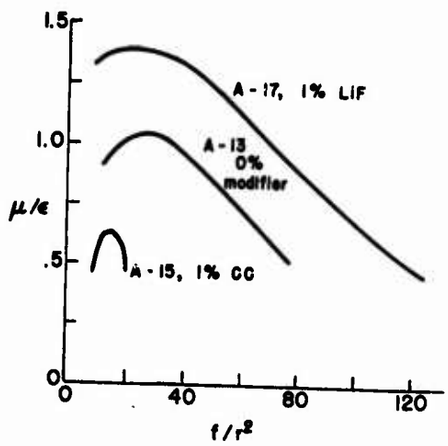

(c) 76% 80μ AP, 815 psia.

FIG. 13. Effect of Ballistic Modifiers on Response Function (PBAN Binder).

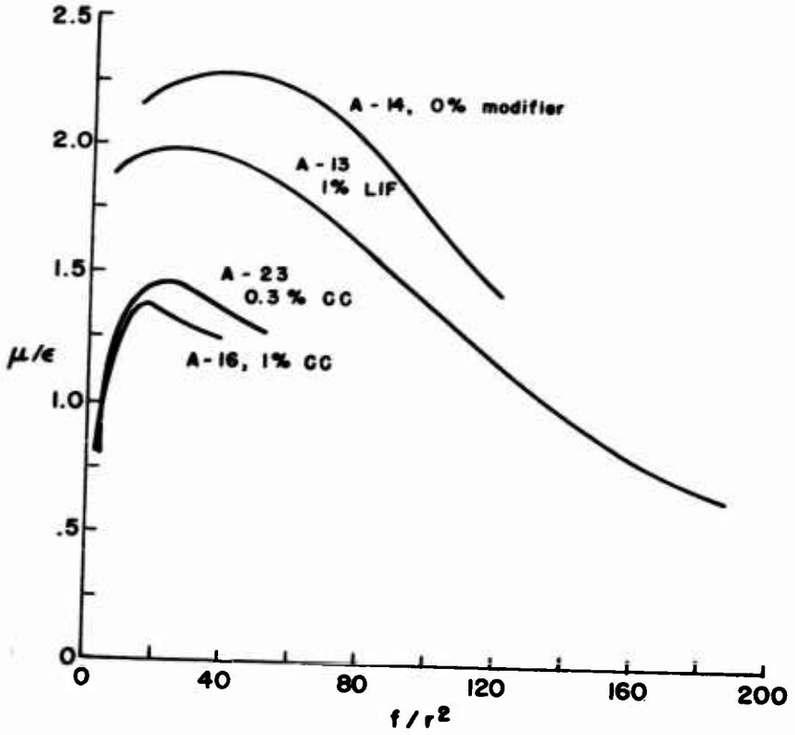

(d) 76% 15μ AP, 215 psia.

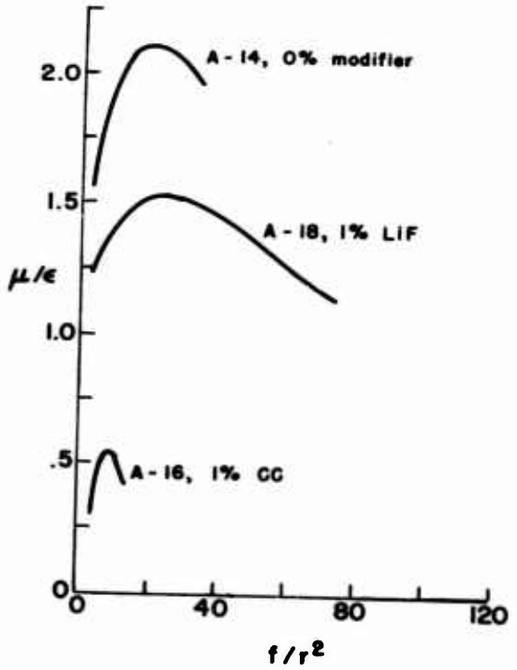

(e) 76% 15μ AP, 815 psia.

FIG. 13. Effect of Ballistic Modifiers on Response Function (PBAN Binder).

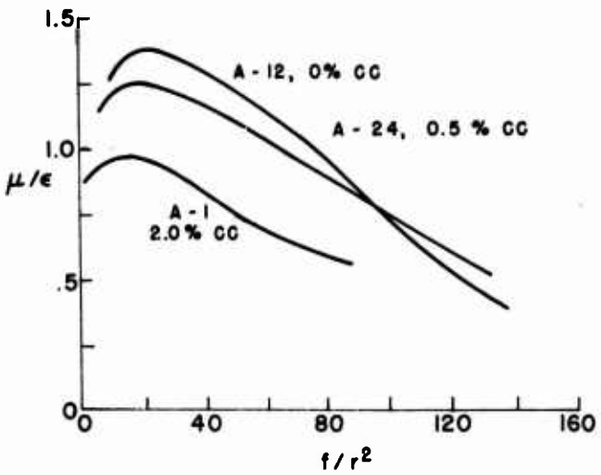

FIG. 13(f). Effect of Ballistic Modifiers on Response Function (PBAN Binder), 80% Bimodal AP (50-50 Mix of Micropulverized and As-Received), 215 psia.

In the case of bimodal AP, the μ/ε curves were again similar when plotted against f/r^2 (Fig. 13(f)). The value of μ/ε was depressed by increases in copper chromite content, although the corresponding increases in burning rate were larger than the decreases in μ/ε. This implies greater susceptibility to instability with copper chromite (when rated on a per-unit burning areas basis). Thus, with all oxidizer sizes, copper chromite increased r, reduced μ/ε, and left the product roughly constant.

Effect of Aluminum and Al_2O_3

Aluminized formulations were prepared as modifications of A-1 and A-14 by substitution of Al for binder. The A-1 modifications had 80% bimodal AP (50-50 mix of micropulverized and as-received), and 2% copper chromite. The aluminum variations were 0.5% 5μ Al, 1.0% 5μ Al, 1.0% 20μ Al, and 0.4% 0.02μ Al. The response functions obtained for these formulations are shown in Fig. 14. The difference between the behavior of the unaluminized A-1 and the other formulations is of doubtful significance considering the experimental uncertainties. In general, the addition of 20μ Al reduced μ/ε, 5μ Al had almost no effect, and 0.02μ Al increased μ/ε. Modification of A-14 (which used 5μ AP) by addition of 20μ Al significantly reduced μ/ε.

One formulation was prepared as a modification of A-1 by replacement of 1% of binder with 1% of Al_2O_3. This modification produced a small decrease of μ/ε, of marginal significance (Fig. 14).

Double-Base Propellants

Of the four double-base propellants tested, two (N-4 and N-5) are of roughly the same energy level as the composites tested, while two (JPN and X-14) are fairly high energy and high burning rate. Two (N-5 and X-14) are plateau type propellants (i.e., they exhibit a low dependence of burning rate on pressure over a pressure interval in the rocket motor operating range). The test results do not seem to reveal any conspicuous difference in response functions (see Appendix B). The values of μ/ε are somewhat higher than for most of the composites, but not as high as the highest given with composites. The values of μ/ε obtained with the lower energy formulations were about the same as with the higher energy formulations. Of course the high energy formulations are much more unstable (on a per unit burning surface area basis) because of the high burning rate and high value of c (Eq. 37). The difference between the plateau and nonplateau propellants was not conspicuous enough to belabor in the absence of more systematic studies, although the plateau propellants had somewhat lower values of μ/ε (particularly in the case of N-5 versus N-4 at 815 psia). It is notable that the variation of μ/ε with pressure was less consistent for the double-base propellants than with the composites.

Effect of Pressure

The present studies have provided considerable data on the effect of pressure on μ/ε, as evident from the foregoing discussion. The most complete studies of pressure dependence are provided by the tests on PBAN formulations A-13, A-15, A-17, A-14, A-16, A-18 and A-19 (Table 2, Fig. 12(c) and (d) and Fig. 15(a)-(c) respectively). As noted earlier, correlation of the response function data by constant pressure curves plotted against f/r^2 instead of f yields improved similarity among the constant pressure curves, as suggested by current one-dimensional theories. On the other hand, these same theories do not generally predict the conspicuous pressure dependence of μ/ε. The nature of the pressure dependence was the same for all the composite propellants tested, with high response function at low pressure and declining μ/ε as pressure increased. The degree of pressure dependence was roughly the same for all formulations except A-14 and A-19, which had low pressure dependence of μ/ε. These two formulations were without ballistic modifiers and were effectively fine AP (and high burning rate, high μ/ε). As suggested earlier, the low pressure sensitivity may be due to the relatively high importance of exothermic surface reactions related to the high interfacial area between binder and oxidizer.

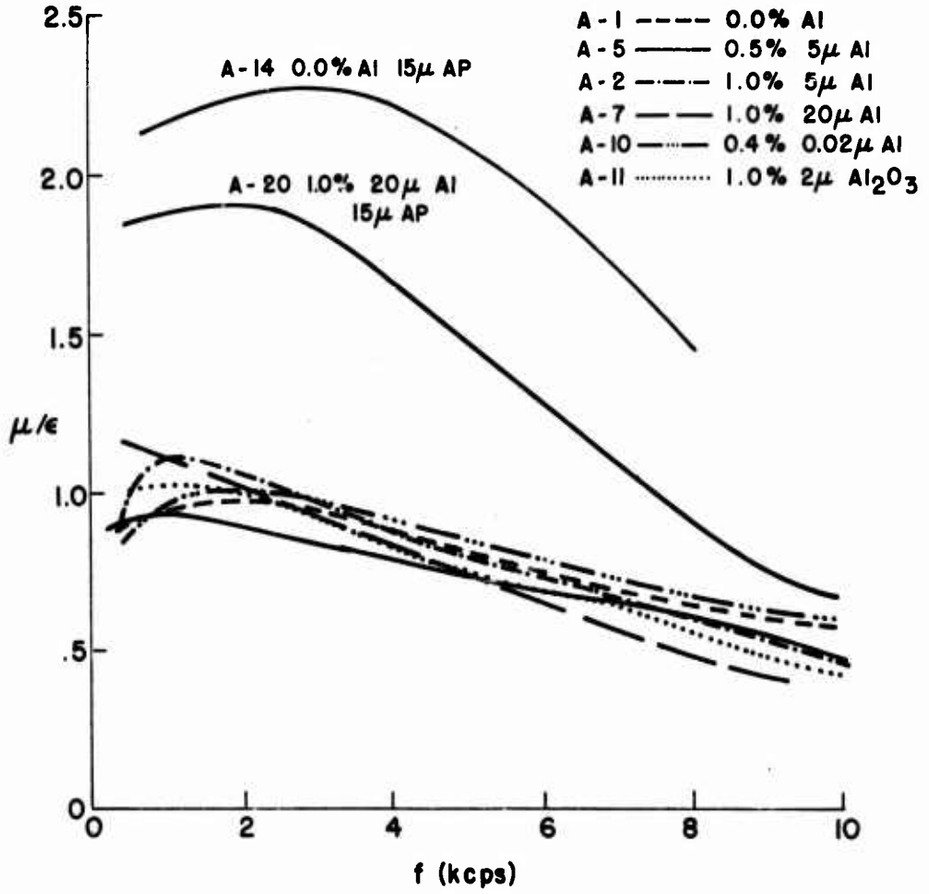

FIG. 14. Effect of Aluminum and Al_2O_3 on Response Function (PBAN Binder. A-14 and A-20 are 76% 15 μ AP, Others are 80% Bimodal AP, 50-50 Mix of Micro-pulverized and As-Received 2% Copper Chromite) 215 psia.

Effect of Additives on Attenuation

The effect of condensed phase products has been discussed in many references, the most appropriate for the present purpose being Ref. 16 (which shows calculated α_2 versus frequency for several particle sizes). In the present work, the condensed phase material presumably consists of copper chromite, Al, Al_2O_3 and carbon. Particle sizes were not measured. Copper chromite is roughly 1 to 2 μ in diameter when added to the propellant. Aluminum size (burning droplets) is presumably of the same order as the ingredient material. Al_2O_3 reaction products are presumably either in the < 2 μ range (smoke product), or of a size related to the original Al or agglomerates (products of surface reaction on Al droplets). Carbon is probably submicron in size.

Looking at the results in Fig. 9, the α_2's for A-13 and A-14 are lowest, as would be expected since no additives were present. The effect of addition of copper chromite can be estimated by comparison of results for A-13 or A-14 with A-1 (1% copper chromite), which led to a 40% increase in α_2. This result is important because all of the other curves except one showing effect of additives include the presence of 1 to 2 μ copper chromite.

The largest attenuations were obtained with A-2 propellant, containing 1% 5 μ Al and 2% copper chromite. Experience with aluminum combustion suggests that 5 μ Al would burn quickly to ∿ 1 μ Al_2O_3 smoke, which is a relatively good size for attenuation (see Fig. 3 of Ref. 16). The value of α_2 is somewhat low but in qualitative agreement with the theory. The result with 0.5% 5 μ Al (A-5) lies halfway between the results for 1.0% Al and 0.0% Al (A-1 and A-2). A-20 provides an indication of the effect of adding 1% of 20 μ Al to a formulation with no copper chromite (e.g., A-14). The increase in α_2 is not very great--possibly because 20 μ Al is too coarse for effective attenuation and may not react fast enough to convert to finer Al_2O_3. Addition of 1% 20 μ Al to a formulation with 2% copper chromite had a more conspicuous effect (compare A-7 and A-14), although less effect than 5 μ Al. Addition of 1% 2 μ Al_2O_3 (A-11) and of 0.4% 0.02 μ Al had negligible effect on α_2 (compare with A-1). This result is surprising in the case of the Al_2O_3, since the particle size was near optimum for damping: it is possible that the oxide was agglomerated to an ineffective size, possibly during propellant processing. No direct information on this point is available.

Stability Limits

In the present work, considerable effort was devoted to testing near the stability limits of the combustor--primarily to extend the range of μ/ε data. In the process, considerable information regarding the stability limit of this type of T-burner was developed, and curve-fitting procedures were contrived to maximize the generalization of

these results. The ultimate application of these results could be either (a) as an empirical guide to choice of test variables in future work, or (b) development or evaluation of loss and scaling laws for T-burners. The former of these applications can be made from the results as they are presented (Table 5 and Appendix A)--at least for similar propellants and T-burners. The second application is beyond the scope of the present study, but the data may be a stimulus to such studies.

It should be clear that the curve fitting procedure that was chosen was a matter of expediency in the face of limited data. The resulting stability limit curves differ markedly as a function of propellant, and consequently can be used as qualitative indicators of the stability "personality" of the propellant. In practice, of course, one would be more concerned with how high the response function becomes inside the stability limit, but the limit is an indicator of the range of frequency and pressure over which instability might occur.

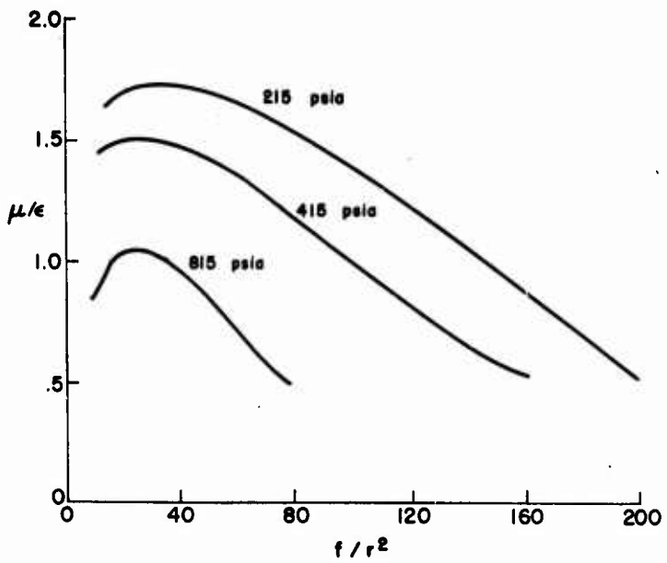

(a) 76% 80μ AP.

FIG. 15. Effect of Pressure on Response Function (PBAN Binder, No Ballistic Modifier).

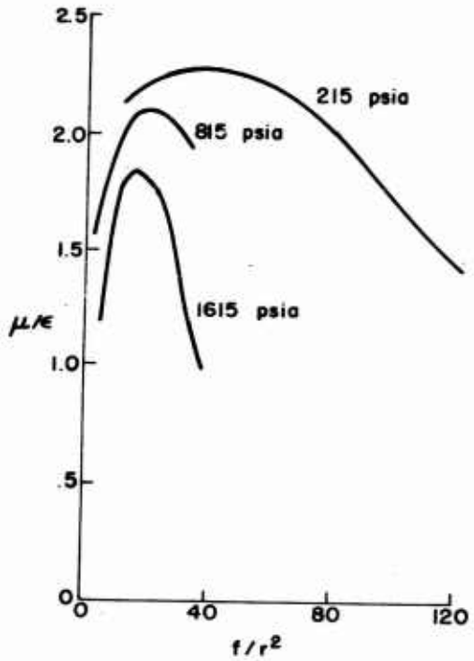

(b) 76% 15μ AP.

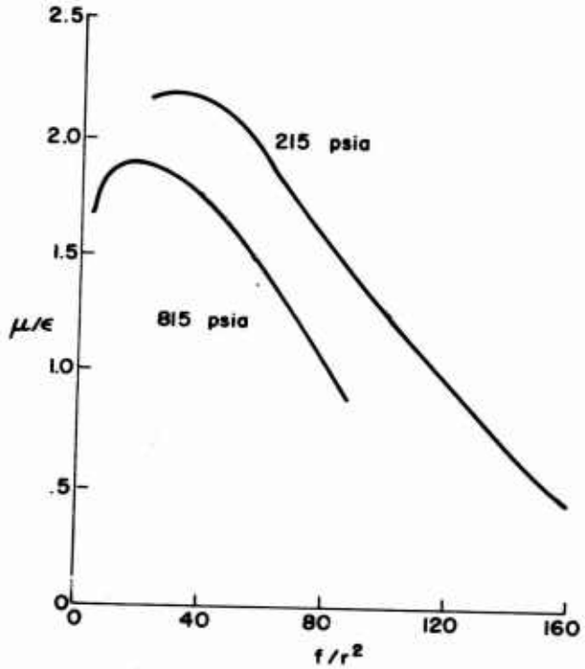

(c) 76% Bimodal AP, 50-50 15μ, 80μ.

FIG. 15. Effect of Pressure on Response Function (PBAN Binder, No Ballistic Modifier).

Appendix A

RESULTS UNDER LIMITED PRESSURE COVERAGE

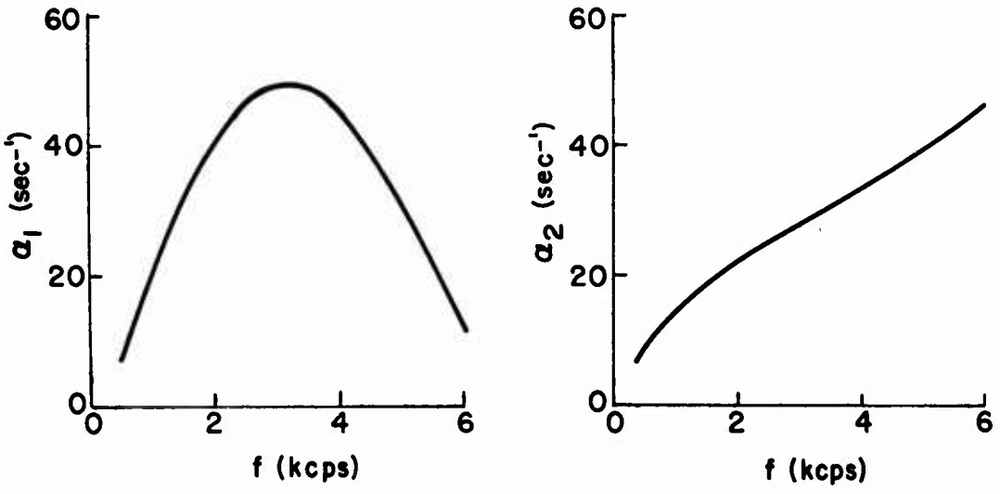

Propellant (1) A-12	
Composition	**Ballistic Data**
Binder. . . . PBAN, 20%	Pressure, psia. 215
Aluminum. . . None	r, in/sec 21
Oxidizer. . . AP(BM), 80%	P/r 1024
	c, in/sec . . .38,500
Catalyst. . . None	Kr. 40.7

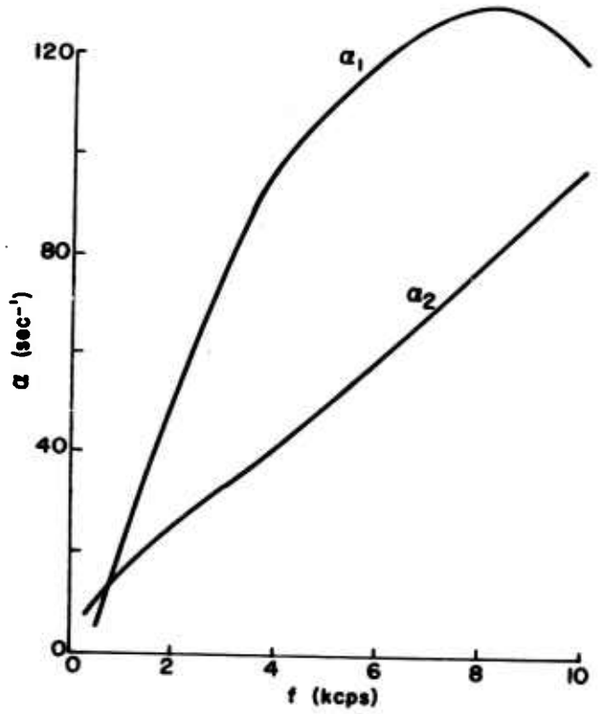

(a)

Propellant (2) A-1	
Composition	Ballistic Data
Binder. . . . PBAN, 18% Aluminum. . . None Oxidizer. . . AP(BM), 80% Catalyst. . . cc, 2%	Pressure, psia. 215 r, in/sec . . . .34 P/r . . . . . 632 c, in/sec . . .38,500 Kr. 25.1

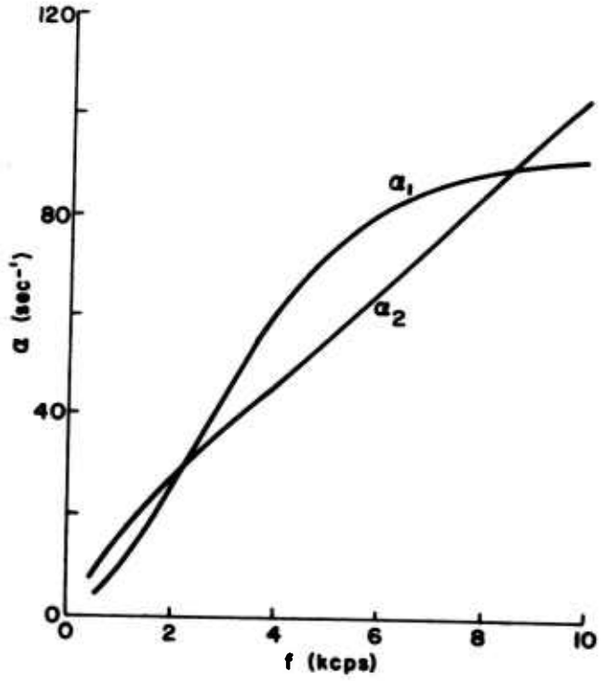

(b)

Propellant (2) A-1	
Composition	Ballistic Data
Binder. . . . PBAN, 18% Aluminum. . . None Oxidizer. . . AP(BM), 80% Catalyst. . . cc, 2%	Pressure, psia. 415 r, in/sec . . . .47 P/r . . . . . 883 c, in/sec . . 38,500 Kr. 35.1

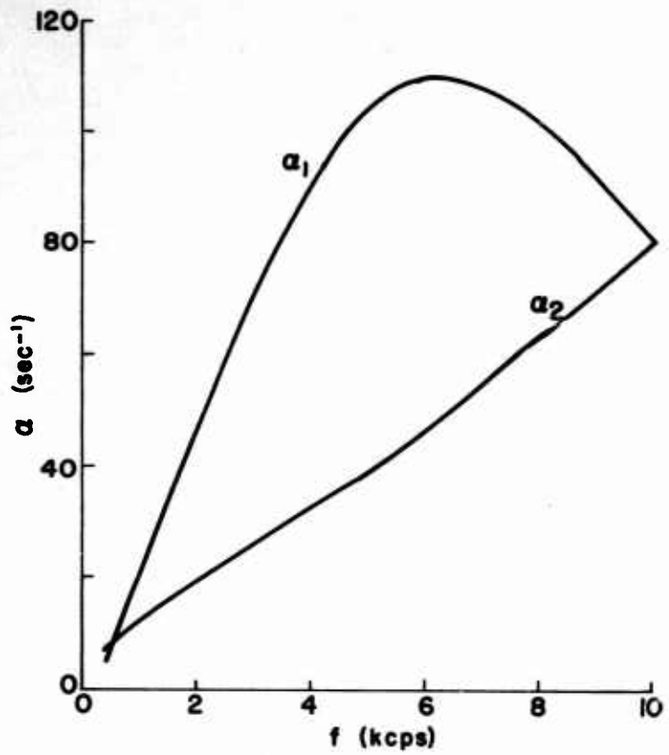

Propellant (3) A-24

Composition	Ballistic Data
Binder. . . PBAN, 19.5% Aluminum. . None Oxidizer. . AP(BM), 80% Catalyst. . None	Pressure, psia. 215 r, in/sec . . . .28 P/r . . . . . 768 c, in/sec . . .35,500 Kr. 35.5

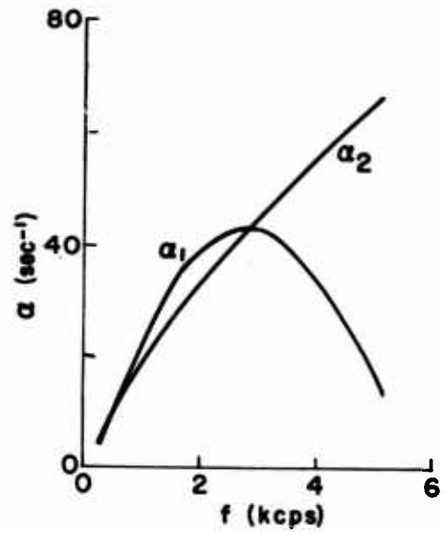

Propellant (4) A-22

Composition	Ballistic Data
Binder. . . . PS, 20% Aluminum. . . None Oxidizer. . . AP(BM), 80% Catalyst. . . None	Pressure, psia. . 215 r, in/sec . . . . .29 P/r . . . . . 742 c, in/sec . . .36,900 Kr. 30.7

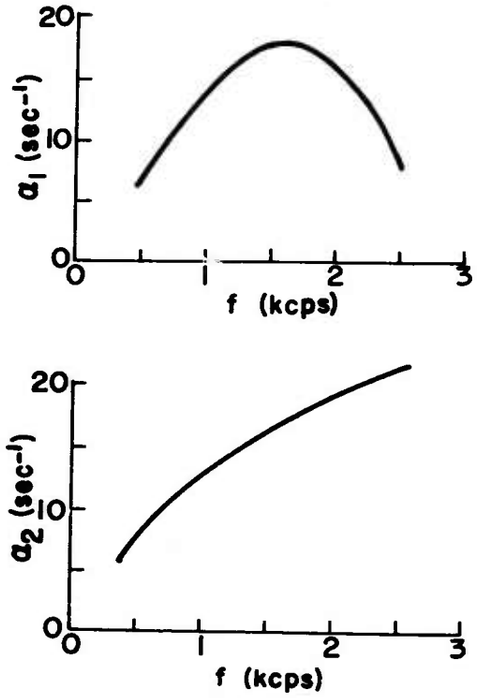

Propellant (5) A-25	
Composition	**Ballistic Data**
Binder. . . . PU, 20%	Pressure, psia. . 215
Aluminum. . . None	r, in/sec 19
Oxidizer. . . AP(BM), 80%	P/r 1131
Catalyst. . . None	c, in/sec . . . 37,700
	Kr. 48.3

NONALUMINIZED COMPOSITE PROPELLANTS

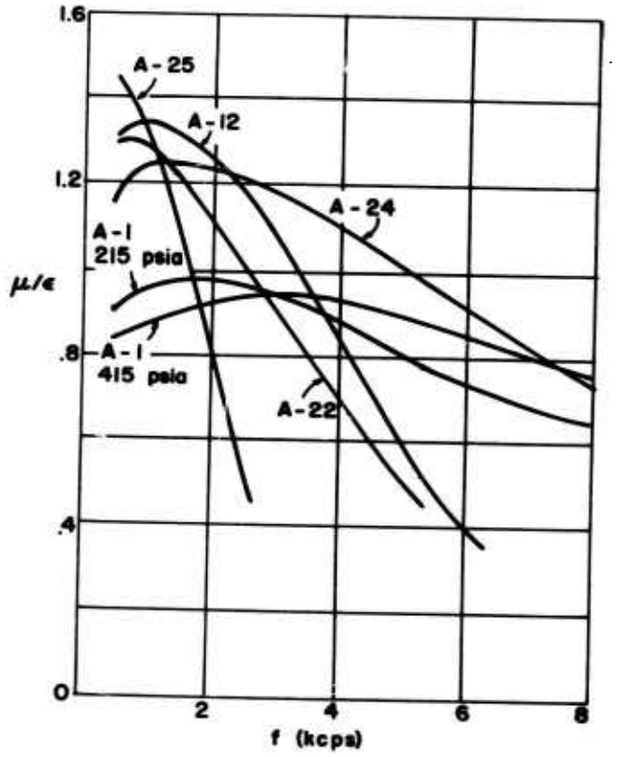

Response Function Results for Propellants A-12, A-24, A-22 and A-25 at 215 psia and A-1 at 215 and 415 psia.

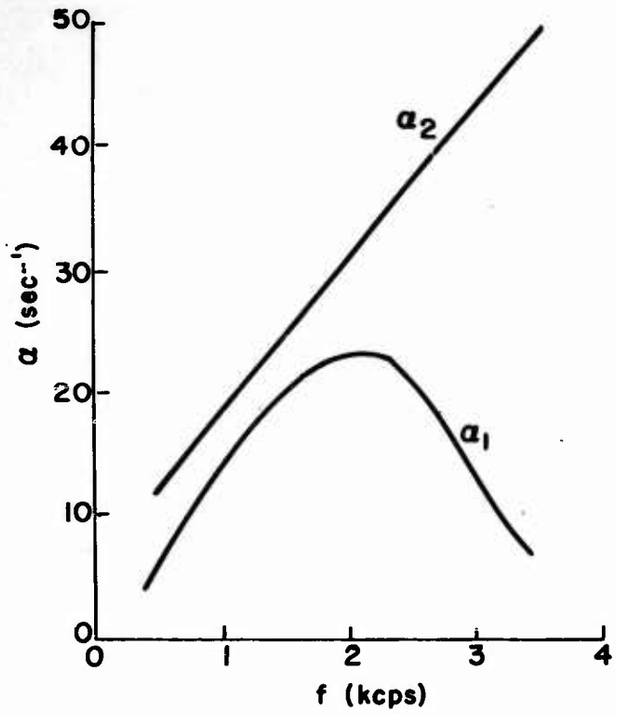

Propellant (6) A-28

Composition	Ballistic Data
Binder. . . . PBAN, 10% Aluminum. . . None Oxidizer. . . AP(80μ), 90% Catalyst. . . None	Pressure, psia. 215 r, in/sec . . . .24 P/r . . . . . 896 c, in/sec . . .36,600 Kr. 38.7

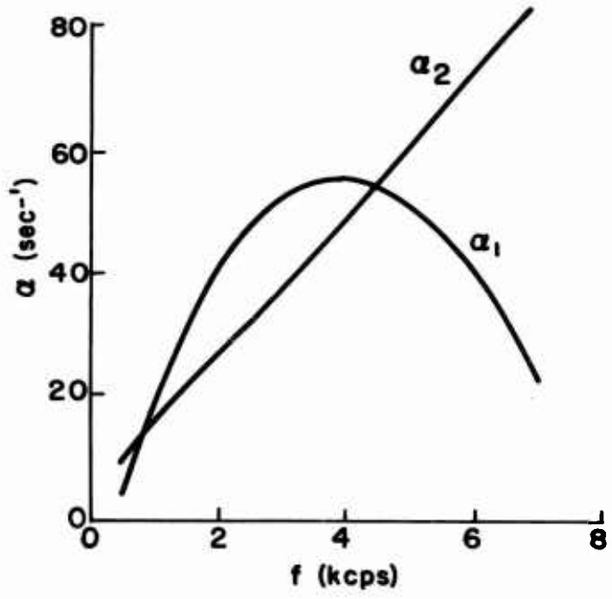

Propellant (7) A-27

Composition	Ballistic Data
Binder. . . . PBAN, 15% Aluminum. . . None Oxidizer. . . AP(80μ), 85% Catalyst. . . None	Pressure, psia 215 r, in/sec . .28 P/r . . . . 768 c, in/sec . 37,200 Kr. 33.2

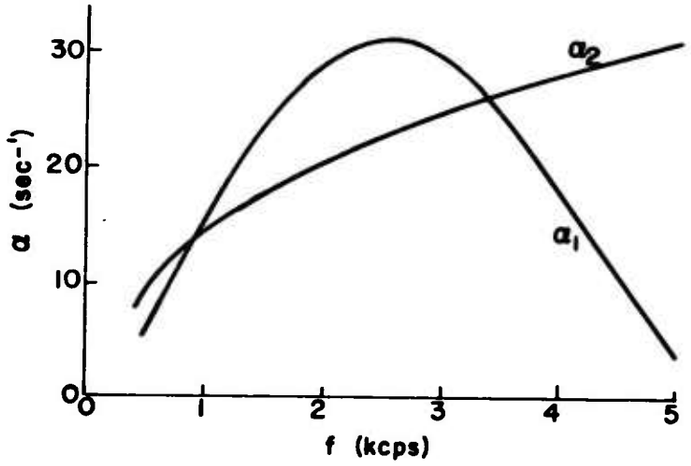

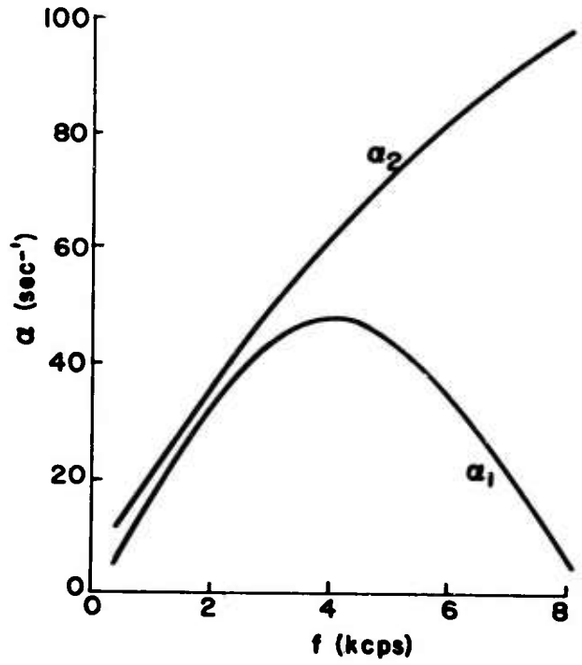

Propellant (8) A-26	
Composition	Ballistic Data
Binder. . . . PBAN, 23.5% Aluminum. . . None Oxidizer. . . AP(80μ), 76% Catalyst. . . CB, .5%	Pressure, psia. 215 r, in/sec . . . .16 P/r . . . . . 1344 c, in/sec . . .35,000 Kr. 65.2

Propellant (9) A-44	
Composition	Ballistic Data
Binder. . . . PS, 25% Aluminum. . . None Oxidizer. . . AP(80μ), 75% Catalyst. . . None	Pressure, psia 215 r, in/sec. . . .32 P/r. . . . . 672 c, in/sec. . .37,000 Kr 28.4

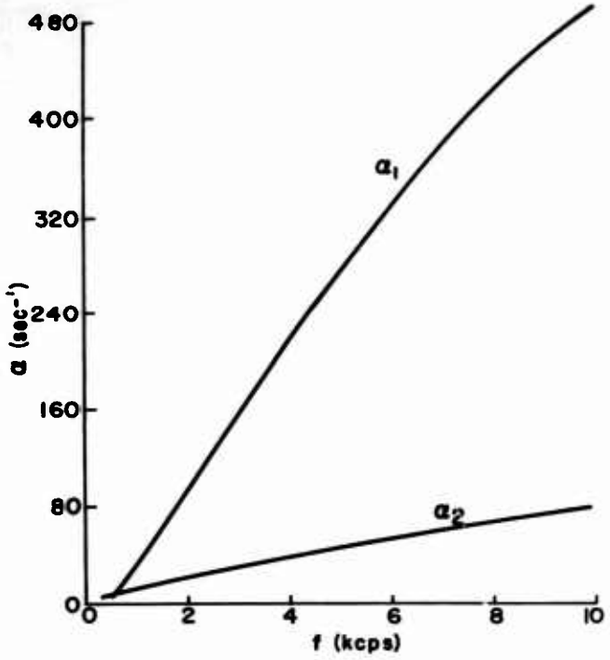

Propellant (10) A-23	
Composition	**Ballistic Data**
Binder. . . PBAN, 23.7%	Pressure, psia. . 215
Aluminum. . None	r, in/sec 44
Oxidizer. . AP(15μ), 76%	P/r 489
Catalyst. . cc, .3%	c, in/sec 37,000
	Kr. 22.3

NONALUMINIZED COMPOSITE PROPELLANTS

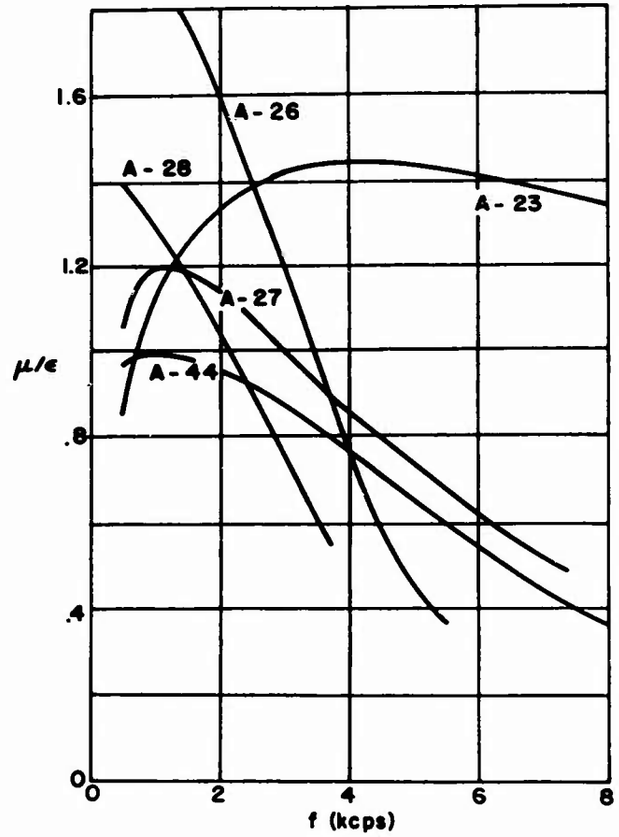

Response Function Results for Propellants A-28, A-27, A-26, A-44 and A-23 at 215 psia.

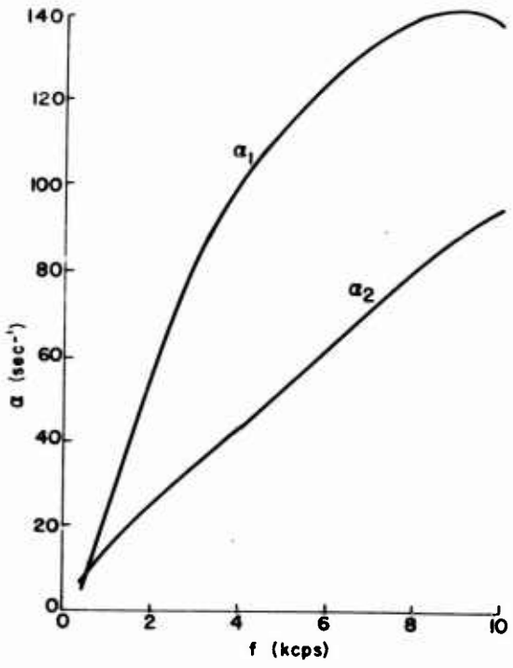

Propellant (11) A-10	
Composition	**Ballistic Data**
Binder. . . PBAN, 17.6%	Pressure, psia . 215
Aluminum. . .02μ, 14%	r, in/sec. 34
Oxidizer. . AP(BM), 80%	P/r. 632
Catalyst. . cc, 2%	c, in/sec. . . .38,500
	Kr 25.1

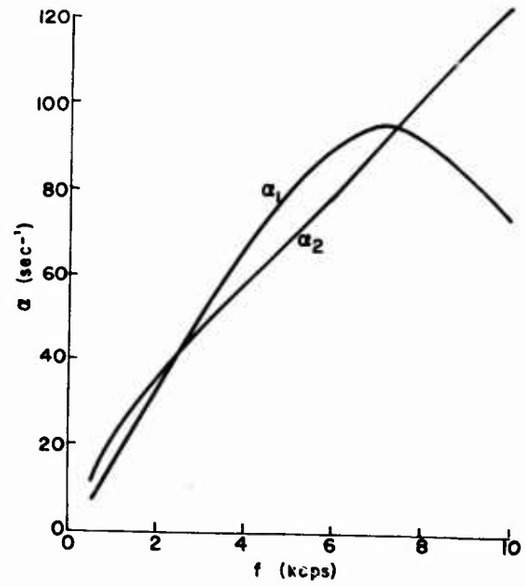

Propellant (12) A-5	
Composition	**Ballistic Data**
Binder. . . PBAN, 17.5%	Pressure, psia. 215
Aluminum. . 5μ, 15%	r, in/sec 34
Oxidizer. . AP(BM), 80%	P/r 632
Catalyst. . cc, 2%	c, in/sec . . .38,500
	Kr. 25.1

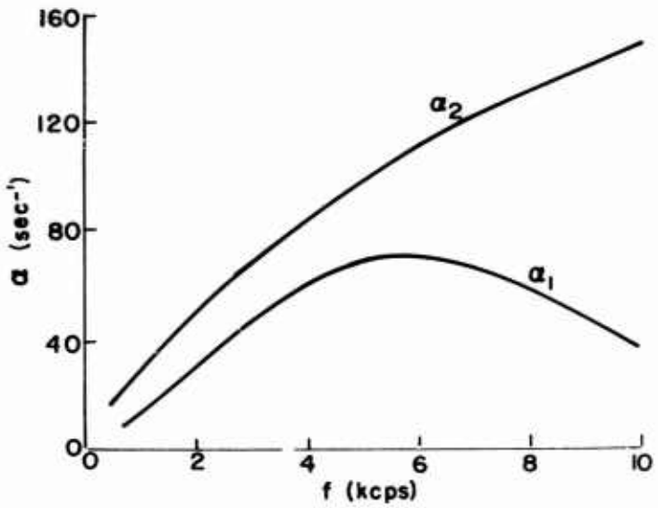

(a)

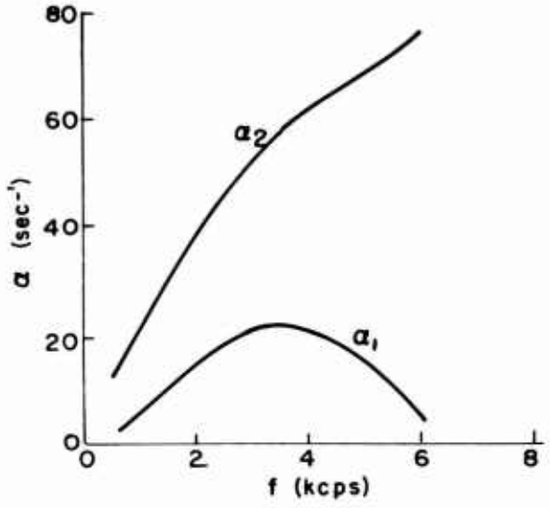

(b)

Propellant (13) A-2	
Composition	Ballistic Data
Binder. . . PBAN, 17% Aluminum. . 5μ, 1% Oxidizer. . AP(BM), 80% Catalyst. . cc, 2%	Pressure, psia . 215 r, in/sec. . . . .34 P/r. . . . . 632 c, in/sec. . . .38,500 Kr 25.1

Propellant (13) A-2	
Composition	Ballistic Data
Binder. . . PBAN, 17% Aluminum. . 5μ, 1% Oxidizer. . AP(BM), 80% Catalyst. . cc, 2%	Pressure, psia . 415 r, in/sec. . . . .45 P/r. . . . . 922 c, in/sec. . . .38, 500 Kr 36.7

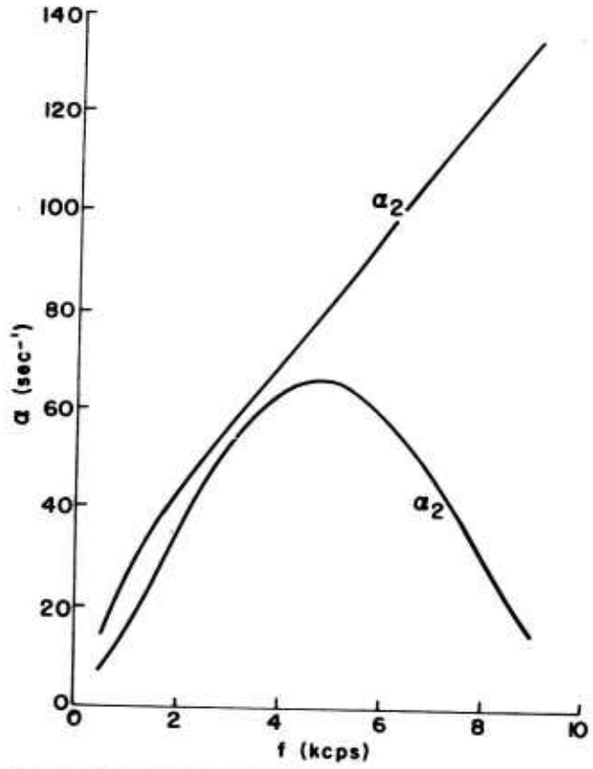

Propellant (14) A-7	
Composition	**Ballistic Data**
Binder. . . PBAN, 17% Aluminum. . 20μ, 1% Oxidizer. . AP(BM), 80% Catalyst. . cc, 2%	Pressure, psia . 215 r, in/sec. . . . .34 P/r. . . . . 632 c, in/sec. . . .38,500 Kr 25.1

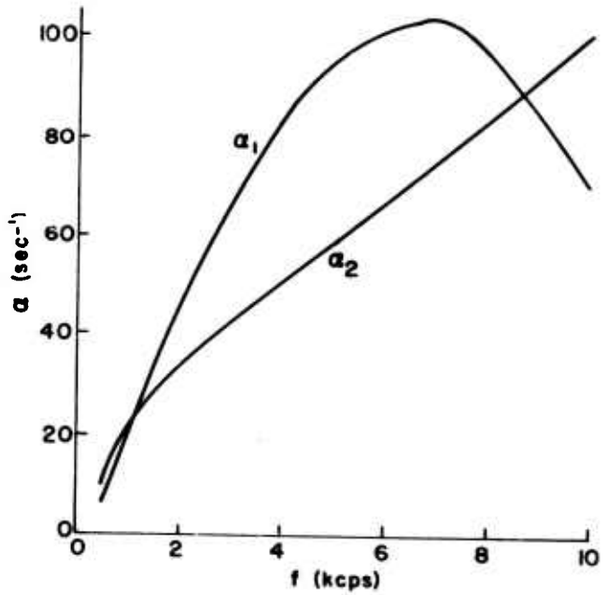

Propellant (15) A-11	
Composition	**Ballistic Data**
Binder. . PBAN, 17% Aluminum. 2μ,1%(Al_2O_3) Oxidizer. AP(BM), 80% Catalyst. cc, 2%	Pressure, psia. 215 r, in/sec . . . .34 P/r . . . . . 632 c, in/sec . . .38,500 Kr. 25.1

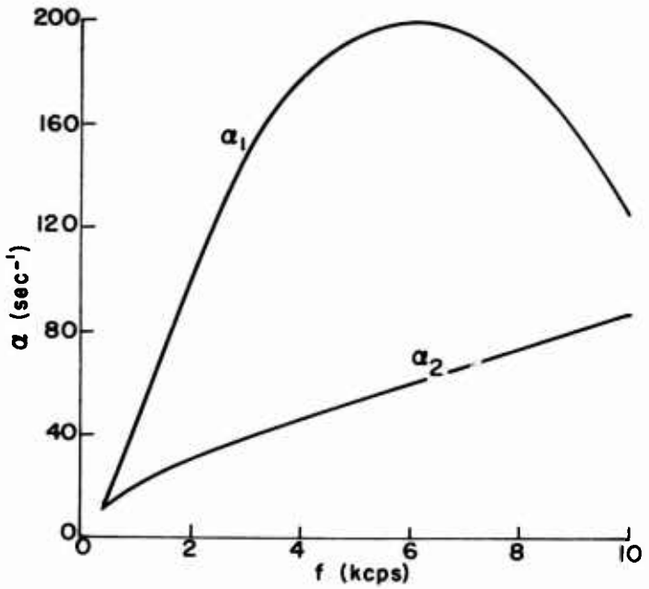

Propellant (16) A-20	
Composition	**Ballistic Data**
Binder. . . PBAN, 23%	Pressure, psia. . 215
Aluminum. . 20μ, 1%	r, in/sec 33
Oxidizer. . AP(15μ), 76%	P/r 726
Catalyst. . None	c, in/sec 37,200
	Kr. 29.6

ALUMINIZED COMPOSITE PROPELLANTS

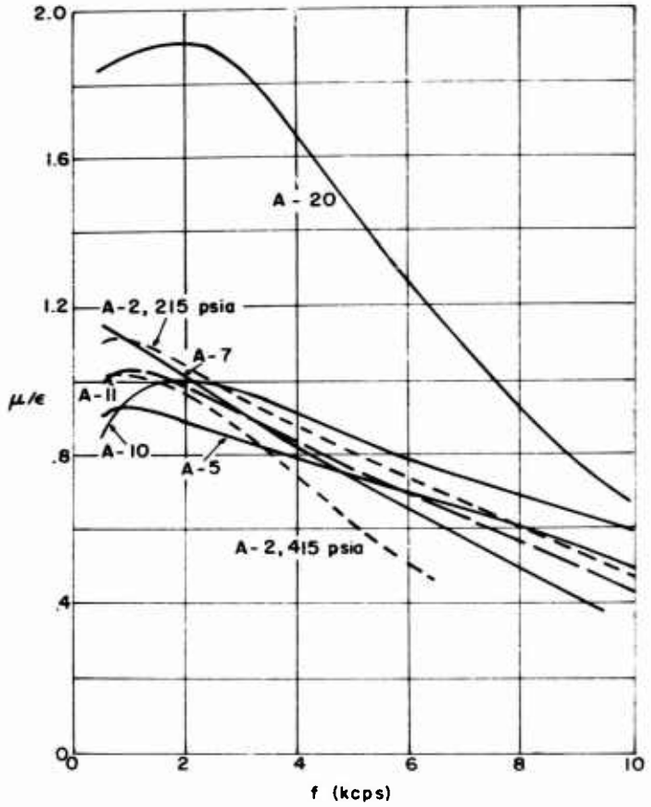

Response Function Results for Propellants A-10, A-5, A-7, A-11 and A-20 at 215 psia and A-2 at 215 and 415 psia.

Appendix B

EXTENDED PRESSURE COVERAGE

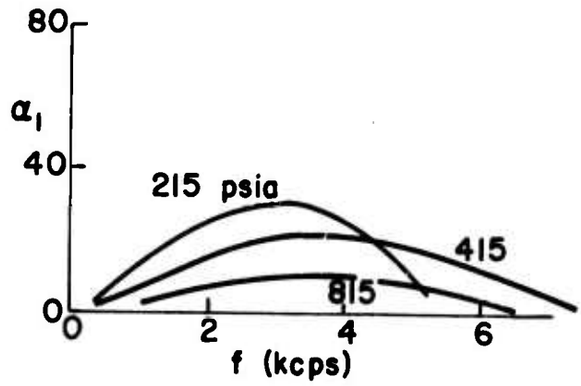

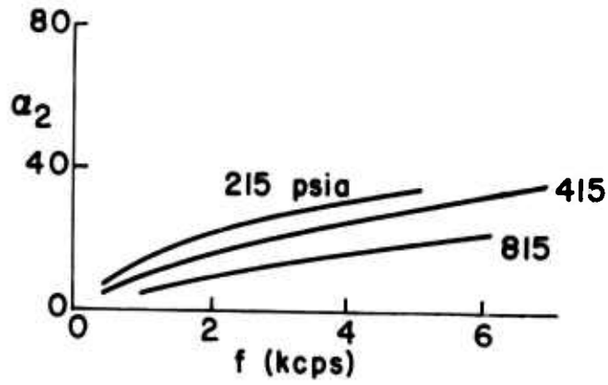

Propellant (17) A-13

Composition	Ballistic Data		
Binder. . . . PBAN, 24% Aluminum. . . None Oxidizer. . . AP(80μ), 76% Catalyst. . . None	Pressure, psia. . . 215 r, in/sec . . . . . .16 P/r . . . . . 1344 c, in/sec . . . . .35,400 Kr. 64.1	415 .21 1976 36,700 91.2	815 .28 2911 37,600 130.0

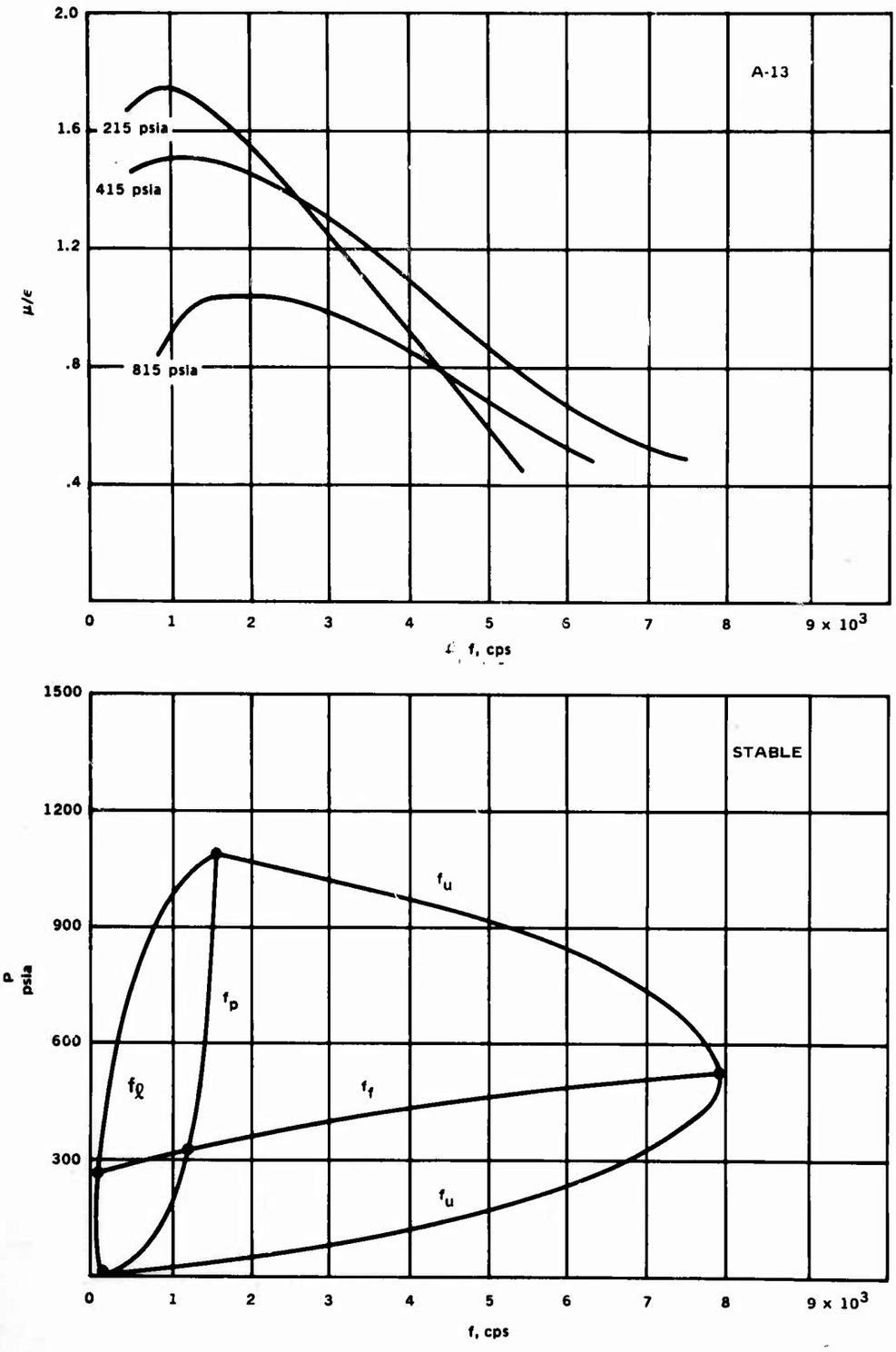

Response Function Results and Neutral Boundary for A-13 Propellant.

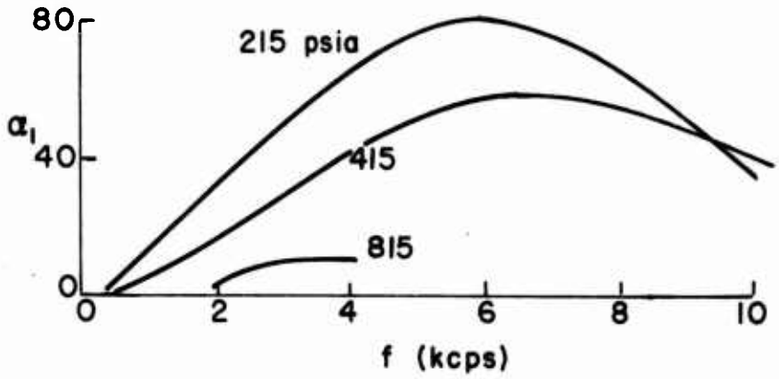

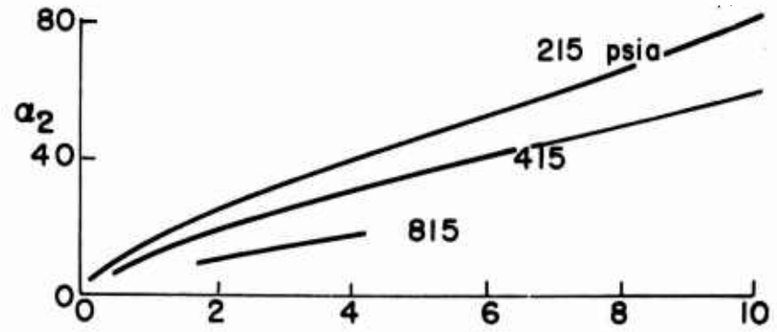

Propellant (18) A-15

Composition	Ballistic Data		
Binder. . . . PBAN, 23%	Pressure, psia. . . 215	415	815
Aluminum. . . None	r, in/sec 26	.35	.47
Oxidizer. . . AP(80μ), 76%	P/r 827	1186	1734
Catalyst. . . cc, 1%	c, in/sec 36,500	37,200	37,700
	Kr. 37.9	54.1	77.6

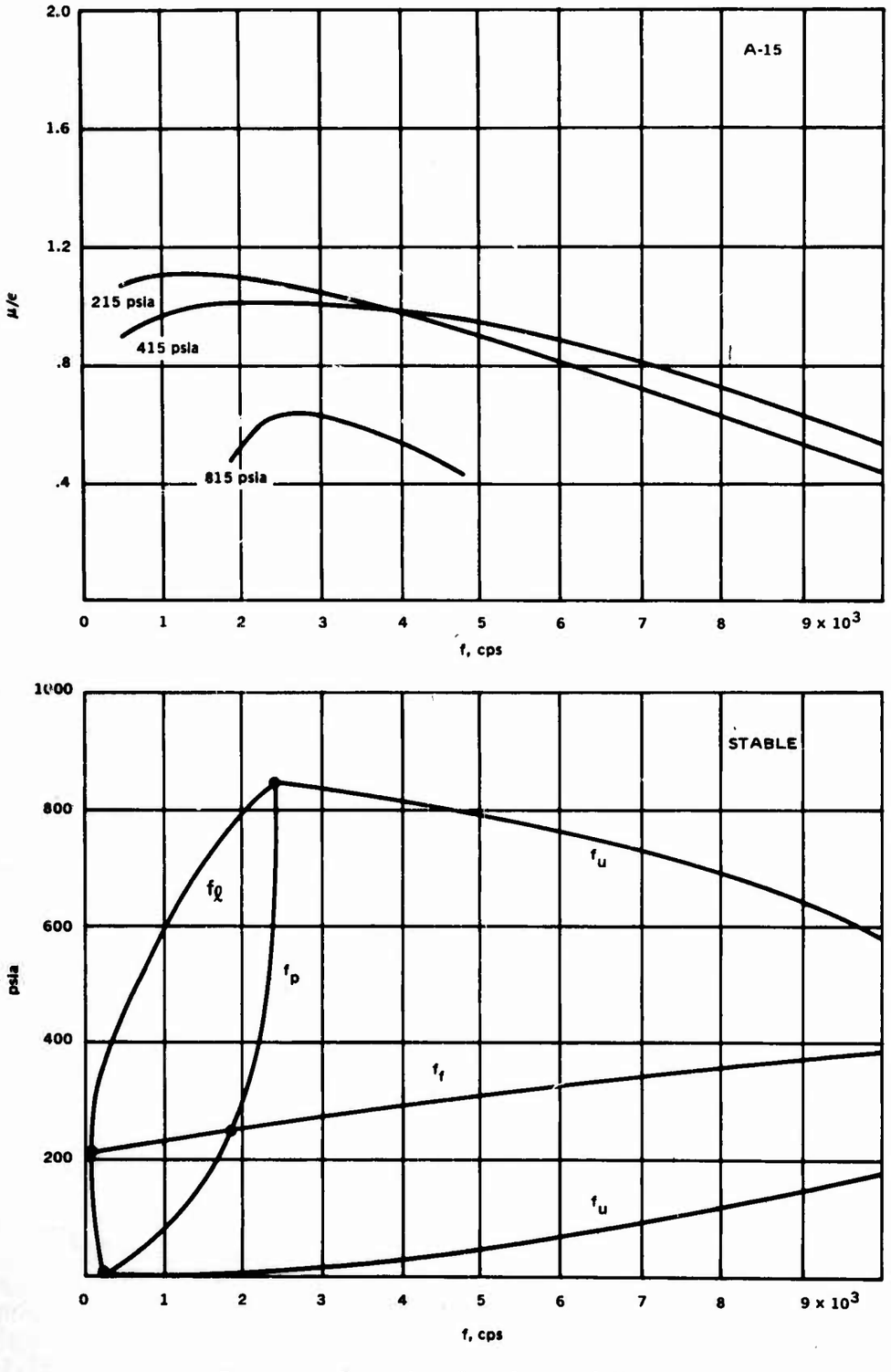

Response Function Results and Neutral Boundary for A-15 Propellant.

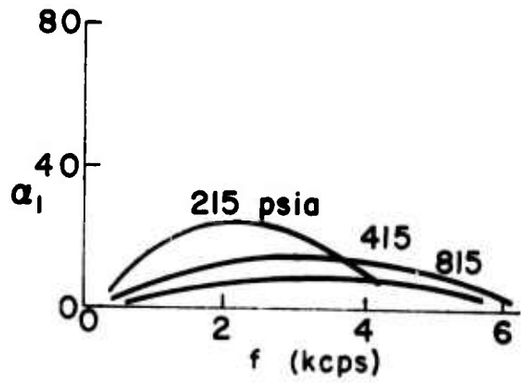

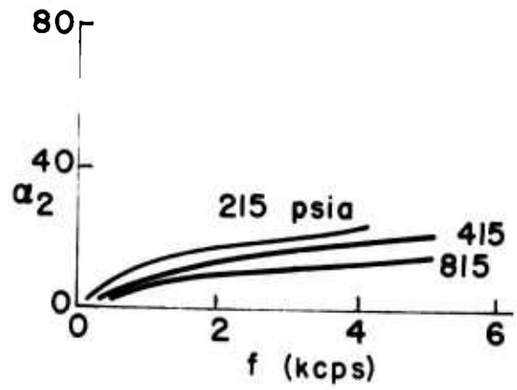

Propellant (19) A-17

Composition	Ballistic Data		
Binder. . . . PBAN, 23% Aluminum. . . None Oxidizer. . . AP(80μ), 76% Catalyst. . . LF, 1%	Pressure, psia. . . 215 r, in/sec . . . . . .12 P/r . . . . . 1791 c, in/sec . . . . .34,200 Kr. 88.7	415 .16 2593 35,600 123.2	815 .22 3704 37,000 169.8

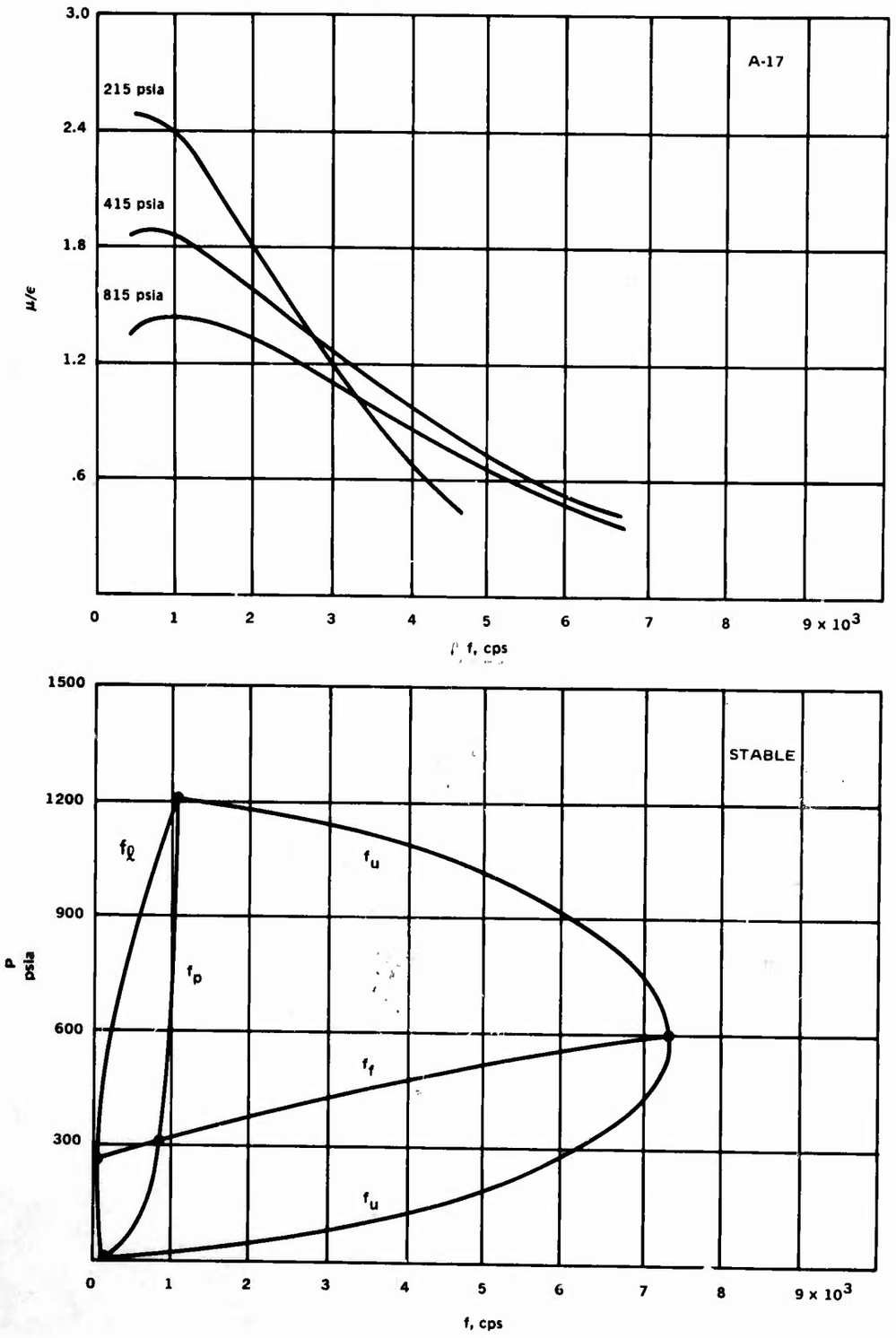

Response Function Results and Neutral Boundary for A-17 Propellant.

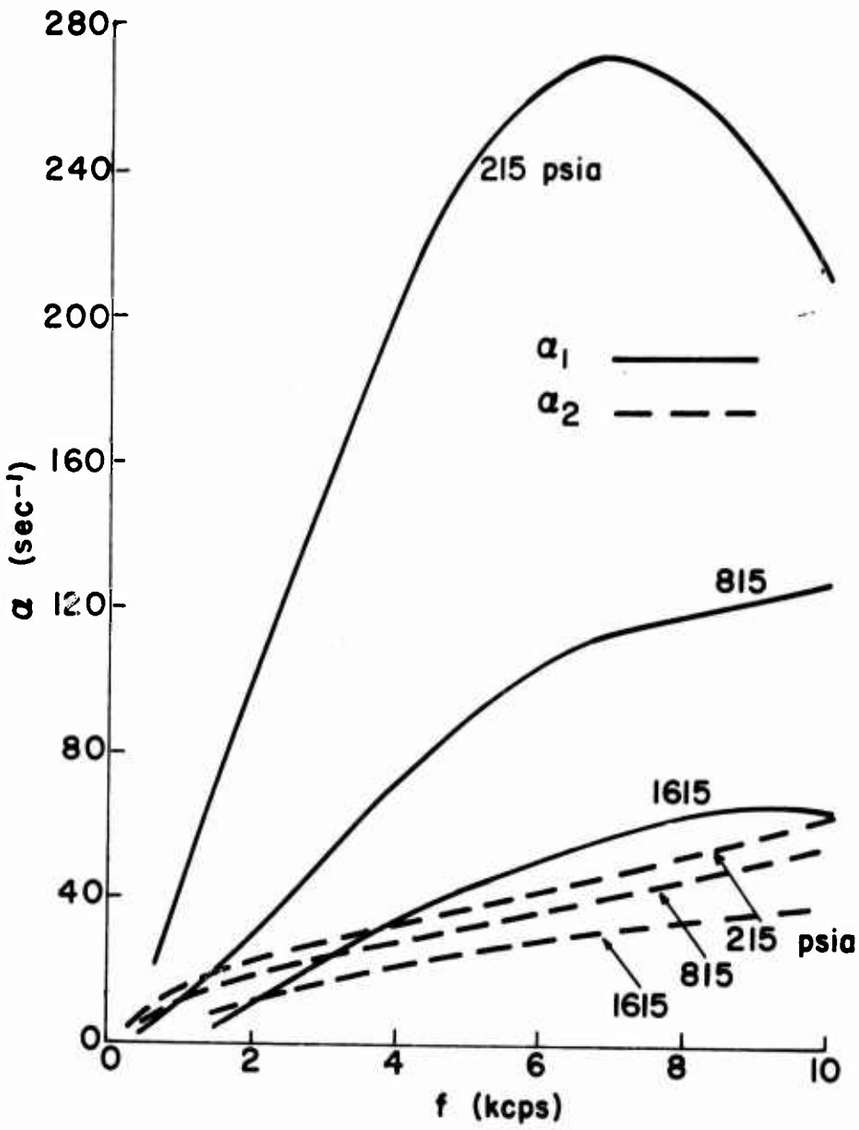

Propellant (21) A-14			
Composition	Ballistic Data		
Binder. . . . PBAN, 24%	Pressure, psia. . . 215	815	1615
Aluminum. . . None	r, in/sec 26	.42	.53
Oxidizer. . . AP(15μ), 76%	P/r 827	1940	3047
Catalyst. . . None	c, in/sec 37,200	38,800	38,500
	Kr. 37.6	84.9	134.0

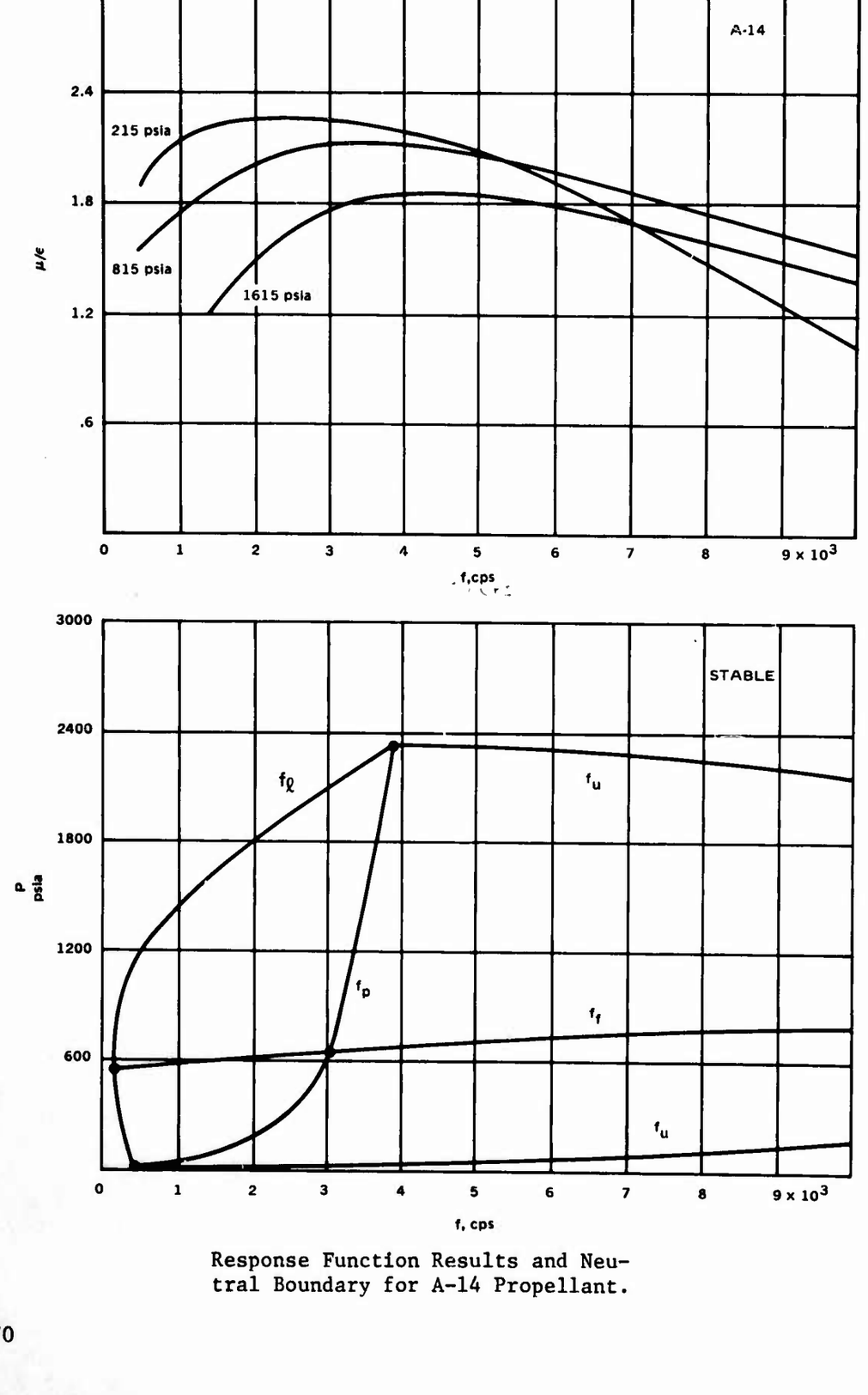

Response Function Results and Neutral Boundary for A-14 Propellant.

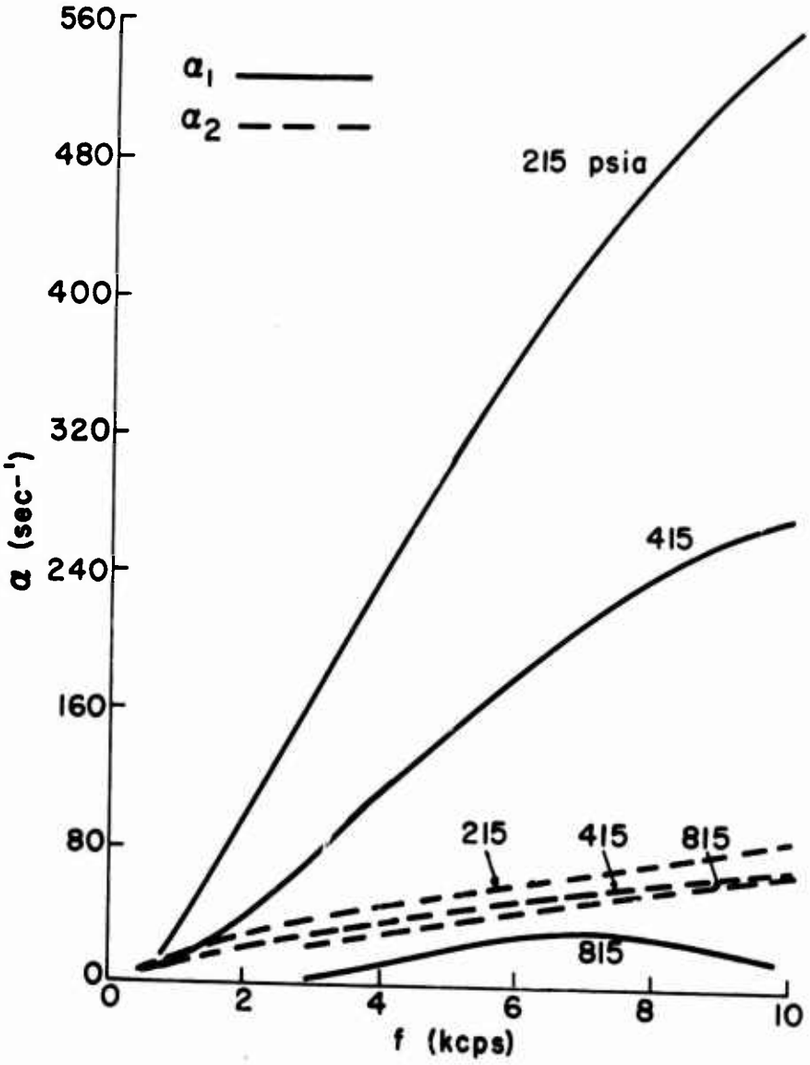

Propellant (22) A-16			
Composition	Ballistic Data		
Binder. . . . PBAN, 23%	Pressure, psia. . . 215	415	815
Aluminum. . . None	r, in/sec 51	.64	.82
Oxidizer. . . AP(15μ), 76%	P/r 422	648	994
Catalyst. . . cc, 1%	c, in/sec 37,000	38,200	38,000
	Kr. 19.3	28.7	44.3

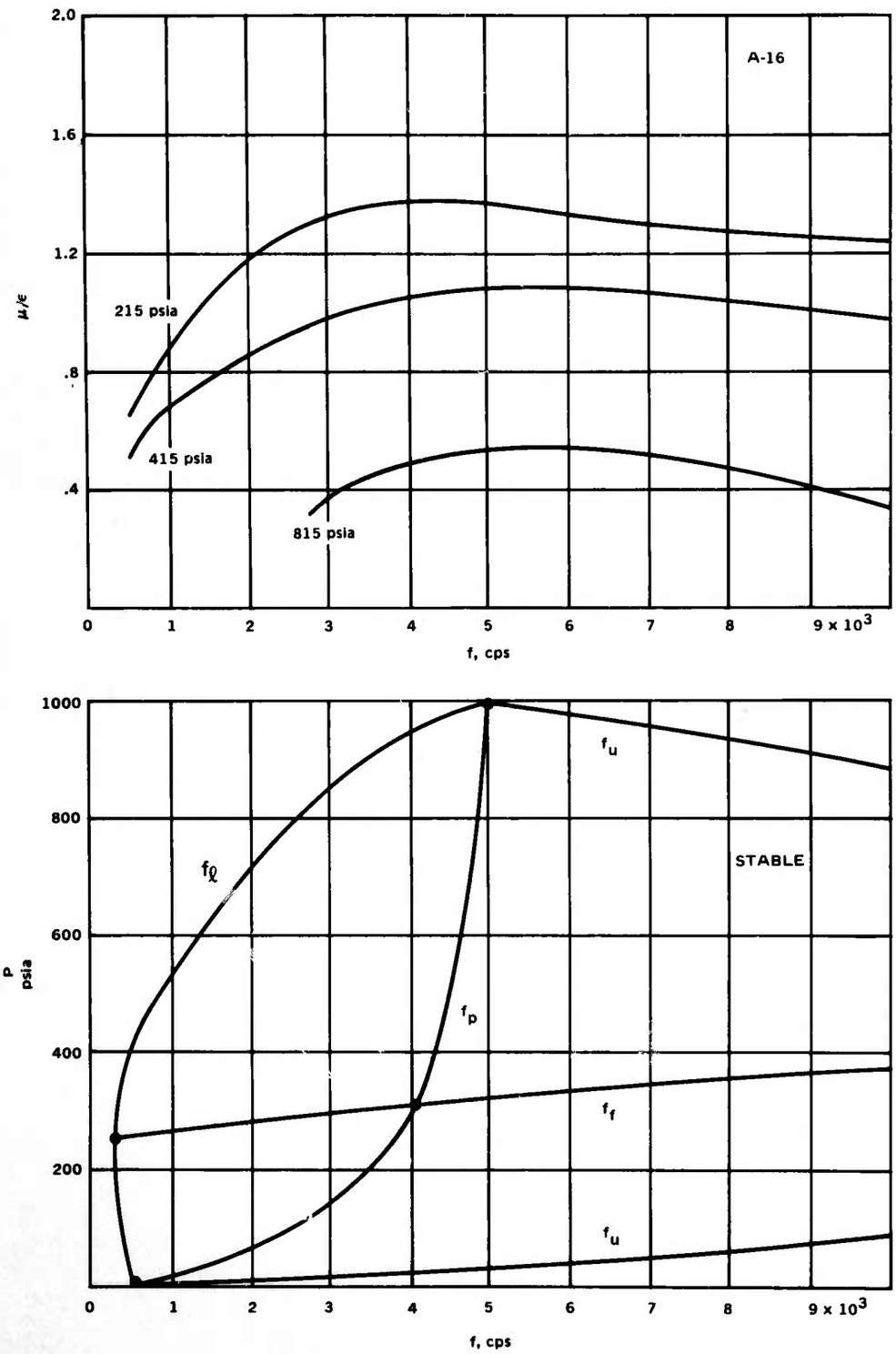

Response Function Results and Neutral Boundary for A-16 Propellant.

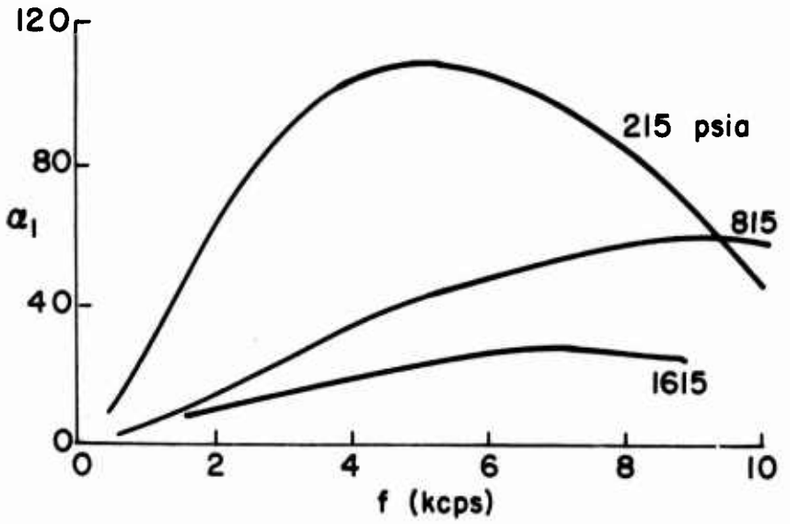

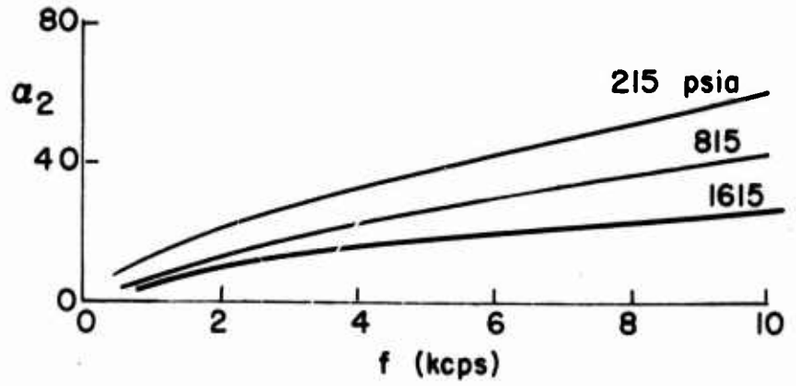

Propellant (23) A-18

Composition	Ballistic Data		
Binder. . . . PBAN, 23%	Pressure, psia. . . 215	815	1615
Aluminum. . . None	r, in/sec 22	.35	.45
Oxidizer. . . AP(80μ), 76%	P/r 977	2329	3589
Catalyst. . . LF, 1%	c, in/sec 35,800	37,200	38,000
	Kr. 46.3	105.8	160.0

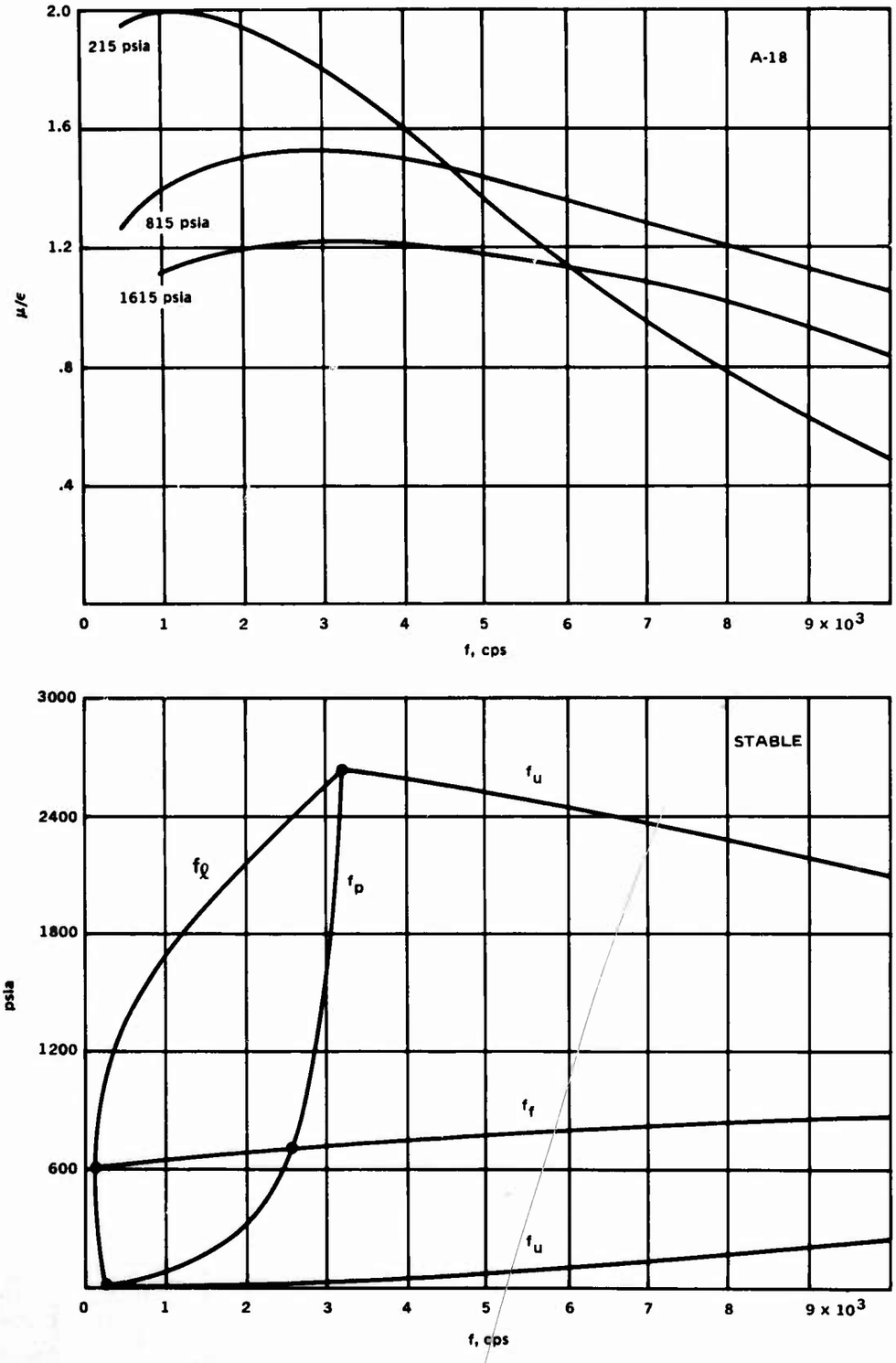

Response Function Results and Neutral Boundary for A-18 Propellant.

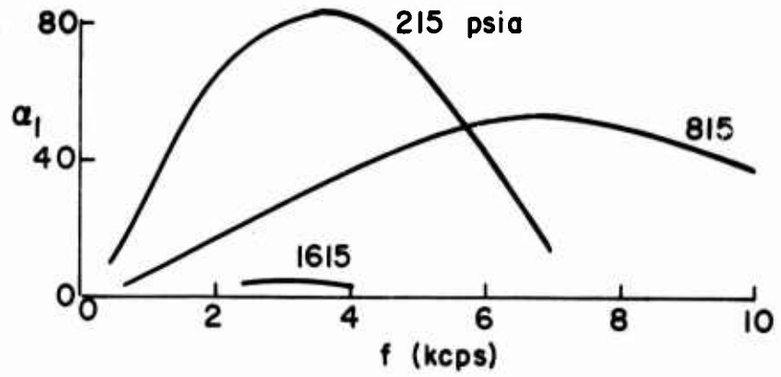

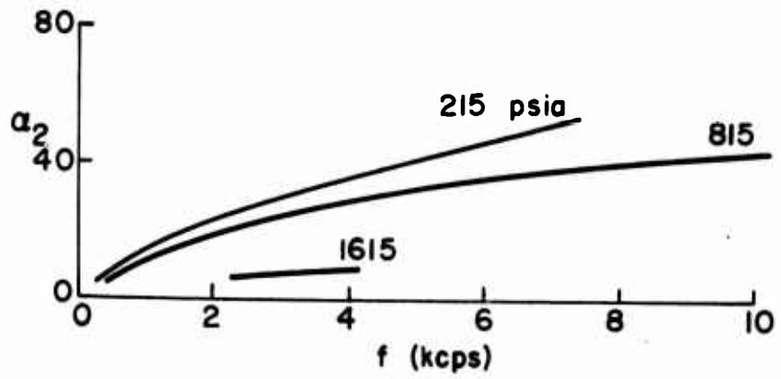

Propellant (24) A-19			
Composition	Ballistic Data		
Binder. . . . PBAN, 24% Aluminum. . . None Oxidizer. . . AP(80μ), 76% Catalyst. . . LF, 1%	Pressure, psia. . . 215 r, in/sec . . . . . .21 P/r . . . . . 1024 c, in/sec . . . . .35,900 Kr. 48.2	815 .34 2397 37,600 108.2	1615 .44 3670 38,100 163.1

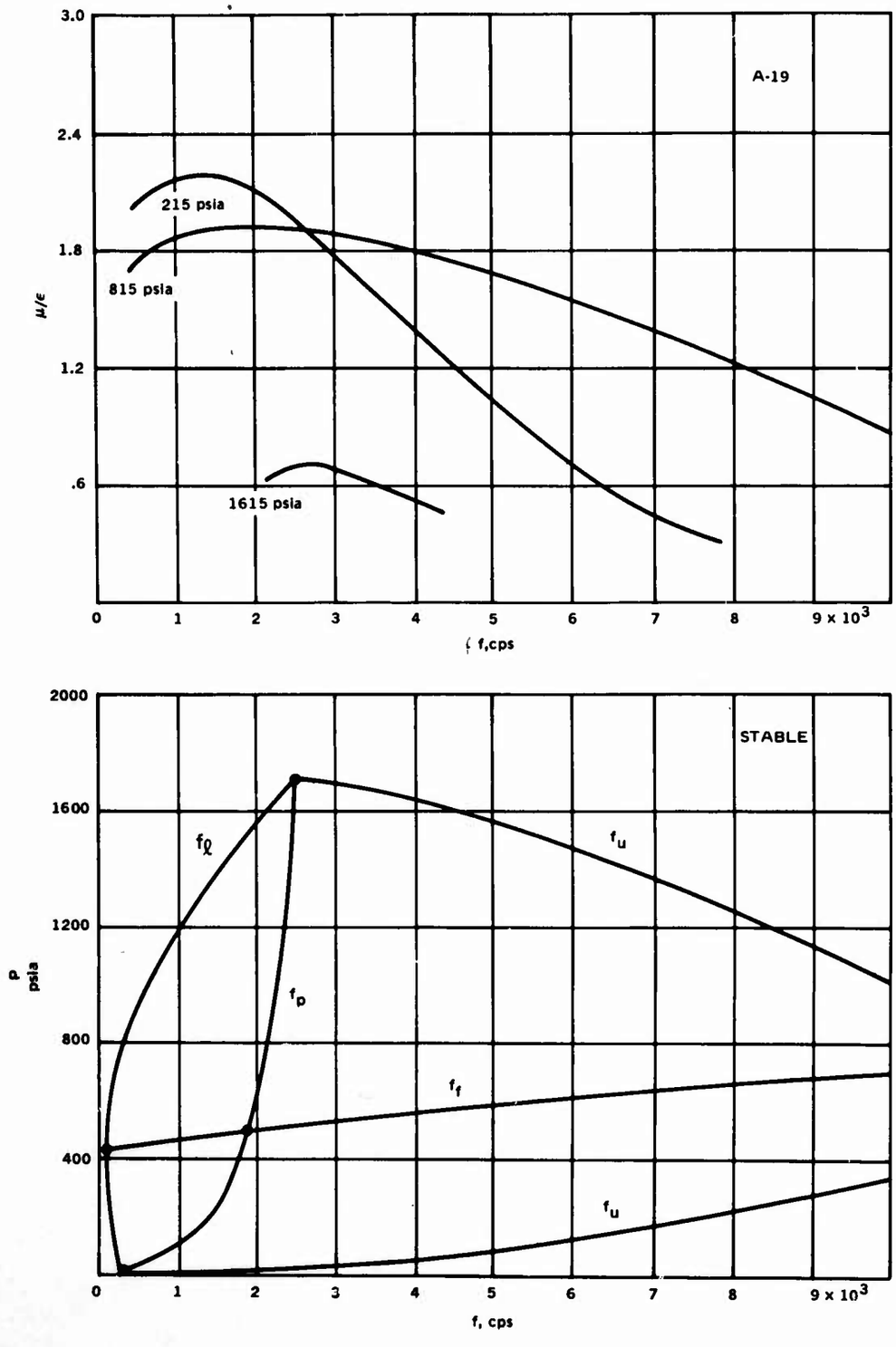

Response Function Results and Neutral Boundary for A-19 Propellant.

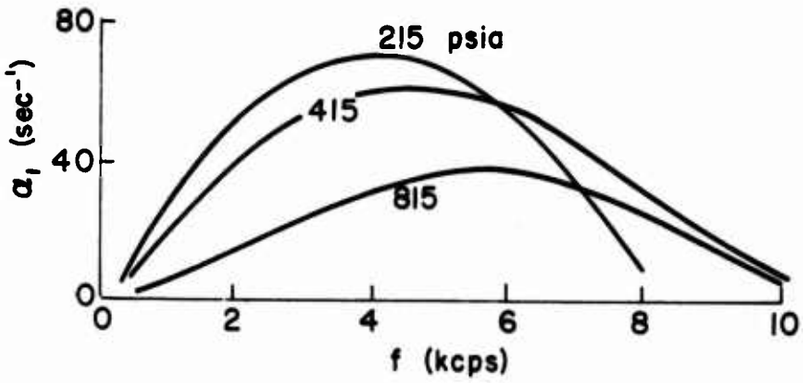

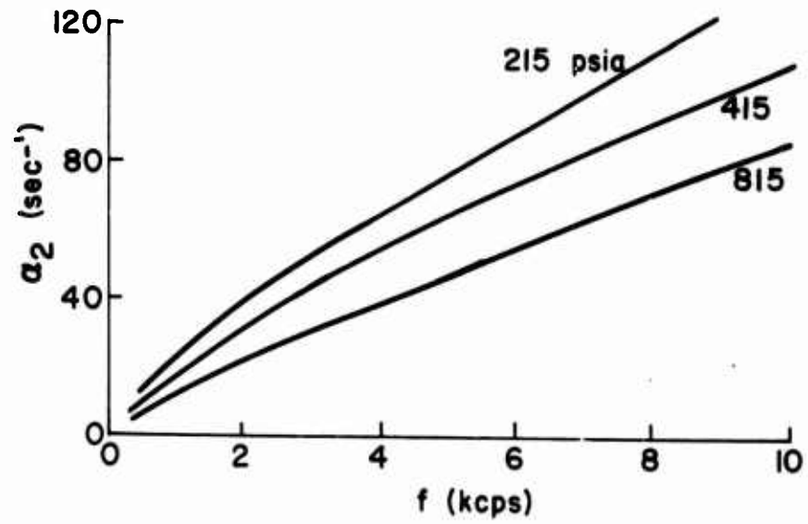

Propellant (25) T-35			
Composition	Ballistic Data		
Binder. . . . PS, 26%	Pressure, psia. . . 215	415	815
Aluminum. . . None	r, in/sec 44	.56	.72
Oxidizer. . . AP(15μ), 71%	P/r 488	741	1132
Catalyst. . . MgO, 1% FeO, 2%	c, in/sec 35,200	36,300	37,600
	Kr. 21.6	31.8	46.9

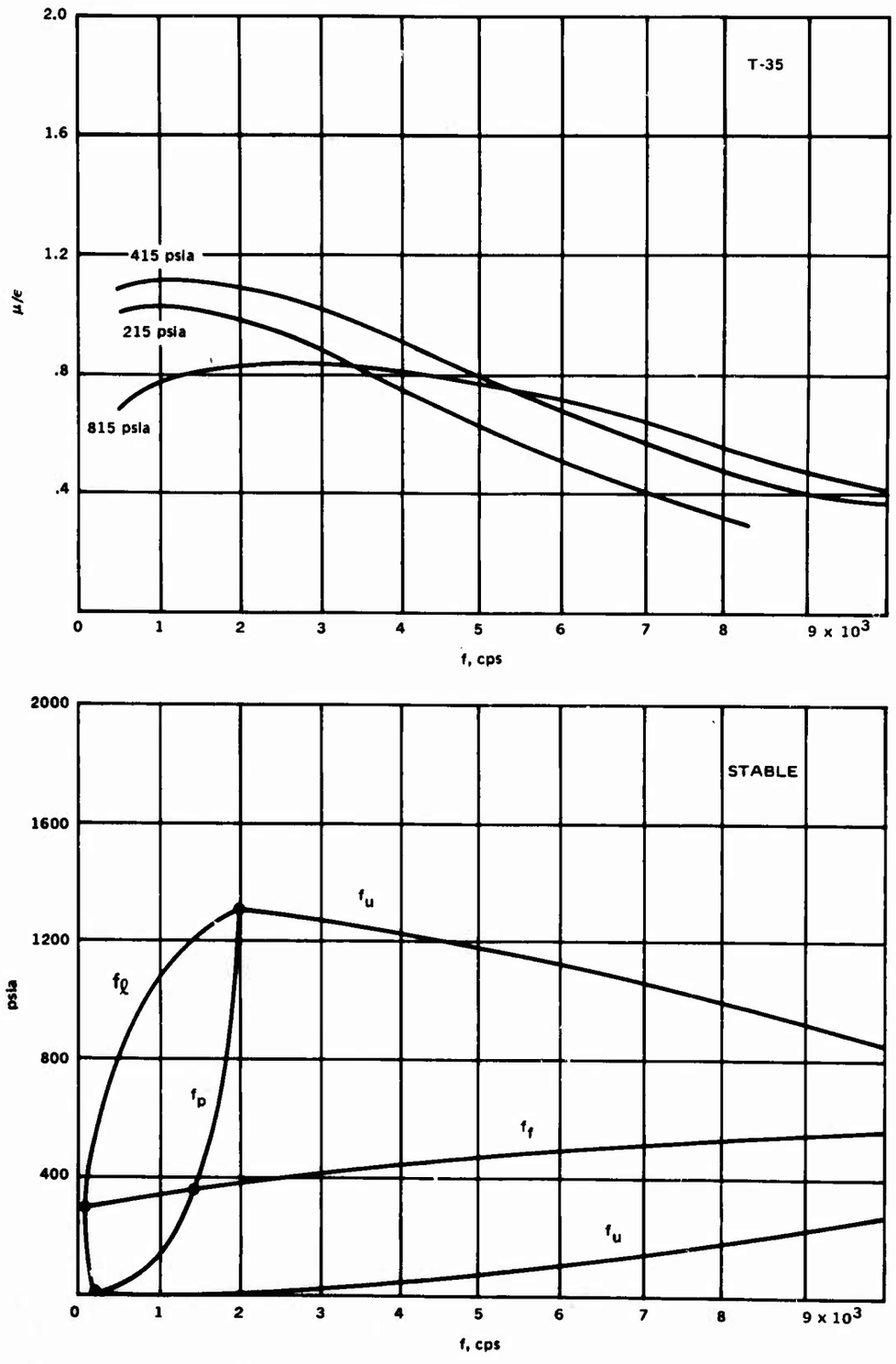

Response Function Results and Neutral Boundary for T-35 Propellant.

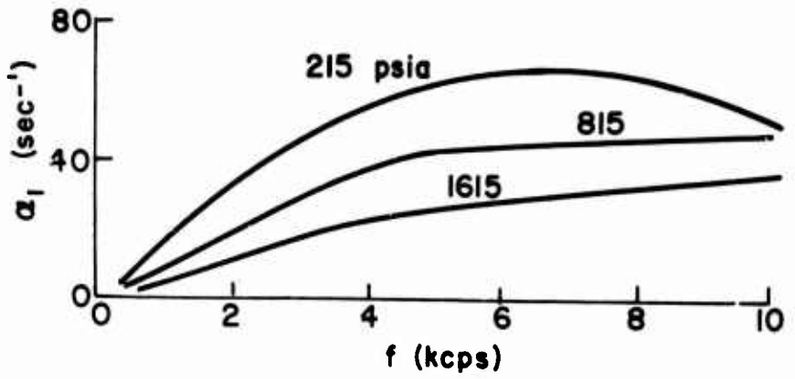

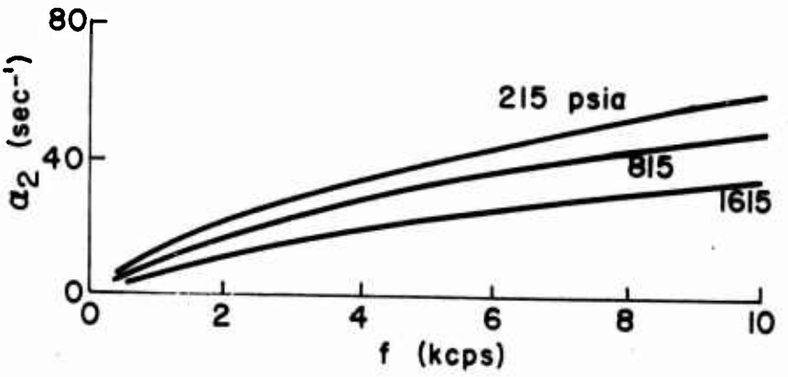

Propellant (32) N-4			
Ballistic Data			
Pressure, psia. . .	215	815	1615
r, in/sec	.17	.34	.48
P/r	1265	2397	3365
c, in/sec	34,600	36,300	37,800
Kr.	62.9	114.0	153.4

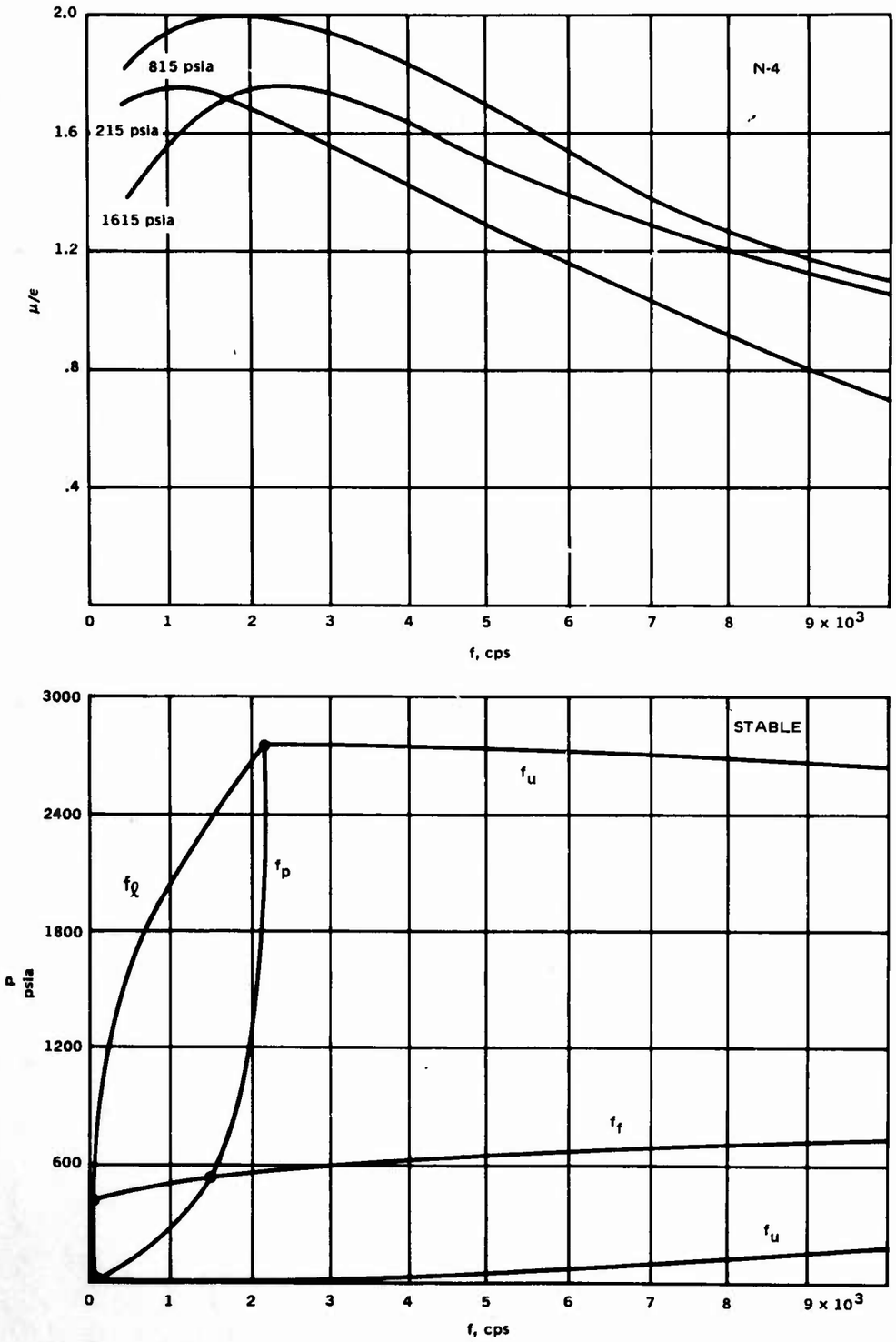

Response Function Results and Neutral Boundary for N-4 Propellant.

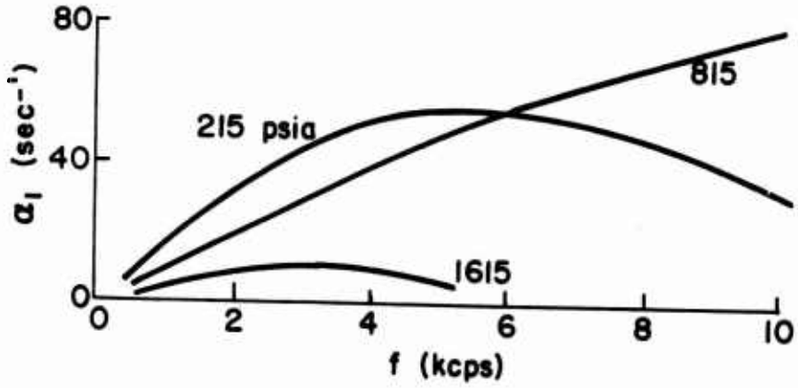

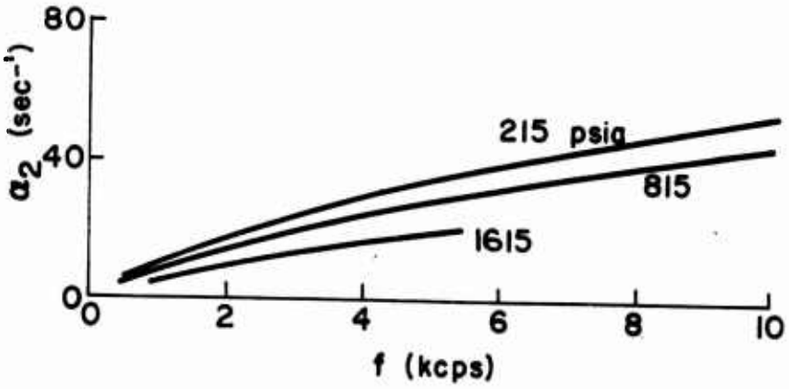

Propellant (33) N-5			
Ballistic Data			
Pressure, psia. . .	215	815	1615
r, in/sec	.16	.44	.41
P/r	1344	1852	3939
c, in/sec	34,700	38,200	37,500
Kr.	66.7	83.6	181.1

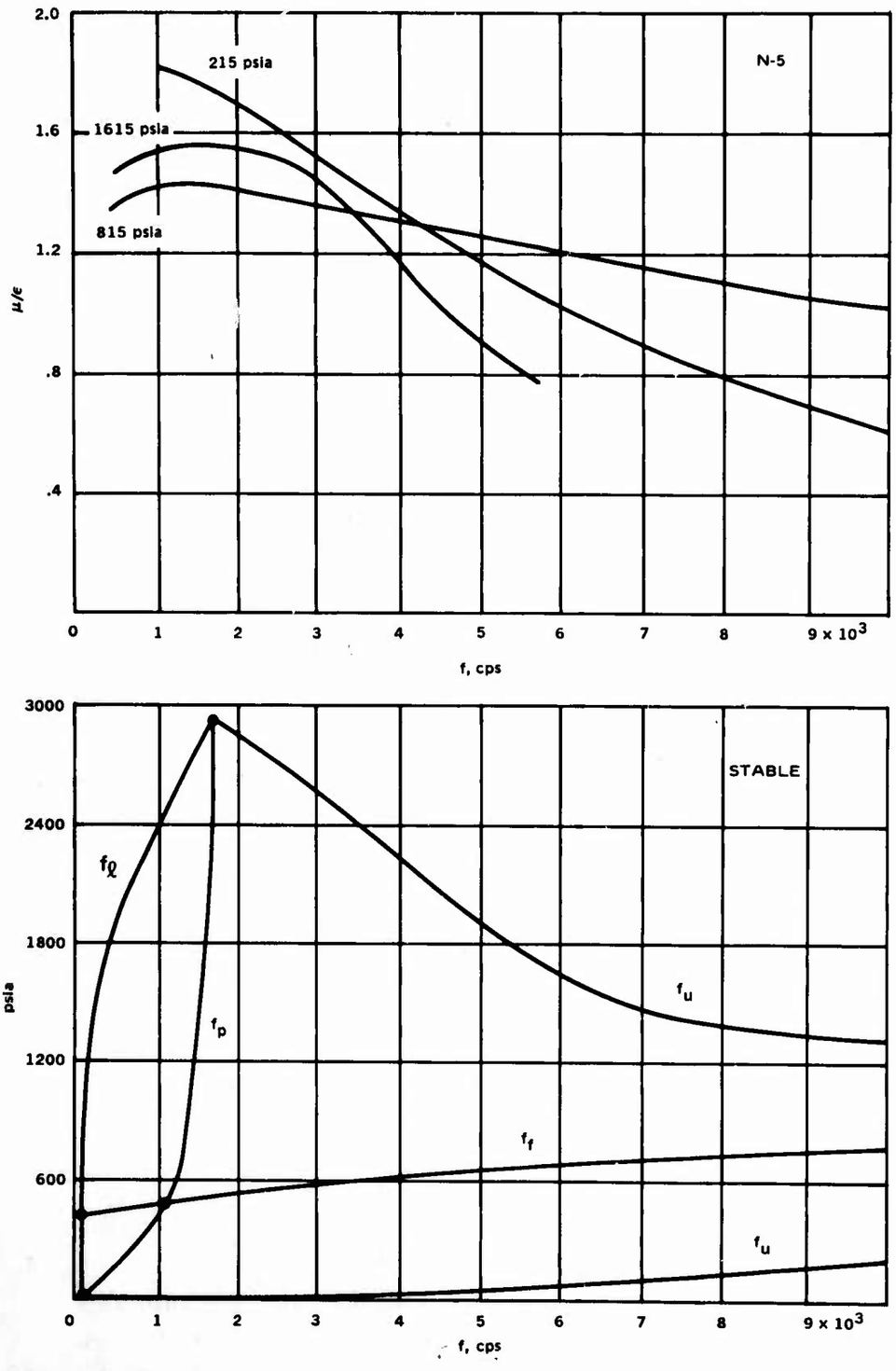

Response Function Results and Neutral Boundary for N-5 Propellant.

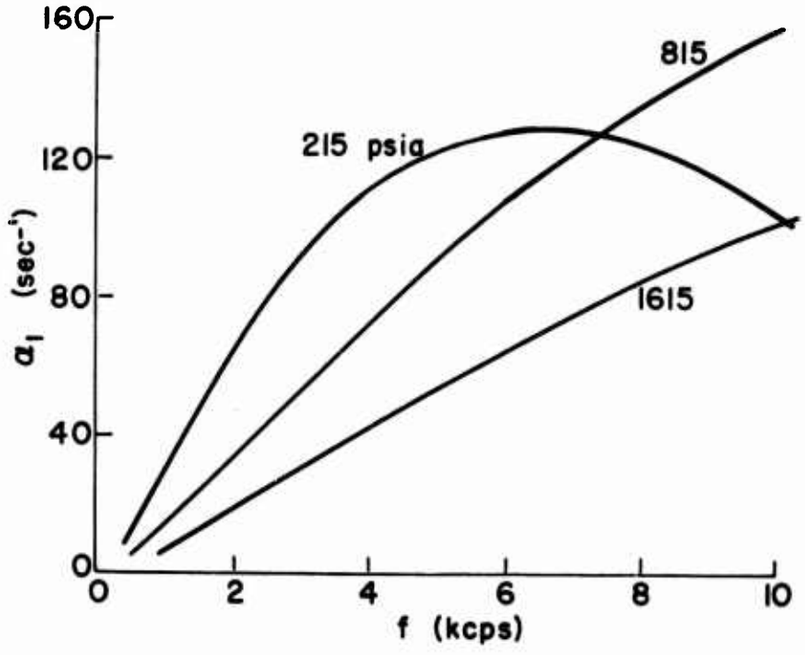

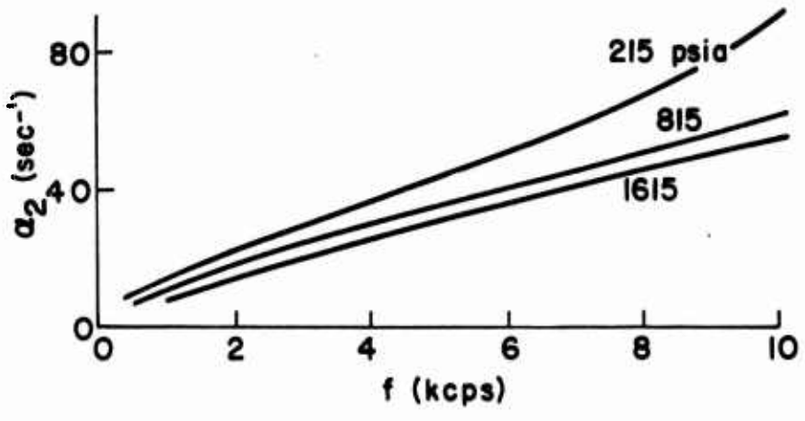

Propellant (34) JPN			
Ballistic Data			
Pressure, psia. . .	215	815	1615
r, in/sec	.22	.55	.89
P/r	977	1473	1815
c, in/sec	37,400	38,200	39,000
Kr.	42.6	63.4	75.9

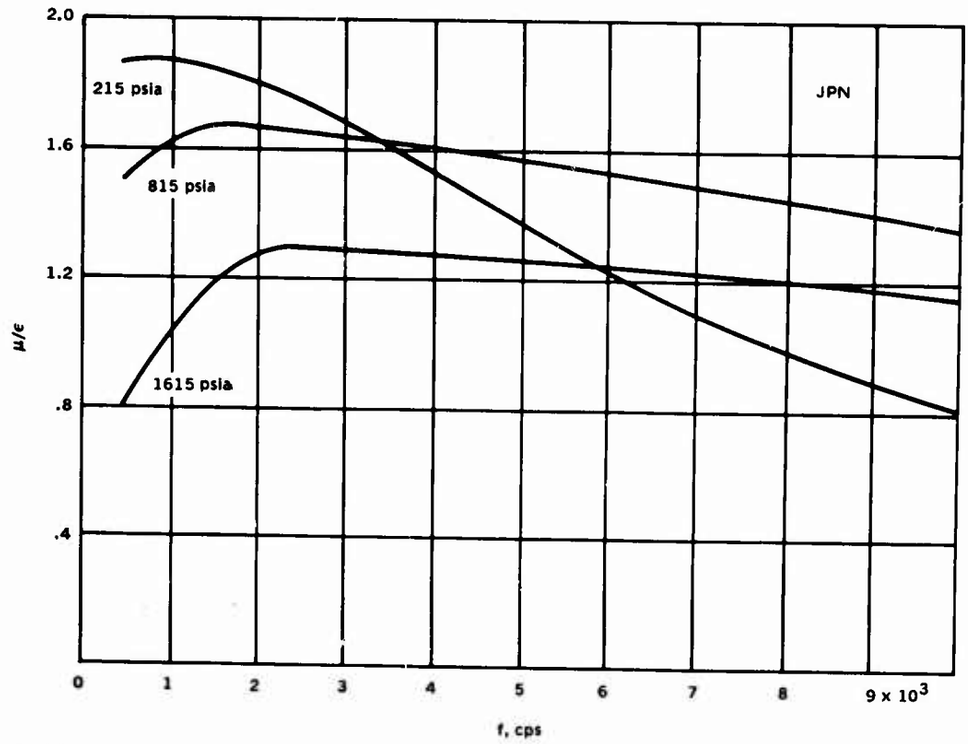

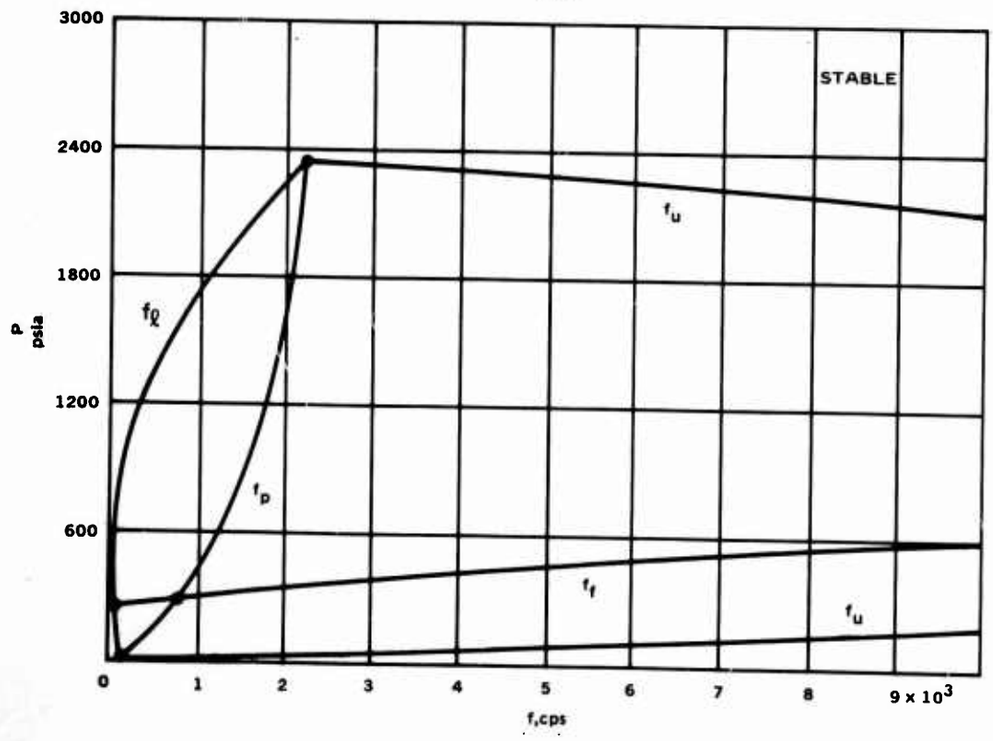

Response Function Results and Neutral Boundary for JPN Propellant.

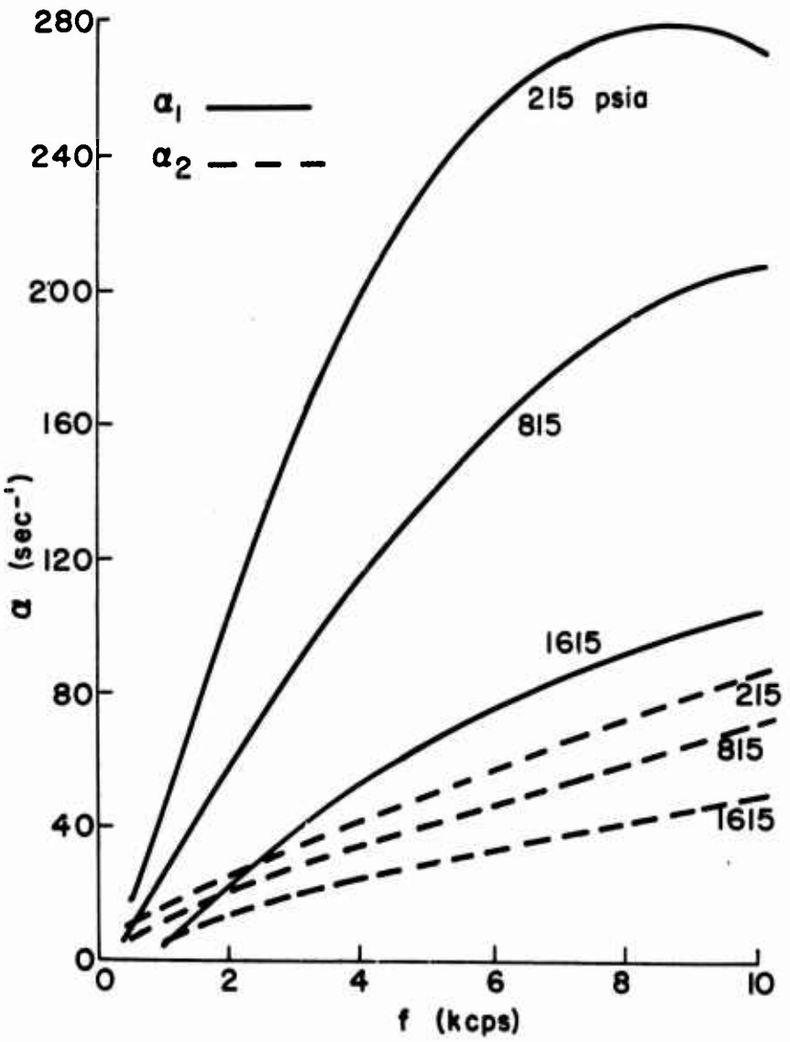

Propellant (35) X-14			
Ballistic Data			
Pressure, psia. . .	215	815	1615
r, in/sec	.51	.93	1.08
P/r	421	876	1495
c, in/sec	38,000	38,800	39,100
Kr.	18.5	37.5	63.6

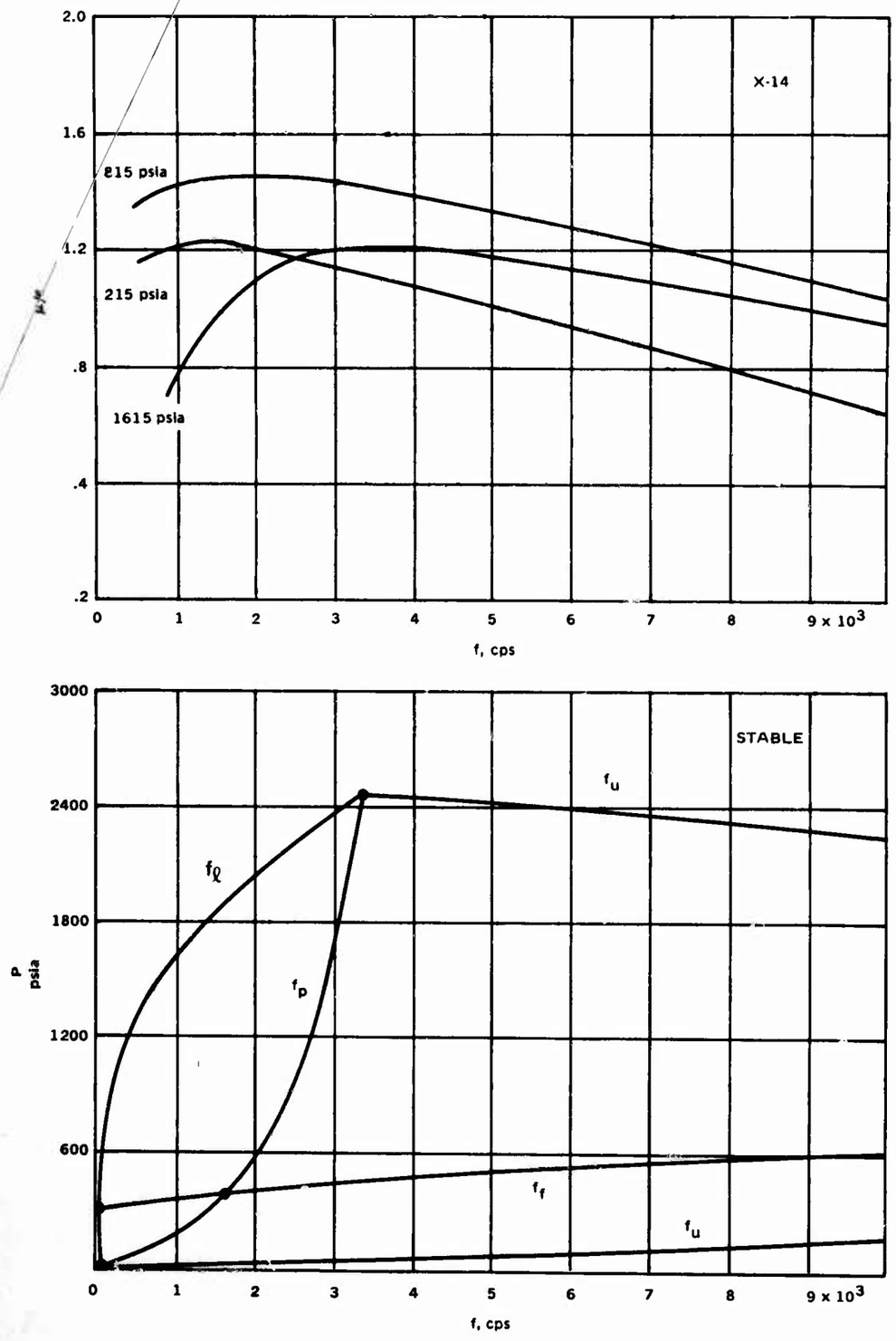

Response Function Results and Neutral Boundary for X-14 Propellant.

Appendix C

CHARACTERIZATION OF THE STABILITY LIMIT AND $[\partial(\mu/\epsilon)/\partial f]_p$, $[\partial(\mu/\epsilon)/\partial p]_f = 0$ CURVES

Experience with the 1.5-inch diameter T-burner has shown that, at any given mean pressure, there is a limited frequency range in which $\alpha_1 > 0$, and at any given frequency (burner length) there is a limited pressure range in which $\alpha_1 > 0$. While the cost and accuracy of determination of the $\alpha = 0$ stability limit has previously discouraged determination of the limit, the present investigation has explored this subject as thoroughly as the need seems to warrant. This investigation included an analytical representation of the stability limit designed to extract as much information as possible from the rather limited data available.

The stability limit is characterized by upper and lower pressure limits P_c and P_o beyond which the burner is stable for all lengths (frequencies) (Fig. 7). Likewise there are upper and lower frequencies f_c and f_o, beyond which the burners are stable at all pressures. Joining the points P_c and P_o is a curve (designated f_p in Fig. 7) indicating the frequencies for maximum response function, at each pressure, $[\partial(\mu/\epsilon)/\partial f]_p = 0$; and a corresponding curve (designated f_f) joining points f_n and f_m is the locus of pressures for maximum μ/ϵ for each frequency, $[\partial(\mu/\epsilon)/\partial p]_f = 0$. The intersection of these curves in the unstable region (point designated P*, f*) is the condition for maximum response function.

A study of stability limit data obtained from test series at various mean pressures showed that the upper frequency, f_u, for $x = 0$ could be correlated with pressure, by a linear relation between f_u/r^2 and P_u. Accordingly, this functional form was adopted for correlation of all upper frequency limit data. The detailed form was modified for convenience to represent the upper and lower absolute pressure limits, P_c and P_o, and the upper frequency limit, f_m, as singular points:

$$\frac{f_u}{r^2} = \frac{f_o}{r_o^2}\left(\frac{P_c - P}{P_c - P_o}\right) + \frac{f_c}{r_c^2}\left(\frac{P_o - P}{P_o - P_c}\right) \tag{41}$$

The forms showing P_m and f_m as singular points are determined by solving Eq. 41 for P, setting $\partial P/\partial f = \infty$, and using the result to obtain P_m from the equation for P. The result, using also the burning rate relation $r = CP^n$, is

$$P_m = \left(\frac{2n}{1+2n}\right)\left(\frac{f_o r_c^2 P_c - f_c r_o^2 P_o}{f_o r_c^2 - f_c r_o^2}\right) \tag{42}$$

which is approximated by the simpler form

$$P_m = \left(\frac{2n}{1+2n}\right) P_c \tag{43}$$

for the combinations of $f_c r_o^2 P_o$ with $f_o r_c^2 P_c$ and of $f_c r_o^2$ with $f_o n_c^2$ encountered in this work. Corresponding forms for the frequency at maximum are

$$f_m = \frac{r_m^2}{2n}\left(\frac{f_o}{r_o^2} - \frac{r_c}{r_c^2}\right)\left(\frac{P_m}{P_c - P_o}\right) \tag{44}$$

and

$$f_m = \frac{1}{1+2n}\left(\frac{r_m}{r_o}\right)^2 r_o \tag{45}$$

A study of the experimental data for the low frequency limit data lead to correlation by the function

$$f_\ell = f_o\left(\frac{P_c - P}{P_c - P_o}\right)^3 + r_c\left(\frac{P - P_o}{P_c - P_o}\right)^3 \tag{46}$$

Most of the experimental f_ℓ values seem to indicate an exponent for the pressure terms somewhat smaller than 3, but taking into account the uncertainty due to data scattering, the exponent 3 provides a more conservative estimate. The terminal point (P_n, f_n), where f_n is the lowest frequency sustaining unstable burning and P_n the corresponding pressure, is calculated by applying the condition for minimum, $df_\ell/dP = 0$, to Eq. 46. The equation for P_n becomes

$$P_n = \frac{P_c\left[(f_o f_c)^{1/2} - f_o\right] + P_o\left[f_c - (f_o f_c)^{1/2}\right]}{(f_c - f_o)} \tag{47}$$

and the approximate solution for f_n is given by

$$f_n = f_o \left[\frac{f_c - (f_o f_c)^{\frac{1}{2}}}{f_c - f_o}\right]^3 + f_c \left[\frac{(f_o f_c)^{\frac{1}{2}} - f_o}{f_c - f_o}\right]^3 \tag{48}$$

The locus lines $[\partial(\mu/\epsilon)/\partial f]_p = 0$ and $[\partial(\mu/\epsilon)/\partial p]_f = 0$ were assumed (after examination of available data) to be of the form

$$f_p = f_o \left(\frac{r}{r_o}\right)\left(\frac{P_c - P}{P_c - P_o}\right) + f_c \left(\frac{r}{r_c}\right)\left(\frac{P - P_o}{P_c - P_o}\right) \tag{49}$$

and

$$f_f = f_n \left(\frac{r}{r_n}\right)\left(\frac{P_m - P}{P_m - P_n}\right) + f_m \left(\frac{r}{r_m}\right)\left(\frac{P - P_n}{P_m - P_n}\right) \tag{50}$$

where the functional form has been chosen so that the curves go through the points (f_c, P_c) and (f_o, P_o) in one case and (f_n, P_n) and (P_m, P_m) in the other case. Sample curves are shown in Fig. 6.

The intersection of the $[\partial(\mu/\epsilon)/\partial f]_p = 0$ and $[\partial(\mu/\epsilon)/\partial P]_f = 0$ curves is the point of maximum response function, denoted here by (f* P*). This intersection could be calculated by graphical means, or estimates could be made with the approximate relations

$$P^* = \frac{1-n}{2} P_c$$

$$f^* = \frac{1+n}{2} \frac{r^*}{r_o} f_o$$

Appendix D

MAXIMUM ACOUSTIC PRESSURE $(\Delta P)_m$, PSIA, AND $(\Delta P)_m/P$ RATIOS

A-13			A-14			A-15		
f	$(\Delta P)_m$	$(\Delta P)_m/P$	f	$(\Delta P)_m$	$(\Delta P)_m/P$	f	$(\Delta P)_m$	$(\Delta P)_m/P$
215 psia			215 psia			215 psia		
500	16	.075	500	20	.093	500	14	.065
1,000	28	.130	1,000	39	.182	1,000	26	.120
2,000	35	.164	2,000	50	.232	2,000	36	.168
3,000	30	.140	3,000	54	.251	3,000	36	.168
4,000	18	.084	4,000	53	.246	4,000	33	.154
5,000	7	.033	5,000	49	.228	5,000	29	.135
6,000	S	--	6,000	44	.205	6,000	24	.112
			7,000	38	.177	7,000	19	.088
			8,000	33	.154	8,000	13	.061
			9,000	28	.130	9,000	8	.037
			10,000	23	.107	10,000	4	.019
415 psia			815 psia			415 psia		
500	12	.029	500	11	.014	500	9	.022
1,000	22	.053	1,000	27	.033	1,000	19	.046
2,000	33	.079	2,000	46	.057	2,000	34	.082
3,000	38	.091	3,000	58	.071	3,000	40	.096
4,000	34	.082	4,000	65	.080	4,000	38	.092
5,000	25	.060	5,000	69	.085	5,000	35	.084
6,000	14	.034	6,000	72	.088	6,000	30	.072
7,000	4	.010	7,000	71	.087	7,000	25	.060
8,000	S	--	8,000	67	.082	8,000	21	.051
			9,000	64	.079	9,000	17	.041
			10,000	59	.072	10,000	12	.029
815 psia			1615 psia			815 psia		
500	S	--	1,000	S	--			
1,000	5	.006	1,500	18	.011	1,500	S	--
2,000	12	.015	2,000	44	.027	2,000	2	.008
3,000	12	.015	3,000	78	.049	3,000	8	.010
4,000	9	.011	4,000	100	.062	4,000	4	.005
5,000	5	.006	5,000	112	.069	5,000	S	--
6,000	2	.003	6,000	116	.072			
7,000	S	--	7,000	114	.071			
			8,000	106	.065			
			9,000	96	.059			
			10,000	87	.054			

A-16			A-17			A-18		
f	$(\Delta P)_m$	$(\Delta P)_m/P$	f	$(\Delta P)_m$	$(\Delta P)_m/P$	f	$(\Delta P)_m$	$(\Delta P)_m/P$
215 psia			215 psia			215 psia		
500	15	.070	500	13	.061	500	20	.093
1,000	28	.130	1,000	21	.098	1,000	31	.144
2,000	42	.196	2,000	24	.112	2,000	38	.177
3,000	48	.224	3,000	18	.084	3,000	42	.195
4,000	51	.237	4,000	9	.042	4,000	41	.190
5,000	50	.233	5,000	S	--	5,000	39	.181
6,000	47	.219				6,000	34	.158
7,000	42	.196				7,000	28	.130
8,000	36	.168				8,000	22	.102
9,000	31	.144				9,000	16	.074
10,000	27	.126				10,000	11	.051
415 psia			415 psia			815 psia		
500	4	.010	500	8	.019	500	4	.005
1,000	15	.036	1,000	17	.041	1,000	12	.015
2,000	31	.075	2,000	26	.063	2,000	27	.033
3,000	42	.101	3,000	25	.060	3,000	40	.049
4,000	49	.118	4,000	19	.046	4,000	50	.061
5,000	54	.130	5,000	12	.029	5,000	57	.070
6,000	58	.140	6,000	6	.014	6,000	60	.073
7,000	60	.145	7,000	S	--	7,000	59	.072
8,000	59	.142				8,000	56	.069
9,000	57	.138				9,000	52	.064
10,000	50	.121				10,000	46	.056
815 psia			815 psia			1615 psia		
			500	4	.005	500	S	--
			1,000	8	.010	1,000	5	.003
2,500	S	--	2,000	12	.015	2,000	18	.011
3,000	4	.005	3,000	11	.014	3,000	28	.017
4,000	14	.017	4,000	8	.010	4,000	32	.019
5,000	19	.023	5,000	6	.007	5,000	34	.021
6,000	21	.026	6,000	3	.004	6,000	34	.021
7,000	21	.026	7,000	S	--	7,000	33	.020
8,000	19	.023				8,000	30	.018
9,000	17	.021				9,000	25	.015
10,000	14	.017				10,000	20	.012

A-19			T-35			N-4		
f	$(\Delta P)_m$	$(\Delta P)_m/P$	f	$(\Delta P)_m$	$(\Delta P)_m/P$	f	$(\Delta P)_m$	$(\Delta P)_m/P$
215 psia			215 psia			215 psia		
500	28	.130	500	16	.075	500	14	.065
1,000	40	.186	1,000	29	.135	1,000	27	.126
2,000	43	.200	2,000	36	.168	2,000	40	.186
3,000	39	.182	3,000	36	.168	3,000	42	.196
4,000	32	.149	4,000	31	.144	4,000	39	.182
5,000	23	.107	5,000	24	.112	5,000	36	.168
6,000	14	.065	6,000	17	.079	6,000	32	.149
7,000	7	.033	7,000	10	.047	7,000	28	.130
8,000	S	--	8,000	4	.019	8,000	23	.107
			9,000	S	--	9,000	19	.088
						10,000	15	.070
815 psia			415 psia			815 psia		
500	13	.016	500	9	.022	500	21	.026
1,000	24	.030	1,000	20	.048	1,000	42	.052
2,000	40	.049	2,000	35	.084	2,000	69	.085
3,000	52	.064	3,000	42	.102	3,000	75	.092
4,000	61	.075	4,000	45	.108	4,000	78	.095
5,000	66	.081	5,000	43	.104	5,000	77	.094
6,000	68	.084	6,000	39	.094	6,000	74	.091
7,000	67	.082	7,000	34	.082	7,000	68	.083
8,000	64	.079	8,000	27	.065	8,000	62	.076
9,000	60	.074	9,000	20	.048	9,000	54	.066
10,000	54	.066	10,000	10	.024	10,000	46	.056
1615 psia			815 psia			1615 psia		
			500	2	.002	500	3	.002
			1,000	11	.014	1,000	31	.019
2,000	S	--	2,000	27	.033	2,000	105	.065
2,500	10	.006	3,000	40	.049	3,000	144	.089
3,000	9	.006	4,000	49	.060	4,000	148	.092
3,500	6	.004	5,000	50	.062	5,000	140	.087
4,000	3	.002	6,000	46	.057	6,000	122	.076
4,500	S	--	7,000	40	.049	7,000	100	.062
			8,000	32	.040	8,000	80	.050
			9,000	23	.028	9,000	63	.039
			10,000	12	.015	10,000	41	.026

N-5			JPN			X-14		
f	$(\Delta P)_m$	$(\Delta P)_m/P$	f	$(\Delta P)_m$	$(\Delta P)_m/P$	f	$(\Delta P)_m$	$(\Delta P)_m/P$
215 psia			215 psia			215 psia		
500	18	.084	500	23	.107	500	24	.112
1,000	32	.149	1,000	33	.154	1,000	33	.154
2,000	37	.172	2,000	38	.177	2,000	40	.186
3,000	35	.162	3,000	38	.177	3,000	43	.200
4,000	31	.144	4,000	36	.167	4,000	43	.200
5,000	27	.126	5,000	34	.158	5,000	42	.196
6,000	22	.102	6,000	32	.149	6,000	40	.186
7,000	18	.084	7,000	29	.135	7,000	38	.177
8,000	14	.065	8,000	25	.116	8,000	34	.158
9,000	9	.042	9,000	20	.093	9,000	30	.140
10,000	6	.028	10,000	15	.070	10,000	26	.121
815 psia			815 psia			815 psia		
500	35	.043	500	28	.035	500	30	.037
1,000	60	.074	1,000	54	.066	1,000	52	.064
2,000	75	.092	2,000	77	.094	2,000	76	.093
3,000	80	.097	3,000	86	.105	3,000	88	.108
4,000	78	.096	4,000	89	.109	4,000	93	.114
5,000	76	.093	5,000	88	.108	5,000	94	.116
6,000	73	.088	6,000	85	.104	6,000	91	.112
7,000	70	.086	7,000	82	.100	7,000	87	.107
8,000	66	.081	8,000	79	.097	8,000	83	.102
9,000	62	.076	9,000	75	.092	9,000	77	.095
10,000	57	.070	10,000	71	.087	10,000	72	.089
1615 psia			1615 psia			1615 psia		
500	21	.013	500	S	--	500	S	--
1,000	60	.037	1,000	24	.015	1,000	22	.014
2,000	72	.045	2,000	70	.043	2,000	86	.053
3,000	63	.039	3,000	104	.064	3,000	124	.077
4,000	42	.026	4,000	125	.077	4,000	150	.093
5,000	20	.012	5,000	143	.087	5,000	173	.107
6,000	S	--	6,000	154	.094	6,000	178	.110
			7,000	160	.097	7,000	175	.108
			8,000	152	.093	8,000	166	.103
			9,000	145	.088	9,000	153	.094
			10,000	135	.082	10,000	134	.082

Appendix E

A-13 PROPELLANT GROWTH AND DECAY CONSTANTS

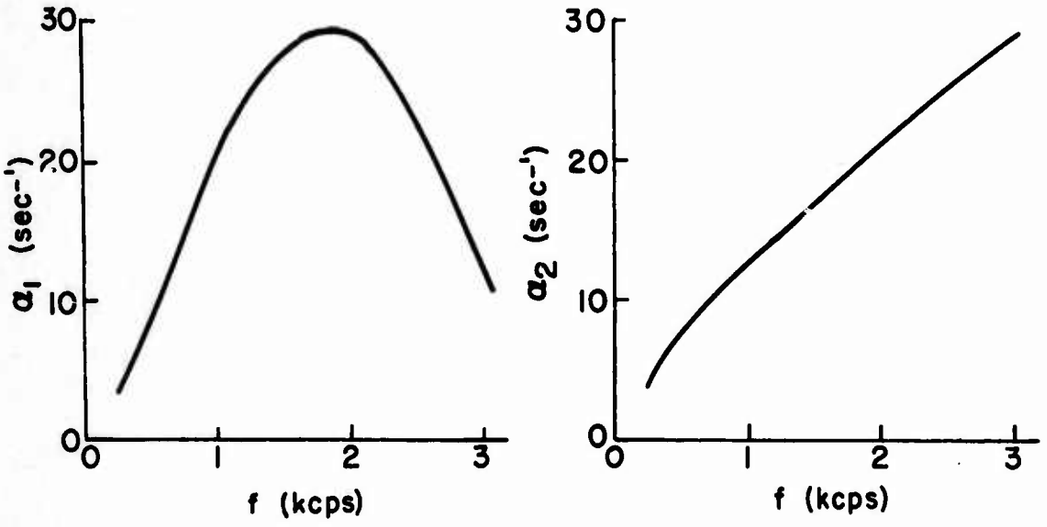

Propellant (17) A-13	
Composition	Ballistic Data
Binder. . . . PBAN, 24%	Pressure, psia. . . 115
Aluminum. . . None	r, in/sec 12
Oxidizer. . . AP(80μ), 76%	P/r 958
Catalyst. . . None	c, in/sec 34,000
	Kr. 47.4

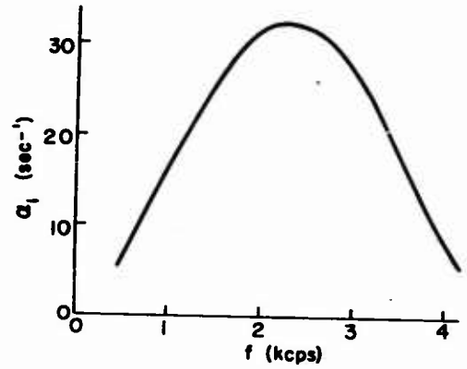

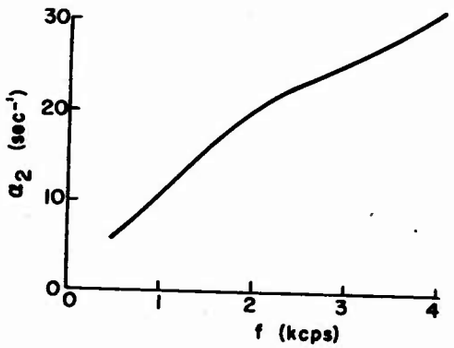

Propellant (17) A-13	
Composition	Ballistic Data
Binder. . . PBAN, 24% Aluminum. . None Oxidizer. . AP(80μ), 76% Catalyst. . None	Pressure, psia. . 165 r, in/sec . . . . .14 P/r . . . . . 1179 c, in/sec . . . .34,700 Kr. 57.0

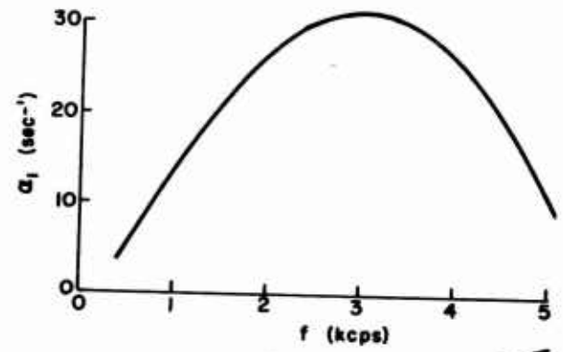

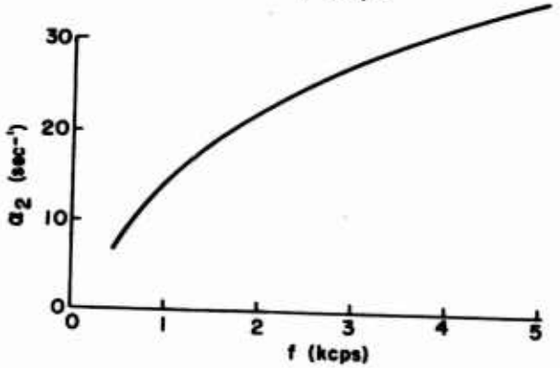

Propellant (17) A-13	
Composition	Ballistic Data
Binder. . . PBAN, 24% Aluminum. . None Oxidizer. . AP(80μ), 76% Catalyst. . None	Pressure, psia. . 215 r, in/sec . . . . .16 P/r . . . . . 1344 c, in/sec . . . .35,400 Kr. 64.1

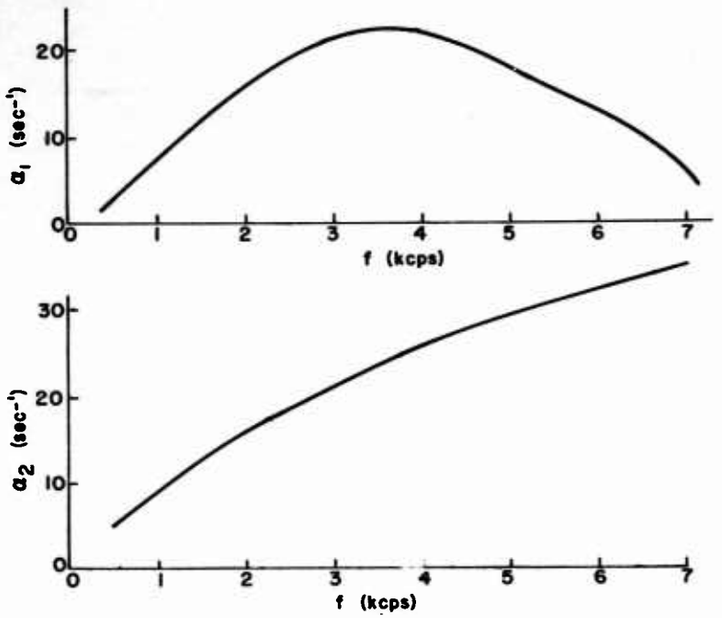

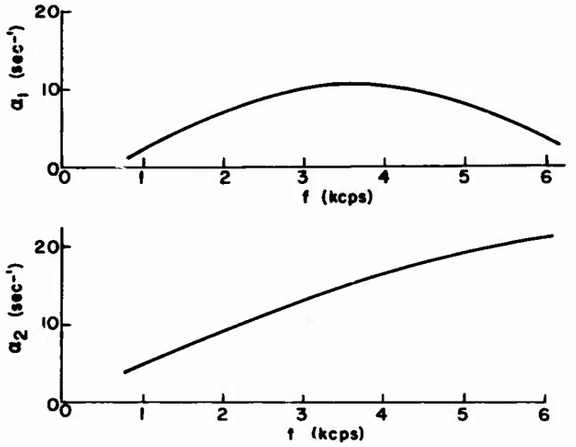

Propellant (17) A-13	
Composition	Ballistic Data
Binder. . . PBAN, 24% Aluminum. . None Oxidizer. . AP(80μ), 76% Catalyst. . None	Pressure, psia. . 415 r, in/sec . . . . .21 P/r . . . . . 1976 c, in/sec . . . .36,700 Kr. 91.2

Propellant (17) A-13	
Composition	Ballistic Data
Binder. . . PBAN, 24% Aluminum. . None Oxidizer. . AP(80μ), 76% Catalyst. . None	Pressure, psia. . 815 r, in/sec . . . . .28 P/r . . . . . 2911 c, in/sec . . . .37,600 Kr. 130.0

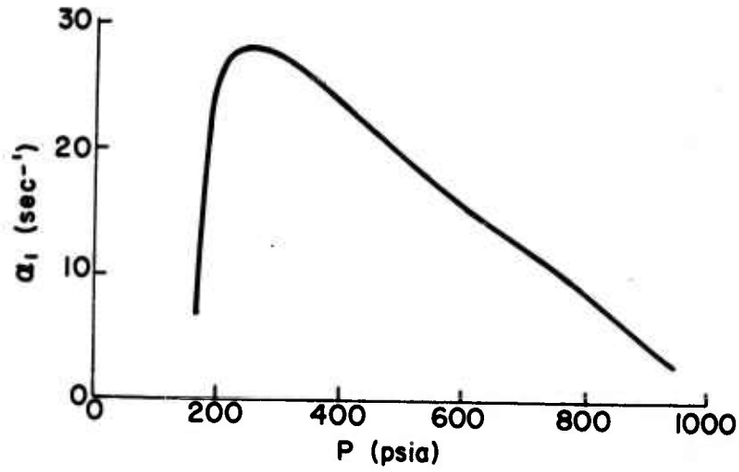

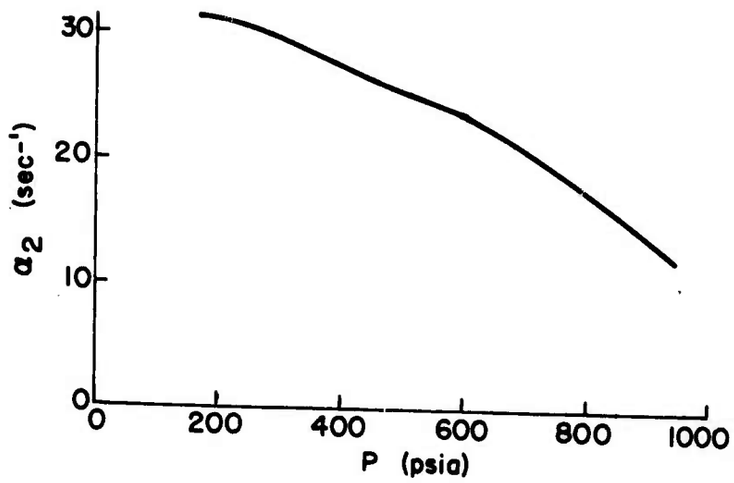

Propellant (17) A-13	
Composition	Ballistic Data
Binder. . . PBAN, 24% Aluminum. . None Oxidizer. . AP(80μ), 76% Catalyst. . None	Frequency, sec^{-1}. . 4200 cps

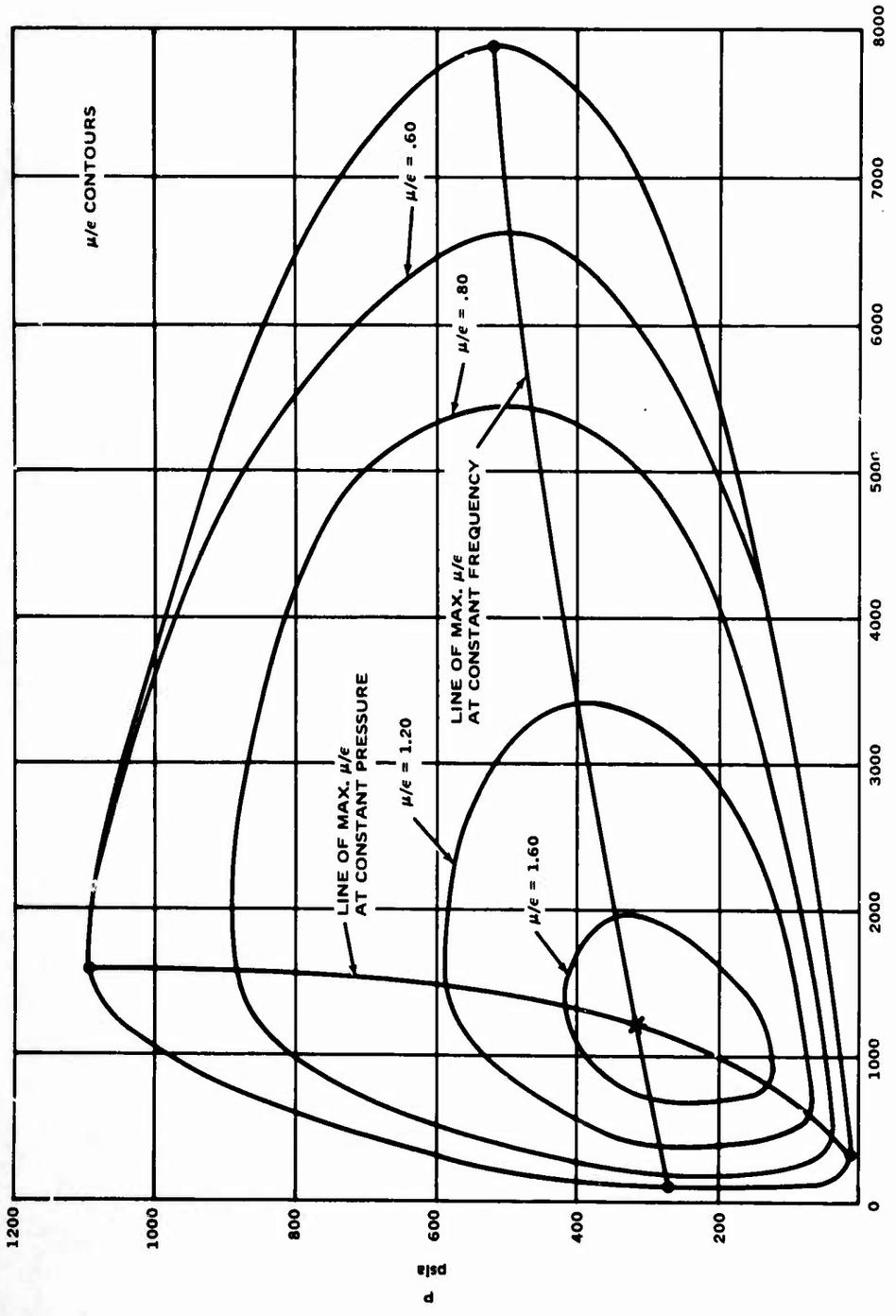

FIG. 16. Isoresponse Function Contours for A-13 Propellant.

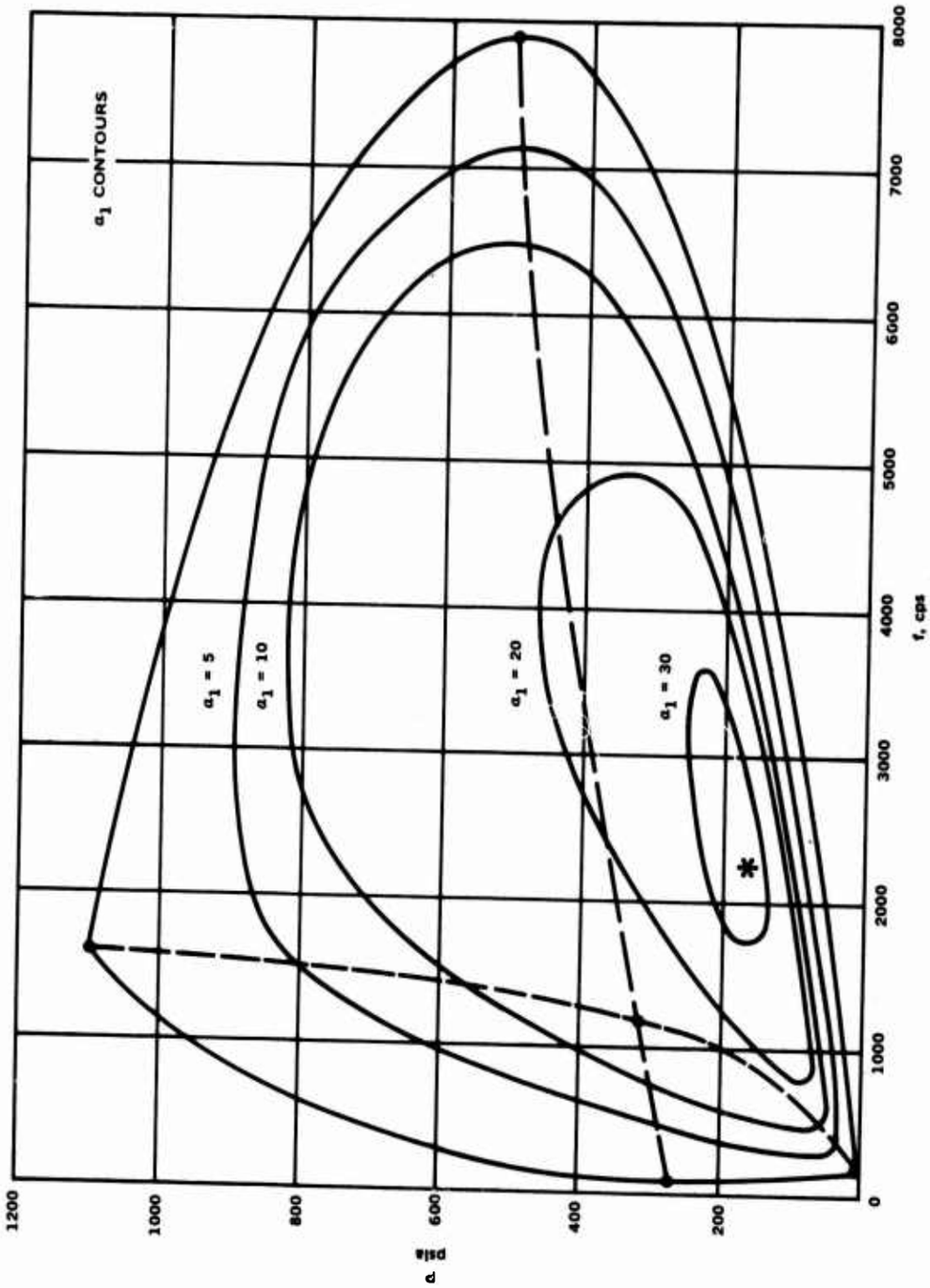

FIG. 17(a). Iso-a_1 Contours for A-13 Propellant.

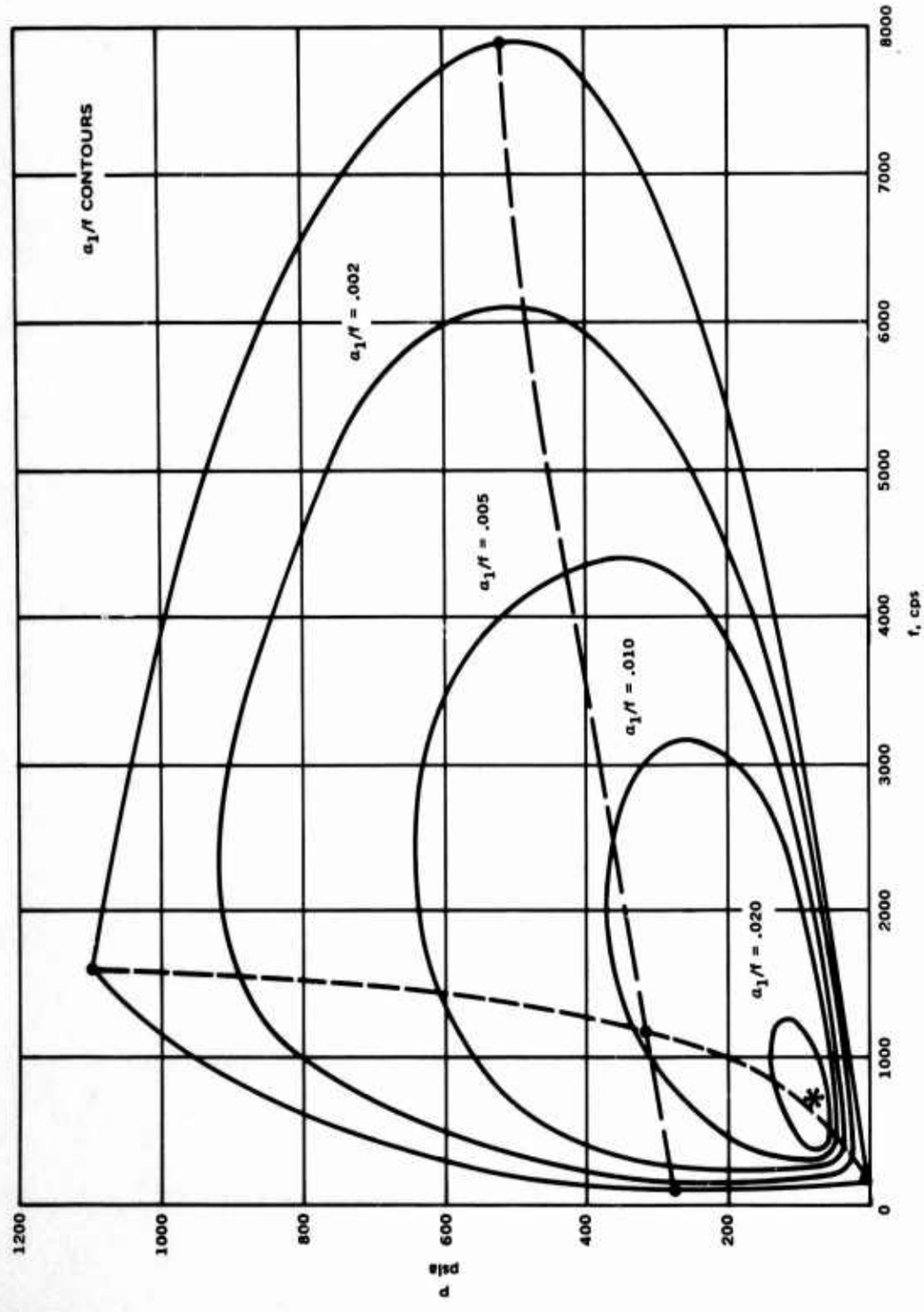

FIG. 17(b). Iso-a_1/f Contours for A-13 Propellant.

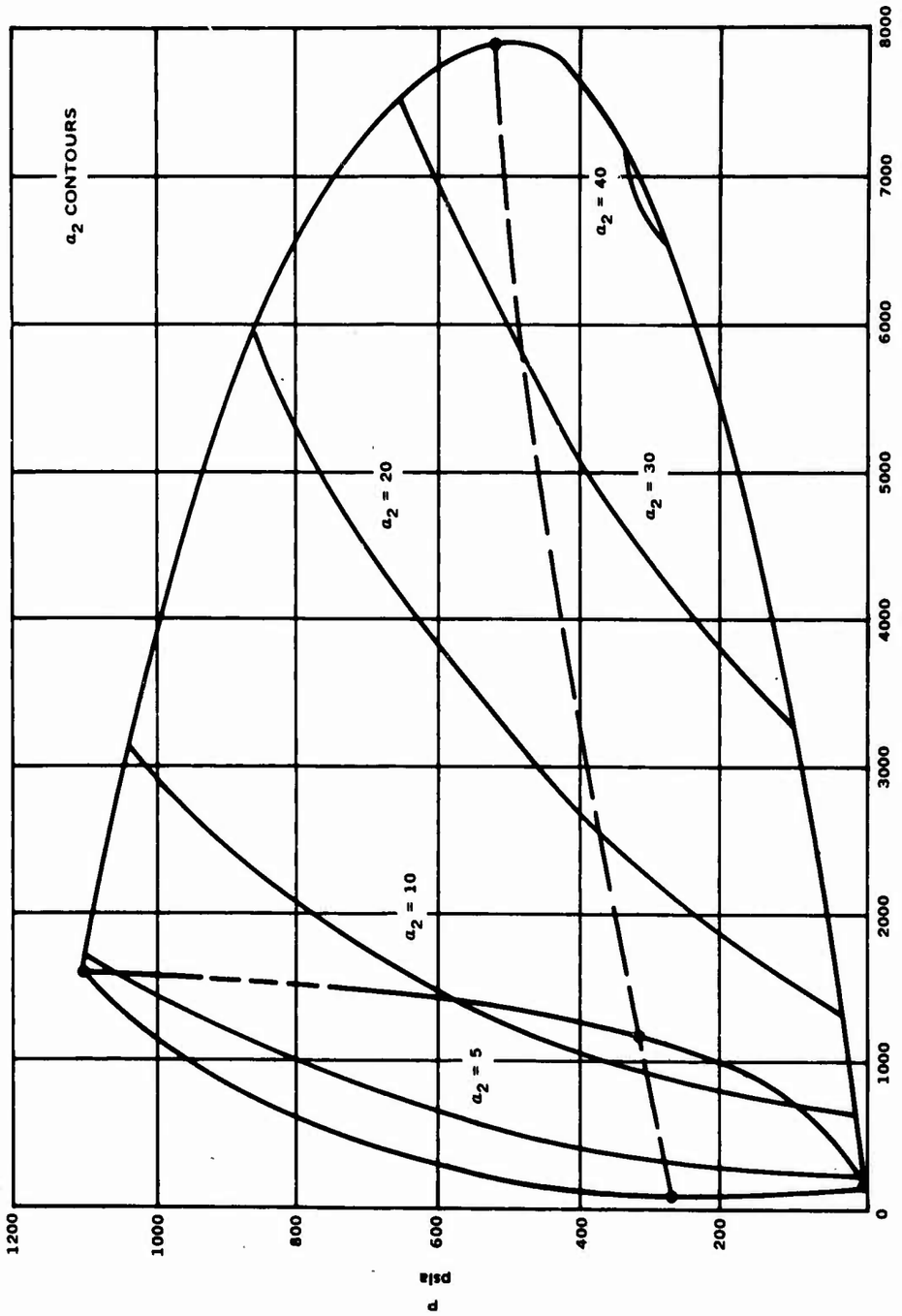

FIG. 18(a). Iso-α_2 Contours for A-13 Propellant.

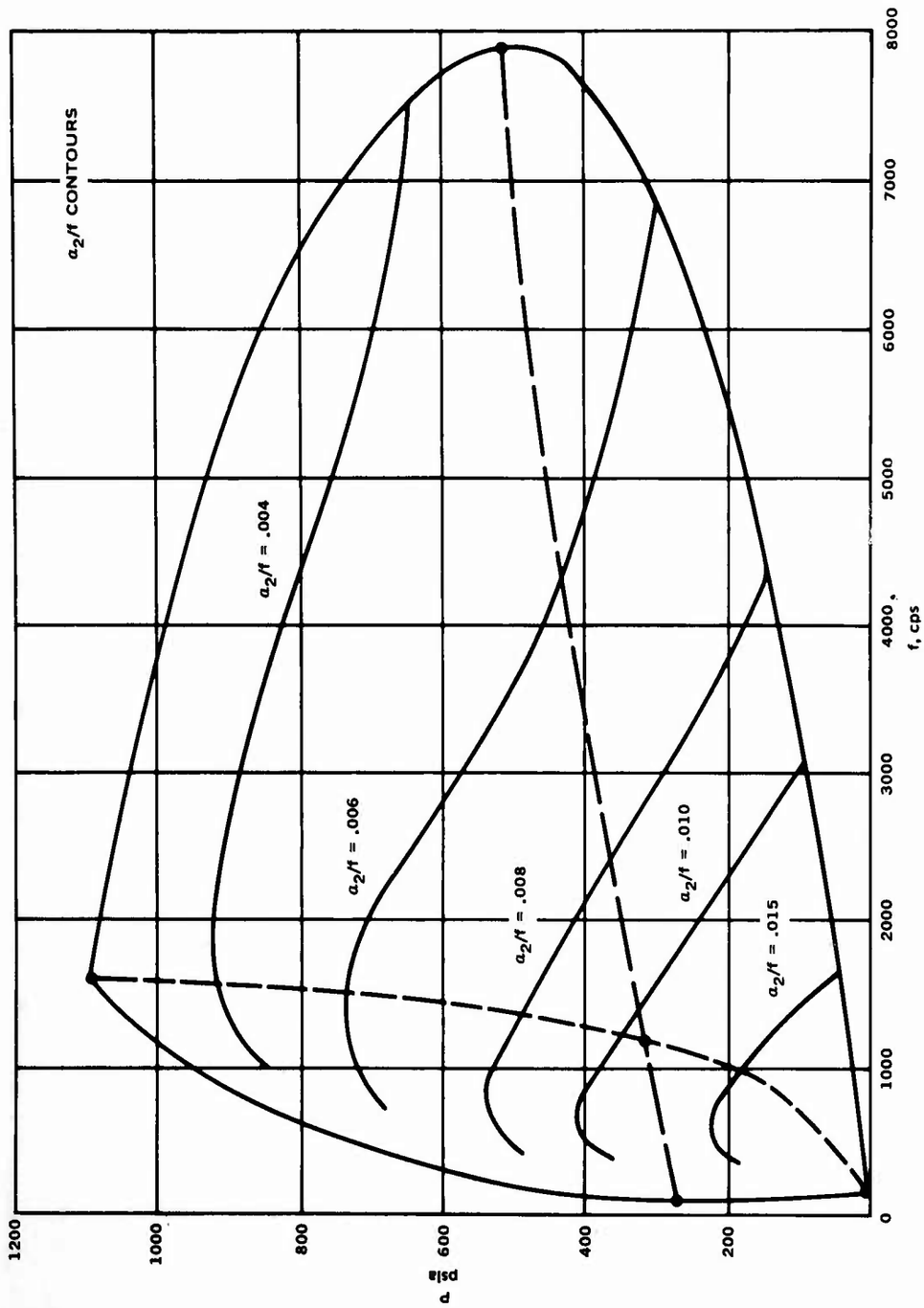

FIG. 18(b). Iso-α_2/f Contours for A-13 Propellant.

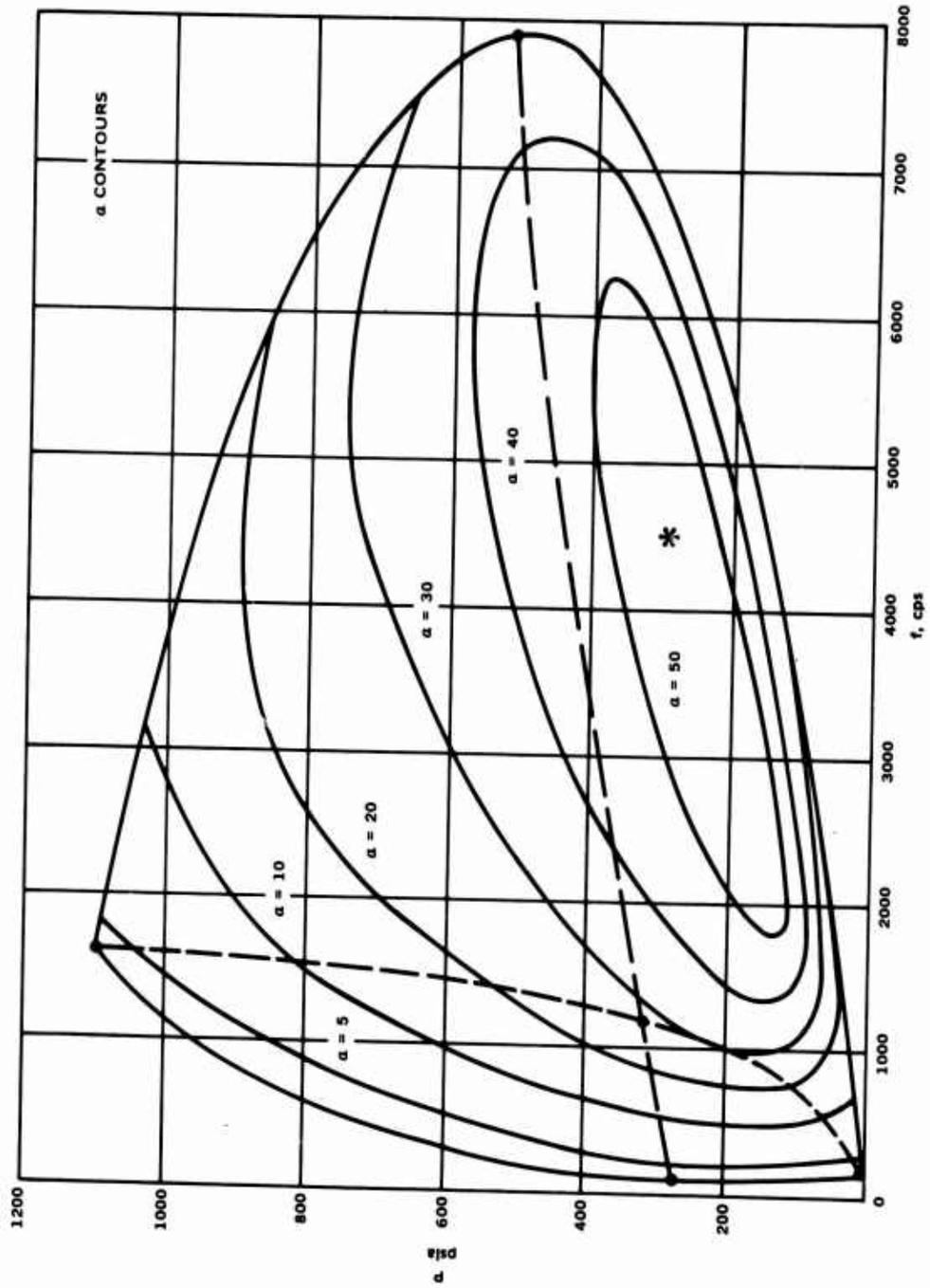

FIG. 19(a). Iso-α Contours for A-13 Propellant.

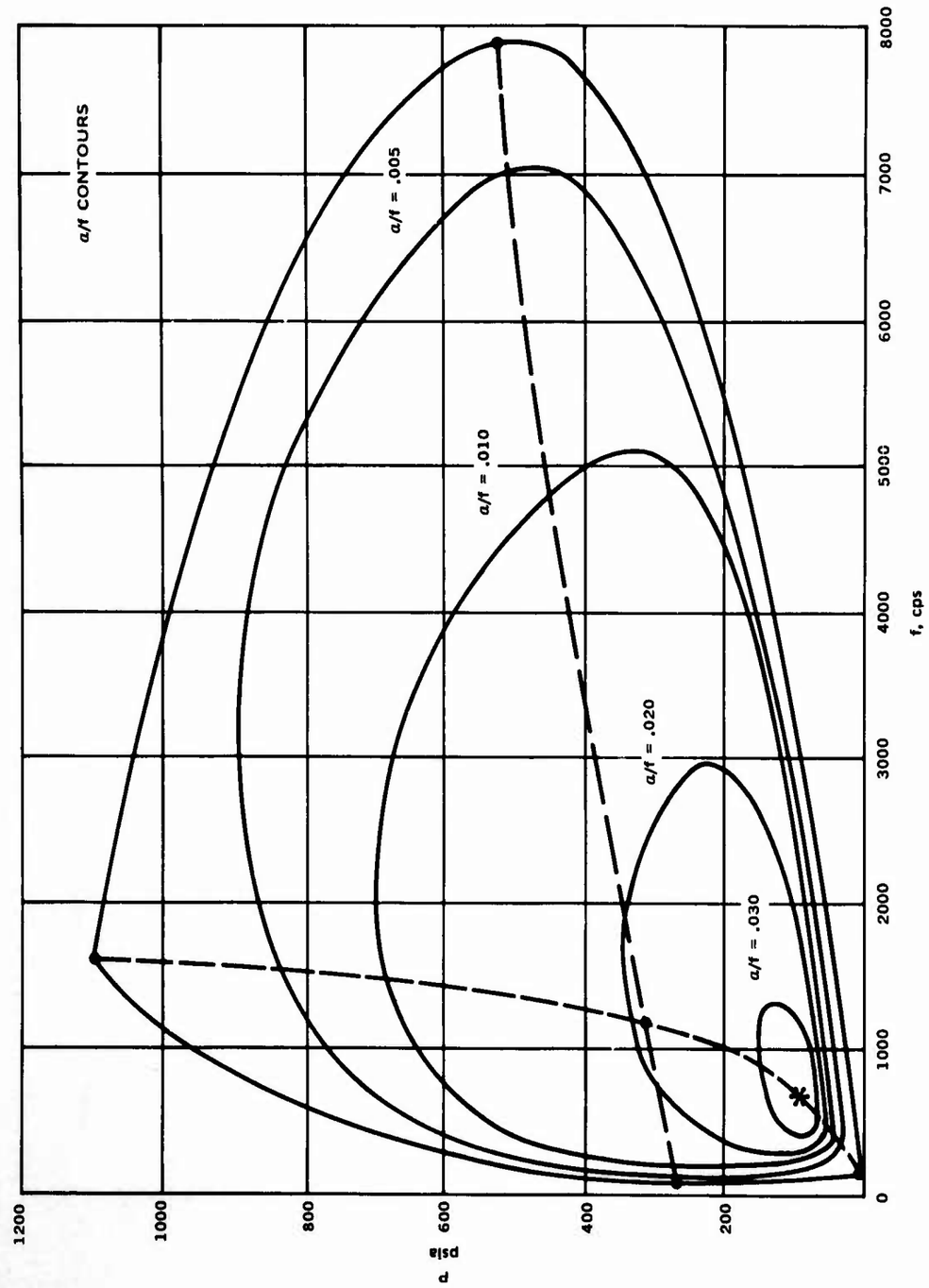

FIG. 19(b). Iso-α/f Contours for A-13 Propellant.

REFERENCES

1. Price, E. W. Experimental Solid Rocket Combustion Instability, in Tenth Symposium (International) on Combustion. Pittsburgh, Pa., Combustion Institute, 1965. Pp. 1067-82.

2. Report of the Committee on Standardization of Combustion Instability Measurements, Interagency Chemical Rocket Propulsion Group. Minutes of the October 1968 meeting of the Solid Propellant Combustion Working Group. Chemical Propulsion Information Agency, Johns Hopkins Applied Physics Laboratory, Silver Spring, Md.

3. Ballistic Research Laboratory. Combustion Instability in Army Solid Propellant Rockets--Serious Problem or Not?, by L. A. Watermeier and R. C. Strittmater. Aberdeen Proving Ground, Md., BRL, March 1966. (BRL Memo. Report No. 1729).

4. Horton, M. D. Use of the One-Dimensional T-Burner to Study of Oscillatory Combustion, AMER INST AERONAUT ASTRONAUT J, Vol. 2, No. 6 (June 1964), pp. 1112-18.

5. Princeton University, Department of Aerospace and Mechanical Sciences. Solid Propellant Combustion Instability: Oscillatory Burning of Solid Rocket Propellants, by R. H. Woodward Waesche and Martin Summerfield. Princeton, N. J., Princeton Univ., August 1965. (Aerospace and Mechanical Sciences Report No. 751, under AFOSR Grant-448-63, Project Task No. 920F-3814.)

6. McClure, F. T., R. W. Hart, and R. H. Cantrell. Interaction Between Sound and Flow: Stability of T-Burners, AMER INST AERONAUT ASTRONAUT J, Vol. 1, No. 3 (March 1963), pp. 586-90.

7. Strittmater, R. C., L. A. Watermeier, and S. P. Pfaff. Virtual Specific Acoustic Admittance Measurements of Burning Solid Propellant Surfaces by a Resonant Tube Technique, in Ninth Symposium (International) on Combustion. New York, Academic Press, 1963. Pp. 311-15.

8. Dehority, G. L., and H. B. Mathes. Acoustic Response Function Equation for a T-Burner with High Heat Loss, Technical Notes, AMER INST AERONAUT ASTRONAUT J, Vol. 6, No. 4 (April 1968), pp. 741-42.

9. U. S. Naval Ordnance Test Station. Testing the Dynamic Stability of Solid Propellants: Techniques and Data, by M. D. Horton. China Lake, Calif., NOTS, August 1964. 50 pp. (NAVWEPS Report 8596, NOTS TP 3610), UNCLASSIFIED.

10. Rice, D. W. Effect of Oxidizer Concentration on Combustion Instability of a Solid Propellant, AMER INST AERONAUT ASTRONAUT J, Vol. 2, No. 9 (September 1964), pp. 1654-55.

11. Horton, M. D., and D. W. Rice. The Effect of Compositional Variables Upon Oscillatory Combustion of Solid Rocket Propellants, COMBUST AND FLAME, Vol. 8, No. 1 (March 1964), pp. 21-28.

12. Eisel, J. L. The Effect of Acoustic Pressure on the Burning Rates of Solid Rocket Propellant, PYRODYNAMICS, Vol. 1 (1964). Pp. 61-70.

13. Crump, J. E., and E. W. Price. Effect of Acoustic Environment on the Burning Rate of Double-Base Solid Propellants, AMER ROCKET SOC, J, Vol. 31, No. 7 (July 1961). Pp. 1026-29.

14. Culick, F. E. C. A Review of Calculations for Unsteady Burning of a Solid Propellant, AMER INST AERONAUT ASTRONAUT J, Vol. 6, No. 12 (December 1968), pp. 2241-55.

15. Hightower, J. D., and E. W. Price. Combustion of Ammonium Perchlorate, in Eleventh Symposium (International) on Combustion. Pittsburgh, Pa., Combustion Institute, 1967. Pp. 463-72.

16. Horton, M. D., and M. R. McGie. Particulate Damping of Oscillatory Combustion, AMER INST AERONAUT ASTRONAUT J, Vol. 1, No. 6 (June 1963), pp. 1319-26.

UNCLASSIFIED

Security Classification

DOCUMENT CONTROL DATA - R&D

(Security classification of title, body of abstract and indexing annotation must be entered when the overall report is classified)

1. ORIGINATING ACTIVITY (Corporate author) Naval Weapons Center China Lake, California 93555	2a. REPORT SECURITY CLASSIFICATION UNCLASSIFIED 2b. GROUP

3. REPORT TITLE

EXPERIMENTAL STUDIES ON THE OSCILLATORY COMBUSTION OF SOLID PROPELLANTS

4. DESCRIPTIVE NOTES (Type of report and inclusive dates)

Research Report

5. AUTHOR(S) (Last name, first name, initial)

Aerothermochemistry Division

6. REPORT DATE	7a. TOTAL NO. OF PAGES	7b. NO. OF REFS
March 1969	108	16

8a. CONTRACT OR GRANT NO. b. PROJECT NO. T.A. RMMP-22 095/216 1/F009-06-04 c. d.	9a. ORIGINATOR'S REPORT NUMBER(S) NWC TP 4393 9b. OTHER REPORT NO(S) (Any other numbers that may be assigned this report)

10. AVAILABILITY/LIMITATION NOTICES

This document is subject to special export controls and each transmittal to foreign governments or foreign nationals may be made only with prior approval of the Naval Weapons Center.

11. SUPPLEMENTARY NOTES	12. SPONSORING MILITARY ACTIVITY
	Naval Ordnance Systems Command Department of the Navy Washington, D. C. 20360

13. ABSTRACT

This report describes the results of testing a series of composite and double-base propellants in a T-burner facility. The investigation reveals the unstable combustion behavior that is susceptible of excitation under acoustic pressure-coupled conditions. The degree of instability is quantitatively described in terms of the response function, which is a well-defined characteristic of the propellant. The effect of pressure and frequency has been systematically investigated for the frequency range of 500-10,000 cps and for pressures up to nearly 3,000 psia. Such an extended coverage has permitted the determination of a very general pattern of behavior, including the maximum instability conditions, the isoresponse function contours, and the neutral boundary separating the unstable and stable combustion regimes in the 1.5-inch T-burner.

DD FORM 1 JAN 64 1473 0101-807-6800

UNCLASSIFIED

Security Classification

UNCLASSIFIED
Security Classification

14. KEY WORDS	LINK A		LINK B		LINK C	
	ROLE	WT	ROLE	WT	ROLE	WT
Combustion instability Propellants						

INSTRUCTIONS

1. **ORIGINATING ACTIVITY:** Enter the name and address of the contractor, subcontractor, grantee, Department of Defense activity or other organization *(corporate author)* issuing the report.

2a. **REPORT SECURITY CLASSIFICATION:** Enter the overall security classification of the report. Indicate whether "Restricted Data" is included. Marking is to be in accordance with appropriate security regulations.

2b. **GROUP:** Automatic downgrading is specified in DoD Directive 5200.10 and Armed Forces Industrial Manual. Enter the group number. Also, when applicable, show that optional markings have been used for Group 3 and Group 4 as authorized.

3. **REPORT TITLE:** Enter the complete report title in all capital letters. Titles in all cases should be unclassified. If a meaningful title cannot be selected without classification, show title classification in all capitals in parenthesis immediately following the title.

4. **DESCRIPTIVE NOTES:** If appropriate, enter the type of report, e.g., interim, progress, summary, annual, or final. Give the inclusive dates when a specific reporting period is covered.

5. **AUTHOR(S):** Enter the name(s) of author(s) as shown on or in the report. Enter last name, first name, middle initial. If military, show rank and branch of service. The name of the principal author is an absolute minimum requirement.

6. **REPORT DATE:** Enter the date of the report as day, month, year; or month, year. If more than one date appears on the report, use date of publication.

7a. **TOTAL NUMBER OF PAGES:** The total page count should follow normal pagination procedures, i.e., enter the number of pages containing information.

7b. **NUMBER OF REFERENCES:** Enter the total number of references cited in the report.

8a. **CONTRACT OR GRANT NUMBER:** If appropriate, enter the applicable number of the contract or grant under which the report was written.

8b, 8c, & 8d. **PROJECT NUMBER:** Enter the appropriate military department identification, such as project number, subproject number, system numbers, task number, etc.

9a. **ORIGINATOR'S REPORT NUMBER(S):** Enter the official report number by which the document will be identified and controlled by the originating activity. This number must be unique to this report.

9b. **OTHER REPORT NUMBER(S):** If the report has been assigned any other report numbers *(either by the originator or by the sponsor)*, also enter this number(s).

10. **AVAILABILITY/LIMITATION NOTICES:** Enter any limitations on further dissemination of the report, other than those imposed by security classification, using standard statements such as:

(1) "Qualified requesters may obtain copies of this report from DDC."

(2) "Foreign announcement and dissemination of this report by DDC is not authorized."

(3) "U. S. Government agencies may obtain copies of this report directly from DDC. Other qualified DDC users shall request through _____."

(4) "U. S. military agencies may obtain copies of this report directly from DDC. Other qualified users shall request through _____."

(5) "All distribution of this report is controlled. Qualified DDC users shall request through _____."

If the report has been furnished to the Office of Technical Services, Department of Commerce, for sale to the public, indicate this fact and enter the price, if known.

11. **SUPPLEMENTARY NOTES:** Use for additional explanatory notes.

12. **SPONSORING MILITARY ACTIVITY:** Enter the name of the departmental project office or laboratory sponsoring *(paying for)* the research and development. Include address.

13. **ABSTRACT:** Enter an abstract giving a brief and factual summary of the document indicative of the report, even though it may also appear elsewhere in the body of the technical report. If additional space is required, a continuation sheet shall be attached.

It is highly desirable that the abstract of classified reports be unclassified. Each paragraph of the abstract shall end with an indication of the military security classification of the information in the paragraph, represented as *(TS), (S), (C), or (U)*.

There is no limitation on the length of the abstract. However, the suggested length is from 150 to 225 words.

14. **KEY WORDS:** Key words are technically meaningful terms or short phrases that characterize a report and may be used as index entries for cataloging the report. Key words must be selected so that no security classification is required. Identifiers, such as equipment model designation, trade name, military project code name, geographic location, may be used as key words but will be followed by an indication of technical context. The assignment of links, roles, and weights is optional.

UNCLASSIFIED
Security Classification